An Emerging Aerosol Climatology via Remote Sensing over Metro Manila, Philippines

Genevieve Rose Lorenzo[1,2], Avelino F. Arellano[1], Maria Obiminda Cambaliza[2,3], Christopher Castro[1], Melliza Templonuevo Cruz[2,4], Larry Di Girolamo[5], Glenn Franco Gacal[2], Miguel Ricardo A. Hilario[1], Nofel Lagrosas[6], Hans Jarett Ong[2], James Bernard Simpas[2,3], Sherdon Niño Uy[2], and Armin Sorooshian[1,7]

[1]Department of Hydrology and Atmospheric Sciences, University of Arizona, Tucson, Arizona, 85721, USA
[2]Air Quality Dynamics-Instrumentation & Technology Development Laboratory, Manila Observatory, Quezon City, 1108, Philippines
[3]Department of Physics, School of Science and Engineering, Ateneo de Manila University, Quezon City, 1108, Philippines
[4]Institute of Environmental Science and Meteorology, University of the Philippines, Diliman, Quezon City, 1101, Philippines
[5]Department of Atmospheric Science, University of Illinois, Urbana-Champlain, Illinois, 61801, USA
[6]Center for Environmental Remote Sensing, Chiba University, Chiba, 263-8522, Japan
[7]Department of Chemical and Environmental Engineering, University of Arizona, Tucson, Arizona, 85721, USA

Correspondence to: armin@arizona.edu

Abstract

Aerosol particles in Southeast Asia ~~have a complex life cycle and consequently~~ are challenging to characterize~~. The~~ due to their complex life cycle within the diverse topography and weather in the region ~~complicate the situation.~~. An emerging aerosol climatology was established based on AERONET data (December 2009 to October 2018) for clear sky days in Metro Manila, Philippines. ~~-~~Aerosol optical depth (AOD) values were highest ~~in~~from August~~, coinciding with the summer southwest monsoon, due~~ to October, partly ~~to~~from fine ~~particles from~~ urban aerosol particles, including soot~~. Also, August corresponds to~~, coinciding with the burning season in Insular Southeast Asia when smoke is often transported to Metro Manila during the southwest monsoon. Clustering of AERONET volume size distributions (VSD) resulted in five aerosol particle sources based on the position and magnitude of their peaks in the VSD and the contributions of specific particle species to AOD per cluster based on MERRA-2. The clustering showed that the majority of aerosol particles above Metro Manila were from a clean marine source (58%), which could be related to AOD values there being relatively smaller than in other cities in the region. The following are the other particle sources over Metro Manila: fine polluted (20%), mixed ~~polluted~~dust (12%), urban/industrial (5%), and cloud processing (5%). Furthermore, MERRA-2 AOD data over Southeast Asia were analyzed using empirical orthogonal functions. Along with AOD fractional compositional contributions and wind regimes, four dominant aerosol particle air masses emerged: two sulfate air masses from East Asia, an organic carbon source from Indonesia, and a sulfate source from the Philippines. Knowing the local and regional aerosol particle air masses that impact Metro Manila is useful in identifying the sources while gaining insight on how aerosol particles are affected by long-range transport and their impact on regional weather.

1. Introduction

Although Southeast Asia is one of the most rapidly developing regions in the world~~, there have been limited studies characterizing~~ with a growing number of extensive research conducted (Reid et al., 2023), there remain knowledge gaps related to aerosol particles in the area (Tsay et al., 2013; Lee et al., 2018; Chen et al., 2020; Amnuaylojaroen, 2023). The region represents a complex geographic, meteorological, and hydrological environment making it challenging to understand aerosol particle characteristics, especially interactions between aerosol particles with their environment (Reid et al., 2013). The island of Luzon in the Philippines in particular is very populated and is characterized by high levels of anthropogenic emissions superimposed on natural emissions from the surrounding waters (AzadiAghdam et al., 2019) and long-range transport of emissions from areas such as Indonesia and East Asia (Braun et al., 2020; Hilario et al., 2020a; Hilario et al., 2020b; Hilario et al., 2021a). Aerosol particle lifecycle in the region is impacted by Philippine weather that is marked by two distinct monsoons, typhoons, the intertropical convergent zone, and impacts from El Niño-Southern Oscillation and Madden-Julian Oscillation (Cruz et al., 2013; Xian et al., 2013; Reid et al., 2012; Reid et al., 2015; Hilario et al., 2021b). Studying this area is informative owing to the wide dynamic range in aerosol particle and weather conditions, which are interconnected. ~~The presence of~~The overlapping of large fraction of cirrus clouds with lower clouds in the area (Hong and Di Girolamo, 2020) makes space-borne remote sensing of aerosol particles very challenging (Reid et al., 2013; Lin et al., 2014). These reasons motivated the NASA Cloud, Aerosol, and Monsoon Processes Philippines Experiment ($CAMP^2Ex$) airborne measurement campaign in 2019 to understand the interaction between tropical meteorology and aerosol particles (Di Girolamo et al., 2015; Reid et al., 2023). ~~Prior to the airborne measurements, intensive surface-based measurements were conducted as part of the $CAMP^2Ex$ weatHEr and CompoSition Monitoring (CHECSM) study between July 2018 and October 2019~~However, those short terms measurements cannot provide an adequate assessment of aerosol behavior across all seasons and over many years.

~~Aerosol climatology studies in different regions have proved beneficial to understand temporal characteristics of aerosol particle concentrations and properties, in addition to identifying potential source regions along with interactions with clouds and rainfall (Stevens and Feingold, 2009; Li et al., 2011; Tao et al., 2012; Crosbie et al., 2014; Kumar et al., 2015; Alizadeh-Choobari and Gharaylou, 2017; Mora et al., 2017; Aldhaif et al., 2021).~~ The NASA AErosol RObotic NETwork (AERONET) (Holben et al., 1998) is pivotal in providing broad temporal coverage of aerosol characteristics in specific locations with a column-based perspective from the ground up. Aerosol climatology studies in different regions have proved beneficial to understand temporal characteristics of aerosol particle concentrations and properties, in addition to identifying potential source regions along with interactions with clouds and rainfall (Stevens and Feingold, 2009; Li et al., 2011; Tao et al., 2012; Crosbie et al., 2014; Kumar et al., 2015; Alizadeh-Choobari and Gharaylou, 2017; Mora et al., 2017; Aldhaif et al., 2021). ~~in specific locations with a column-based perspective from the ground up.~~ To our knowledge, there has not been a remote sensing-based aerosol climatology study for the Metro Manila region of Luzon, which has approximately 16 cities, a population of 12.88 million, and a high population density of 20,800 km^{-2} (PSA, 2016; Alas et al., 2018). ~~Studying this area is informative owing to the wide dynamic range in aerosol particle and weather conditions, which are interconnected.~~ ~~Aerosol particle lifecycle in the region is impacted by Philippine weather that is marked by two distinct monsoons, typhoons, and impacts from El Niño-Southern Oscillation and Madden-Julian~~

Oscillation (Cruz et al., 2013; Xian et al., 2013; Reid et al., 2012; Reid et al., 2015; Hilario et al., 2021b).

Regional analysis of aerosol particles in Southeast Asia and Asia in general show the prevalence of biomass burning in the region, as well as the larger influence of anthropogenic emissions in East Asia (Nakata et al., 2018). These large prevalent sources may overshadow other relevant but weaker sources in the region, such as local sources. Due to the complex nature of aerosol particles, analysis techniques such as principal component analysis and clustering along with recent improvements in gridded datasets help detect spatial and temporal patterns that would otherwise be difficult to make with noise interference and even weak signals (Li et al., 2013; Sullivan et al., 2017; Plymale et al., 2021). Understanding the dominant air masses around Southeast Asia will help in distinguishing local and transported particles that influence the aerosol climatology in Metro Manila.Most of the past studies involving long-term remotely sensed aerosol particle data in Southeast Asia (Cohen, 2014; Nakata et al., 2018; Nguyen et al., 2019b) had no specific focus on the Philippines. The Philippines is considered as part of the Maritime Continent (MC), the island nations sub-region of Southeast Asia. The other Southeast Asia sub-region, Peninsular Southeast Asia (PSEA), comprises those nations within the continental Asia land mass. These two regions have separate aerosol sources and climate, where MC is dependent on the intertropical convergent zone (ITCZ) and PSEA is dependent on both the ITCZ and monsoon systems (Dong and Fu, 2015). Only the southern part of the Philippines is climatologically part of MC (Ramage, 1971), however, and northwest Philippines, where Metro Manila is located, is affected by the monsoons and tropical cyclones aside from the ITCZ (Chang et al., 2005; Yumul Jr et al., 2010; Bagtasa, 2017). These unique meteorological influences and extensive local aerosol particle sources warrant a unique aerosol climatology over Metro Manila, one of a polluted source in a tropical marine environment, and its effects on cloud formation in the area. Aerosol effects on clouds in the marine environment are associated with the largest uncertainties in climate change research (Hendrickson et al., 2021; Wall et al., 2022) and the Philippines was ranked as the 5th country globally as most at risk to climate change and extreme weather from 1997 to 2018 (Eckstein et al., 2018). There have been several surface measurements of aerosol particles made in Metro Manila for the past 20 years (Oanh et al., 2006; Bautista VII et al., 2014; Cruz et al., 2019) but columnar ground-based measurements there are just beginning to be established (Dorado et al., 2001; Ong et al., 2016; Cruz et al., 2023). The AERONET sun photometer is one of the first long-term column-based aerosol instruments in Metro Manila and the Philippines (Ong et al., 2016).

The goal of this study is to use multi-year AERONET data in Manila Observatory along with other complementary datasets (MERRA-2, PERSIANN, MISR, HYSPLIT, and NAAPS) to address the following questions: (1) what are the monthly characteristics of aerosol particles over Metro Manila, Philippines?; (2) what are the possible sources and factors influencing the observed characteristics?; (3) what relationships are evident between aerosol particles and cloud characteristics?; and (4) what are the regional and local aerosol particle air masses that influence Metro Manila?

2. Methods

This work relies on analysis of several datasets summarized in Table 1 and the following subsections. The common time range used for all datasets is between January 2009 and October 2018.

Table 1: Summary of datasets over Metro Manila used in this work covering the period from January 2009 to October 2018.

Parameter	Data Source	Spatial Coverage	~~Data Repository~~Time Coverage
Aerosol Optical Depth (500 nm)	AERONET	14.635°N, 121.078°E	~~(AERONET) https://aeronet.gsfc.nasa.gov~~Jan 2009 - Oct 2018
Asymmetry Factor (440 nm - 1020 nm)	AERONET	14.635°N, 121.078°E	Jan 2009 - Oct 2018
Extinction Angstrom Exponent (440 nm -870 nm)	AERONET	14.635°N, 121.078°E	Jan 2009 - Oct 2018
Fine Mode Fraction	AERONET	14.635°N, 121.078°E	Jan 2009 - Oct 2018
Precipitable Water	AERONET	14.635°N, 121.078°E	Jan 2009 - Oct 2018
Single Scattering Albedo (440 nm - 1020 nm)	AERONET	14.635°N, 121.078°E	Jan 2009 - Oct 2018
Refractive Index (Real and Imaginary; 440 nm - 1020 nm)	AERONET	14.635°N, 121.078°E	Jan 2009 - Oct 2018
Volume Size Distribution	AERONET	14.635°N, 121.078°E	Jan 2009 - Oct 2018
Low Cloud Fraction (MODIS)	MERRA-2	14.~~25~~3°N - 14.~~75~~8°N, 120.~~9375~~75°E - 121.~~5625~~25°E	~~(MERRA-2) https://disc.gsfc.nasa.gov/~~Jan 2009 - Dec 2018
Planetary Boundary Layer Height	MERRA-2	14.~~25~~3°N - 14.~~75~~8°N, 120.~~9375~~75°E - 121.~~5625~~25°E	Jan 2009 - Dec 2018
Relative Humidity (975 mb)	MERRA-2	14.~~25~~3°N - 14.~~75~~8°N, 120.~~9375~~75°E - 121.~~5625~~25°E	Jan 2009 - Dec 2018
Sea Level Pressure	MERRA-2	14.~~25~~3°N - 14.~~75~~8°N, 120.~~9375~~75°E - 121.~~5625~~25°E	Jan 2009 - Dec 2018
Temperature (975 mb)	MERRA-2	14.~~25~~3°N - 14.~~75~~8°N, 120.~~9375~~75°E - 121.~~5625~~25°E	Jan 2009 - Dec 2018
Wind (975 mb)	MERRA-2	14.~~25~~3°N - 14.~~75~~8°N, 120.~~9375~~75°E - 121.~~5625~~25°E	Jan 2009 - Dec 2018
Total Extinction Aerosol Optical Depth (550 nm)	MERRA-2	14.3°N - 14.8°N, 120.75°E - 121.25°E	Jan 2009 - Dec 2018
Sulfate, Black Carbon, Organic Carbon, Dust, and Sea Salt Extinction Aerosol Optical Depth (550 nm)	MERRA-2	14.3°N - 14.8°N, 120.75°E - 121.25°E	Jan 2009 - Dec 2018
Precipitation	PERSIANN	14.~~5~~3°N - ~~15.0~~14.8°N, 120.75°E - 121.25°E	~~(PERSIANN) https://chrsdata.eng.uci.edu/~~Jan 2009 - Dec 2018

2.1 Datasets

2.1.1 AERONET

The central dataset used is that of sun photometer measurements and derived (inversion) parameters from the AERONET (Holben et al., 1998) site at the Manila Observatory in Quezon City, Philippines (14.64° N, 121.08° E, ~70 m. a. s. l.). Direct sunlight extinction measurements were made at nominal wavelengths of 340, 380, 440, 500, 675, 870, 940, and 1020 nm, from which aerosol optical depth (AOD) was calculated (except for 940 nm, which is for water vapor) (Eck et al., 2013). AOD is a commonly used proxy for aerosol particle loading in the air column from the ground up (Holben et al., 2001); higher AOD translates to more aerosol particle extinction in the column above a location. The extinction angstrom exponent (EAE) and the fine mode fraction (FMF) are also AERONET direct sun products that are retrieved after the application of a spectral de-convolution algorithm (O'Neill et al., 2003). For the inversion products, it is through radiative retrievals that the volume size distribution (VSD) and complex refractive index (RI) are gathered ~~(Schuster et al., 2005) and from which single scattering albedo (SSA) and asymmetry factor (AF) are calculated.~~and from which single scattering albedo (SSA) and asymmetry factor (AF) are calculated. The AERONET observations were made during clear sky conditions, which has been shown (Hong and Di Girolamo, 2022) to be able to represent all sky conditions.

For the inversions, four wavelengths (440, 670, 870, and 1020 nm) of the radiometer spectral channels were chosen for diffuse radiance measurements and to avoid gas absorption (Dubovik et al., 1998). Version 3 Direct Sun and Inversion algorithms (AERONET, 2019; Giles et al., 2019) were used with the Almucantar Sky Scan Scenario to derive the following parameters with level 2.0 (automatically cloud-cleared and quality controlled datasets with pre- and post-field calibrations) data quality: column AOD (500 nm), fine mode fraction (500 nm), extinction angstrom exponent (440 – 870 nm), precipitable water (940 nm), ~~SSA~~single scattering albedo (440, 670, 870, and 1020 nm), asymmetry factor (440, 670, 870, and 1020 nm), refractive index (440, 670, 870, and 1020 nm), and VSD. The version 3 products are able to keep fine mode aerosol particle data (haze and smoke) as well as remove optically thin cirrus clouds in order to retain more aerosol particle measurements in the database (Giles et al., 2019). Cloud screening in the version 3 product improves remote sensing measurements in Southeast Asia in general, where cirrus clouds are pervasive (Reid et al., 2013). At most, a total of 29,037 direct sun and 1419 inversion AERONET daytime data points were available between January 2009 and October 2018.

2.1.2 MERRA-2

Modern Era-Retrospective Analysis for Research and Applications, Version 2 (MERRA-2: 0.5° × 0.625° approximate resolution) meteorological and aerosol particle composition reanalysis data (Bosilovich, 2016; Gelaro et al., 2017; Randles et al., 2017) were acquired for the area around Manila Observatory (14.25°N – 14.75°N, 120.9375°E – 121.5625°E). The aerosol reanalysis data includes data assimilation of AOD from the Moderate Resolution Imaging Spectroradiometer (MODIS: Terra, 2000 to present and Aqua, 2002 to present), Advanced Very High Resolution Radiometer (AVHRR, 1979-2002), and Multiangle Imaging SpectroRadiometer (MISR, 2000-2014) (Buchard et al., 2017; Rizza et al., 2019). The following products were used: M2I3NPASM Assimilated Meteorological Fields (3-hourly) for 975 mb level winds, temperature, relative humidity, and sea level pressure; M2T1NXFLX Surface Flux Diagnostics (1-hourly from 00:30 UTC time-averaged) 2D for planetary boundary layer height; ~~and~~ M2T1NXCSP COSP Satellite Simulator (1-hourly from 00:30 UTC time-averaged) for MODIS mean low cloud fraction (cloud top pressure > 680 hPa); and M2T1NXAER Aerosol Diagnostics (1-hourly from 00:30 UTC time-averaged) for Total AOD and speciated AOD (Sulfate, Black Carbon (BC), Organic Carbon (OC), Dust, and Sea Salt).

MERRA-2 meteorological and aerosol particle composition monthly mean reanalysis data (Bosilovich, 2016; Gelaro et al., 2017; Randles et al., 2017) were also acquired for a larger region, , (30° × 30°), the Southeast Asia region (0°–N – 30°N, 105°E – 135°E) for the period from 2009 to 2018. This is within the spatial domain of the CAMP^{2}Ex airborne measurement campaign which, as mentioned earlier, targets the interaction between tropical meteorology and aerosol particles. The following datasets (0.5° latitude and 0.625° longitude resolution) were used: MERRA-2 tavgM_2d_aer_Nx: Aerosol Assimilation (M2TMNXAER) for Total 500 nm AOD and speciated 500 nm AOD (Sulfate, Black Carbon (BC), Organic Carbon (, OC),, Dust, and Sea Salt) and MERRA-2 instM_3d_ana_Np: Analyzed Meteorological Fields (M2IMNPANA) for 1000 hPa and 725 hPa level U and V winds. The total MERRA-2 AOD for the region was used along with MISR AOD data to assess the influence of long-range sources to the aerosol column over Manila Observatory. The monthly meteorological and aerosol particle composition data for the region will be used for empirical orthogonal functions, which will be described later.

2.1.3 MISR

Monthly AOD data (Level 3 Global Aerosol: 0.5° × 0.5° spatial resolution) from 2009 to 2018 are used from the Multi-angle Imaging SpectroRadiometer (MISR), (Diner et al., 2007; Garay et al., 2018). Level 3 products are global maps of parameters available in Level 2 (measurements derived from the instrument data) products. MISR has relatively more accurate AOD and agrees better with AERONET data compared to other satellite products due to its multi-angle measurements (Choi et al., 2019; Kuttippurath and Raj, 2021). Monthly median AOD (bin 0) were extracted for Southeast Asia (0.25° - 30.25°N, 104.75°E – 134.75°E) within the CAMP^{2}Ex region. They are used for comparison to the AERONET (over Metro Manila) and MERRA-2 (Southeast Asia) monthly AOD values.

2.1.4 PERSIANN

Hourly precipitation data were obtained from the Precipitation Estimation from the Remotely Sensed Information using Artificial Neural Networks (PERSIANN) (Nguyen et al., 2019)(Nguyen et al., 2019a) database of the Center for Hydrometeorology and Remote Sensing (CHRS) at the University of California, Irvine (UCI). Hourly data were accumulated for running three-day totals, which were compared to AERONET data. The data were averaged between the four grids that included the area of interest as well as ensuring a similar spatial domain (14.5°N – – 15.0°N, 120.75°E – – 121.25°E) to the MERRA-2 dataset.

2.1.4 MISR

Monthly 500 nm AOD data (Level 3 Global Aerosol: 0.5° × 0.5° spatial resolution) from 2009 to 2018 are used from the Multi-angle Imaging SpectroRadiometer (MISR), (Diner et al., 2007; Garay et al., 2018) as regional (Southeast Asia) baseline remote sensing data to support the Manila Observatory AERONET data. The regional (30° × 30°) MISR data was used to confirm regional sources of aerosols that may be influencing the AOD over Metro Manila. Level 3 MISR products are global maps of parameters available in Level 2 (measurements derived from the instrument data) products. MISR is ideal for remote sensing in the CAMP^{2}Ex region because it has an overpass at 10:30 AM ECT (descending mode) (when cirrus is minimal) and its retrievals have been shown to be unimpacted by small cumulus (Zhao et al., 2009), which are typical in the region. MISR has relatively more accurate AOD and agrees better with AERONET data compared to other satellite products due to its multi-angle measurements (Choi et al., 2019;

Kuttippurath and Raj, 2021). The MISR sampling noise is relatively small due to the large domain and seasonal averages that are considered in this study. MISR is also the only passive sensor that speciates aerosol particle size and shape. All these factors led to the choice of using regional MISR data to associate long-range sources influencing AERONET data in Manila Observatory. Monthly mean AOD (bin 0) were extracted for Southeast Asia (0.25°N – 30.25°N, 104.75°E – 134.75°E) within the CAMP^{2}Ex region. Monthly mean AOD values were then calculated for each 0.5° grid point and then for the 30° × 30° region, where the standard error in the monthly mean for the region is less than 0.002. MISR monthly mean time series of size, shape, and absorption speciated 550 nm AOD and angstrom exponent in the CAMP^{2}Ex domain (6.5°N – 22.5°N, 116.5°E – 128.5°E; March 2000 to December 2020) are also used to support the findings from the AERONET data.

2.1.5 NAAPS

Archived maps of total and speciated optical depths ~~along with~~and surface concentrations of sulfate, dust, and smoke for Southeast Asia are used from the Navy Aerosol Analysis and Prediction System (NAAPS: 1~~/3~~° × 1~~/3~~° spatial resolution) (Lynch et al., 2016), and which ~~is~~are publicly available at https://www.nrlmry.navy.mil/aerosol/. This reanalysis product relies on the Navy Global Environmental Model (NAVGEM) for meteorological fields (Hogan et al., 2014). Hourly maps were downloaded for ~~Southeast Asia for~~ aerosol particle events of interest based on AERONET data. These maps help ~~in the identification of~~associate possible regional emission sources~~.~~ to extreme aerosol loading events in Manila Observatory.

2.1.6 ~~NASA Worldview~~HYSPLIT

~~Archived maps of cloud fraction (Aqua MODIS and Terra MODIS) were downloaded from NASA Worldview (https://worldview.earthdata.nasa.gov) for events of interest based on AERONET data.~~

~~2.2~~2.1 ~~Clustering~~

~~Available AERONET VSD data (0.050 μm to 15.000 μm particle radius in 22 logarithmically equidistant bins, 1419 data points) were clustered via k-means clustering (Lloyd, 1982). The algorithm used was k-means++ (Arthur and Vassilvitskii, 2006). The ideal number of clusters was chosen based on relatively highest (>0.5) average silhouette value and the presence of a cluster with a second peak in the larger accumulation mode of the VSD. The clusters were analyzed based on their associated meteorological conditions and aerosol particle characteristics and were classified into air mass types (Table 2) based on previous studies (Pace et al., 2006; Kaskaoutis et al., 2007; Sorooshian et al., 2013; Kumar et al., 2014; Sharma et al., 2014; Che et al., 2015; Kumar et al., 2015).~~

~~**Table 2:** Summary of threshold values of aerosol optical depth (AOD), angstrom exponent (AE), and fine mode fraction (FMF) used to identify air mass types.~~

~~Air Mass Type~~	~~AOD~~	~~AE~~	~~FMF~~	~~Source~~
~~Clean Fine~~	~~< 0.1~~	~~> 1~~	~~> 0.7~~	~~Sorooshian et al., 2013~~
~~Polluted Fine~~	~~> 0.1~~	~~> 1~~	~~> 0.7~~	~~Sorooshian et al., 2013~~
~~Clean Coarse~~	~~< 0.1~~	~~< 1~~	~~< 0.3~~	~~Sorooshian et al., 2013~~
~~Polluted Coarse~~	~~> 0.1~~	~~< 1~~	~~< 0.3~~	~~Sorooshian et al., 2013~~

~~Desert Dust~~	~~> 0.3~~	~~-~~	~~< 0.6~~	~~Kaskaoutis et al., 2007~~
~~Clean Marine~~	~~< 0.2~~	~~-~~	~~< 0.7~~	~~Kaskaoutis et al., 2007~~
~~Urban/Industrial~~	~~> 0.2~~	~~-~~	~~> 0.8~~	~~Kaskaoutis et al., 2007~~

~~2.3~~2.1 ~~Extreme Event Analysis~~

~~Selected types of aerosol particle events were identified to characterize different types of sources and processes impacting aerosol particle columnar properties above Metro Manila. The three events are described below.~~

~~2.3.1~~2.1.1 ~~Smoke Long Range Transport~~

~~Events related to transported biomass burning/smoke were chosen based on the highest black carbon contribution to total AOD from the MERRA-2 dataset, high smoke contributions to AOD from NAAPS, and a dominant submicrometer peak in the AERONET VSD (Eck et al., 1999) over Metro Manila. Maps of surface smoke contributions from NAAPS as well as back~~Back-trajectories from the National Oceanic and Atmospheric Administration's (NOAA) Hybrid Single-Particle Lagrangian Integrated Trajectory (HYSPLIT) model (Stein et al., 2015; Rolph et al., 2017) were used to ~~identify the likely source and transport pathway for the smoke cases. Three~~provide support for the AERONET monthly aerosol characteristics and the chosen case studies. Three and seven-day back-trajectories with six-hour resolution were generated based on the NCEP/NCAR reanalysis meteorological dataset and with a resolution of 1° and a vertical wind setting of "model vertical velocity". The three-day data were used to map the density of trajectories reaching Manila Observatory in each month from 2008 to 2019. The seven-day data were used in the analysis of the case studies. Trajectories were computed for an end point with an altitude of 500 m above ground level at the Manila Observatory. This altitude represents the mixed layer based on related surface air quality studies (Crosbie et al., 2014; Mora et al., 2017; Schlosser et al., 2017; Aldhaif et al., 2020), including a previous study for the same area (Stahl et al., 2020).

2.1.7 NASA Worldview

Archived maps of cloud fraction (Aqua MODIS and Terra MODIS) over Metro Manila and Southeast Asia were downloaded from NASA Worldview (https://worldview.earthdata.nasa.gov) for events of interest based on AERONET data.

2.2 Clustering

Available AERONET VSD data (0.050 µm to 15.000 µm particle radius in 22 logarithmically equidistant discrete points, 1419 data points) were clustered via k-means clustering (Lloyd, 1982). The algorithm used was k-means++ (Arthur and Vassilvitskii, 2006). The ideal number of clusters was chosen based on relatively highest (>0.5) average silhouette value and the presence of a cluster with a second peak in the larger accumulation mode of the VSD. The clusters were analyzed based on their associated meteorological conditions and aerosol particle characteristics and were classified into air mass types (Table 2) based on estimates from previous studies (Dubovik et al., 2002; Pace et al., 2006; Kaskaoutis et al., 2007; Kaskaoutis et al., 2009; Sorooshian et al., 2013; Kumar et al., 2014; Sharma et al., 2014; Che et al., 2015; Kumar et al., 2015; Deep et al., 2021). The first four mentioned air mass types in Table 2 are the most general, and four more classifications based on aerosol particle sources are included. The urban/industrial air mass type here refers to local combustion along with long-range transported biomass burning

(Kaskaoutis et al., 2009). While these classifications are not rigid definitions of air masses, they help in understanding the sources that contribute to aerosols in Metro Manila and in identifying cases where certain sources are more influential than others.

Table 2: Summary of threshold values of aerosol optical depth (AOD), angstrom exponent (AE), fine mode fraction (FMF), and single scattering albedo (SSA) used to identify air mass types.

Air Mass Type	AOD	AE	FMF	SSA	Source
Clean Fine	< 0.1[a]	> 1[a]	> 0.7[a]	-	Sorooshian et al., 2013
Polluted Fine	> 0.1[a]	> 1[a]	> 0.7[a]	-	Sorooshian et al., 2013
Clean Coarse	< 0.1[a]	< 1[a]	< 0.3[a]	-	Sorooshian et al., 2013
Polluted Coarse	> 0.1[a]	< 1[a]	< 0.3[a]	-	Sorooshian et al., 2013
Clean Marine	< 0.2[b]	< 0.9[d]	-	0.98[e]	Kaskaoutis et al., 2009 Dubovik et al., 2002
Urban/Industrial	> 0.2[b]	> 1[d]	-	0.9-0.98[e]	Kaskaoutis et al., 2009 Dubovik et al., 2002
Biomass Burning	-	> 1.4[a]	-	0.89-0.95[e]	Deep et al., 2021 Dubovik et al., 2002
Desert Dust	> 0.3[c]	< 1[d]	-	0.92-0.93[e]	Kaskaoutis et al., 2009 Deep et al., 2021 Dubovik et al., 2002

[a] from MODIS [c] AOD at 400 nm [e] SSA at 440 nm
[b] AOD at 500 nm [d] AE at 380 nm to 870 nm

2.3 Extreme Event Analysis

Aerosol particle events based on the three clusters with the highest VSD concentrations were identified to characterize different types of sources and processes impacting aerosol particle columnar properties above Metro Manila. The three events are described below.

2.3.1 Smoke Long Range Transport

Events related to transported biomass burning/smoke were chosen from the AERONET VSD data that were clustered as urban/industrial (with a dominant submicrometer peak) (Eck et al., 1999) over Metro Manila. Cases with the highest black carbon contribution to total AOD from the MERRA-2 dataset were considered. Maps from NAAPS of high smoke contributions to AOD and surface smoke contributions in the direction of back-trajectories HYSPLIT were used to provide support for the likely source and transport pathway for the smoke cases.

2.3.2 Dust Long Range Transport

A dust transport case over Metro Manila was identified based on the highest dust contribution to AOD from the MERRA-2 dataset, high dust contributions to AOD from NAAPS, andAERONET VSD dust cluster (with an enhanced coarse peak in the AERONET VSD (compared to the submicrometer fraction) (Eck et al., 1999) over Metro Manila., the highest dust contribution to AOD from the MERRA-2 dataset, and high dust contributions to AOD from NAAPS. Surface dust concentrations from NAAPS along ~~with~~the HYSPLIT back-trajectories ~~confirmed~~improved the plausibility of dust for this case.

2.3.3 Cloud Processing

Cloud processing events were identified based on bimodal submicrometer VSDs (Eck et al., 2012) and a relatively large sulfate contribution to AOD over Metro Manila from the MERRA-2 dataset, since this species is predominantly produced via cloud processing (Barth et al., 2000; Faloona, 2009). The presence of clouds was verified qualitatively with MODIS (Aqua and Terra) imagery from NASA Worldview in the path of air parcels reaching Metro Manila based on HYSPLIT back-trajectories.

2.4 Empirical Orthogonal Functions

Regional analysis of aerosol particles in Southeast Asia and Asia in general show the prevalence of biomass burning in the region, as well as the larger influence of anthropogenic emissions in East Asia (Nakata et al., 2018). These large prevalent sources may overshadow other relevant but weaker sources in the region, such as local sources. Due to the complex nature of aerosol particles, analysis techniques such as principal component analysis and clustering along with recent improvements in gridded datasets help detect spatial and temporal patterns that would otherwise be difficult to make with noise interference and even weak signals (Li et al., 2013; Sullivan et al., 2017; Plymale et al., 2021). Understanding the dominant air masses around Southeast Asia will help in distinguishing local and transported particles that influence the aerosol climatology in Metro Manila.~~Empirical orthogonal function (EOF) analysis was performed to be able to associate the air mass clusters identified earlier with regional scale aerosol particle sources.~~

To contextualize the analysis of aerosol particle masses in Metro Manila, major regional sources of aerosol particles in Southeast Asia were identified based on the dominant principal components from empirical orthogonal (EOF) analysis of AOD. EOF analysis was done on the monthly AOD data (January 2009 to December 2018) from MERRA-2 for the Southeast Asia region for the months similar in scope to the AERONET data. EOF analysis needs a complete dataset with no data gaps, which is not available with pure satellite retrievals~~;~~ like MISR; the MERRA-2 reanalysis ~~data alleviate~~dataset alleviates this issue.

The monthly MERRA-2 AOD maps (0° - 30°N, 105°E – 135°E with 0.5° latitude and 0.625° longitude resolution) (Lat: 61 rows x Lon: 49 columns) for the Southeast Asia region (presented subsequently) were first deseasonalized. Then, the AOD anomaly per grid per year (of the 120 months) was calculated by subtracting the monthly mean AOD from each value of a given month (Li et al., 2013). The anomalies per grid were weighted depending on their latitude by multiplying the anomalies by the square root of the cosine of their latitudes.

EOF, specifically singular value decomposition (SVD), analysis (Björnsson and Venegas, 1997) was then performed. To prepare the data for the analysis, they were transformed such that the final matrix was a 2D matrix (120 x 2989) with each row representing a year, and each column representing a grid in the map. The matrix was analyzed for eigenvalues using SVD in Matlab, which ~~outputted~~outputs the eigenvalue (S) and eigenvector (U: principal components and V: empirical orthogonal functions) matrices. The eigenvalues were, by default, arranged in descending order. Each PC time series was standardized by dividing each PC value by the standard deviation per PC time series (120 months).

An eigenvalue spectrum was also plotted based on the variance explained by each eigenvalue and error bars that were calculated using the North test (North et al., 1982). Then, the unweighted AOD anomalies were regressed onto the first three standardized PCs. Each grid therefore had a regression between 120 pairs (unweighted AOD anomalies vs standardized PCs). From the linear regression equation, the regression coefficient per grid was calculated~~ and plotted~~. Each grid on the Southeast Asia map was colored based on the calculated regression coefficient value.

2.5 Correlations

The first three standardized PCs of AOD anomalies were correlated to deseasonalized compositional AOD fractions (Sulfate, BC, OC, Dust, and Sea Salt). For each correlation, the t-test value was calculated, and the resulting t-score was compared to a t-critical value for ~n= 100 pairs (n is the number of pairs of data, in this case 120 months) for 0.90 confidence level, which is 1.660. Correlations that have t-values exceeding +1.660 or less than -1.660 (two-tailed test) are significant (90% confidence).

3 Results and Discussion

3.1 Meteorology and Atmospheric Circulation

Knowledge of monthly behavior of weather in the study region helps interpretation of aerosol particle data. Philippine climate is influenced both by the winter northeast monsoon (~November to April, Amihan) and the summer southwest monsoon (~May to October, Habagat) (Coronas, 1920; Flores, 1969; Matsumoto et al., 2020). Median 3-hourly temperatures at 975 mb per month (MERRA-2, 975 mb) (Fig. 1a) ranged from 23.2 °C in January during the winter northeast monsoon, to 27.0 °C in May during the transition from the summer season, as defined in (Bañares et al., 2021), to the southwest monsoon. May was also the month with the lowest median 3-hourly relative humidity (76.6%) (MERRA-2, 975 mb) (Fig. 1b). The highest median level of relative humidity at 975 mb for a month was in August (86.5 %) during the summer southwest monsoon, which is also the time of the year (June to August) when rainfall peaks in the region where the sampling station (Manila Observatory) is located (Coronas, 1920; Cruz et al., 2013). The highest mean hourly precipitation (Fig. 1i) per month was from July (0.46 mm hr^{-1}) to September (0.42 mm hr^{-1}), while March exhibited the lowest mean hourly rainfall (0.02 mm hr^{-1}). Like relative humidity and precipitation, median precipitable water (from available AERONET data~~) (Fig.~~ of 513 points in August, 4015 points in February, and 5049 points in March) (Fig. 1h) was highest in August (4.9 cm) and lowest in February and March (3.1 cm and 3.2 cm, respectively).

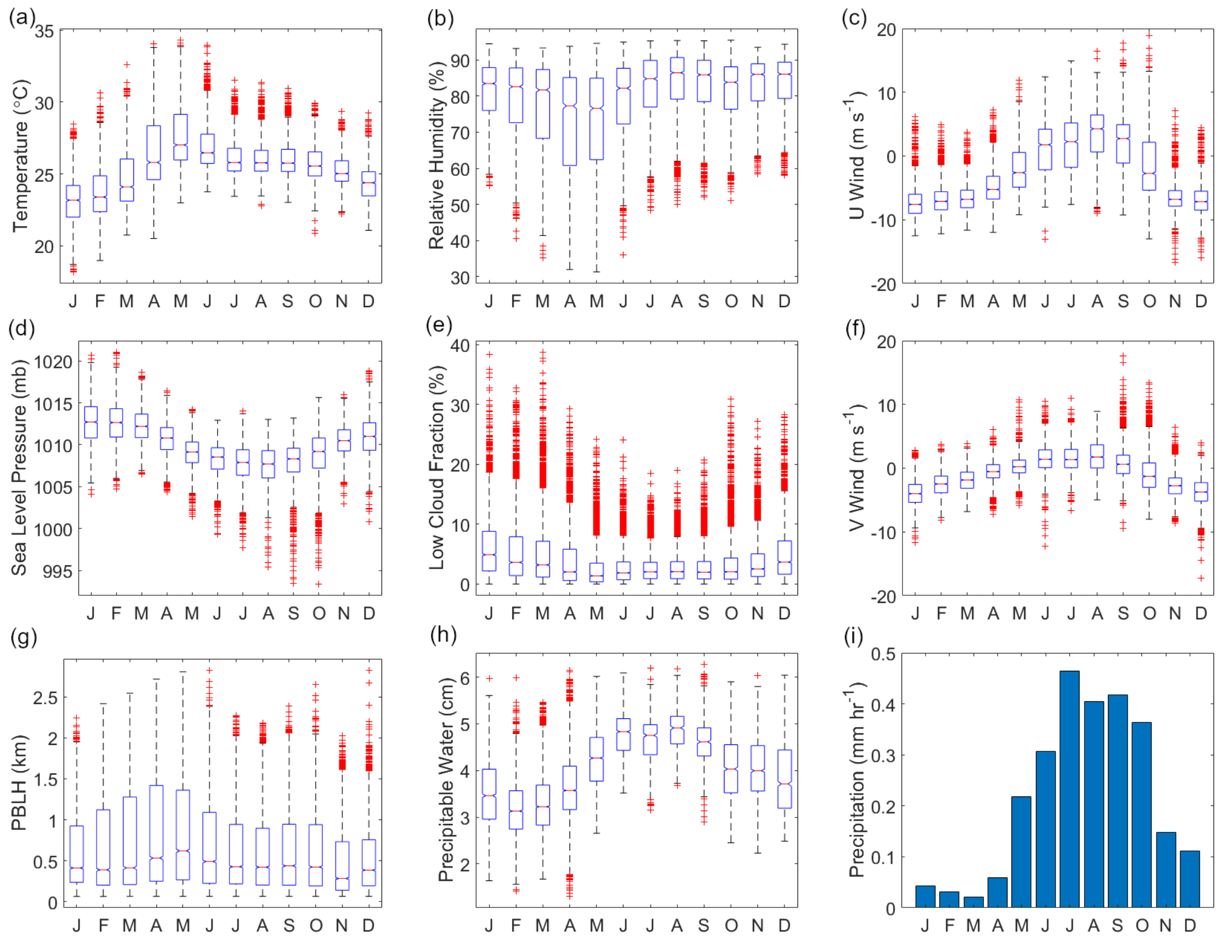

Figure 1: Monthly characteristics of meteorological parameters for Metro Manila, Philippines based on data between January 2009 and October 2018. MERRA-2 parameters: (a) temperature at 975 mb, (b) relative humidity at 975 mb, (c/f) u and v wind at 975 mb, (d) sea level pressure, (g) planetary boundary layer height (PBLH), (e) low cloud fraction; (cloud top pressure > 680 hPa); AERONET: (h) precipitable water; (data counts per month Jan: 2131, Feb: 4015, Mar: 5049, Apr: 5844, May: 3448, Jun: 1696, Jul: 652, Aug: 513, Sep: 753, Oct: 1700, Nov: 2084, Dec: 1449); PERSIANN: (i) mean hourly precipitation per month.

The lowest 3-hourly median pressures (MERRA-2) were observed (Fig. 1d) between July and September during the southwest monsoon season (~985.2 – 985.8 mb). This is also the time when the most number of tropical cyclones pass the island of Luzon (Wu and Choy, 2016). The highest 3-hourly median pressures (988.1 – 990.0 mb) were during the winter northeast monsoon.

Median winds (MERRA-2) were from the south/southwest direction from June to September (Fig. 1c and 1f), associated with the summer southwesterly monsoon. HYSPLIT back-trajectories show the same wind pattern (Fig. 2f to 2i). The highest median 3-hourly wind speeds (MERRA-2) (Fig. 1c and 1f) during the southwest monsoon were recorded for August (u: 4.2 m s^{-1} and v: 1.7 m s^{-1}). Median winds begin to transition in October and November (to the northeast monsoon: Amihan) (Fig. 2j and 2k) coming from the east/northeast and maintained until February (Fig. 2b), which is towards the end of the winter northeast monsoon. There were generally higher wind speeds and the highest median 3-hourly wind speeds of the year (MERRA-2) (Fig. 1c and 1d) in January (u: -7.6 m s^{-1} and v: -4.0 m s^{-1}). Median winds shifted toward a more easterly source from March to May (transition time before the Habagat monsoon) (Fig. 2c to 2e) accompanied by decreasing median 3-hourly wind speeds (u = -6.8 m s^{-1}, v = -1.9 m s^{-1} to u: -2.6 m s^{-1}, v = 0.2 m s^{-1}).

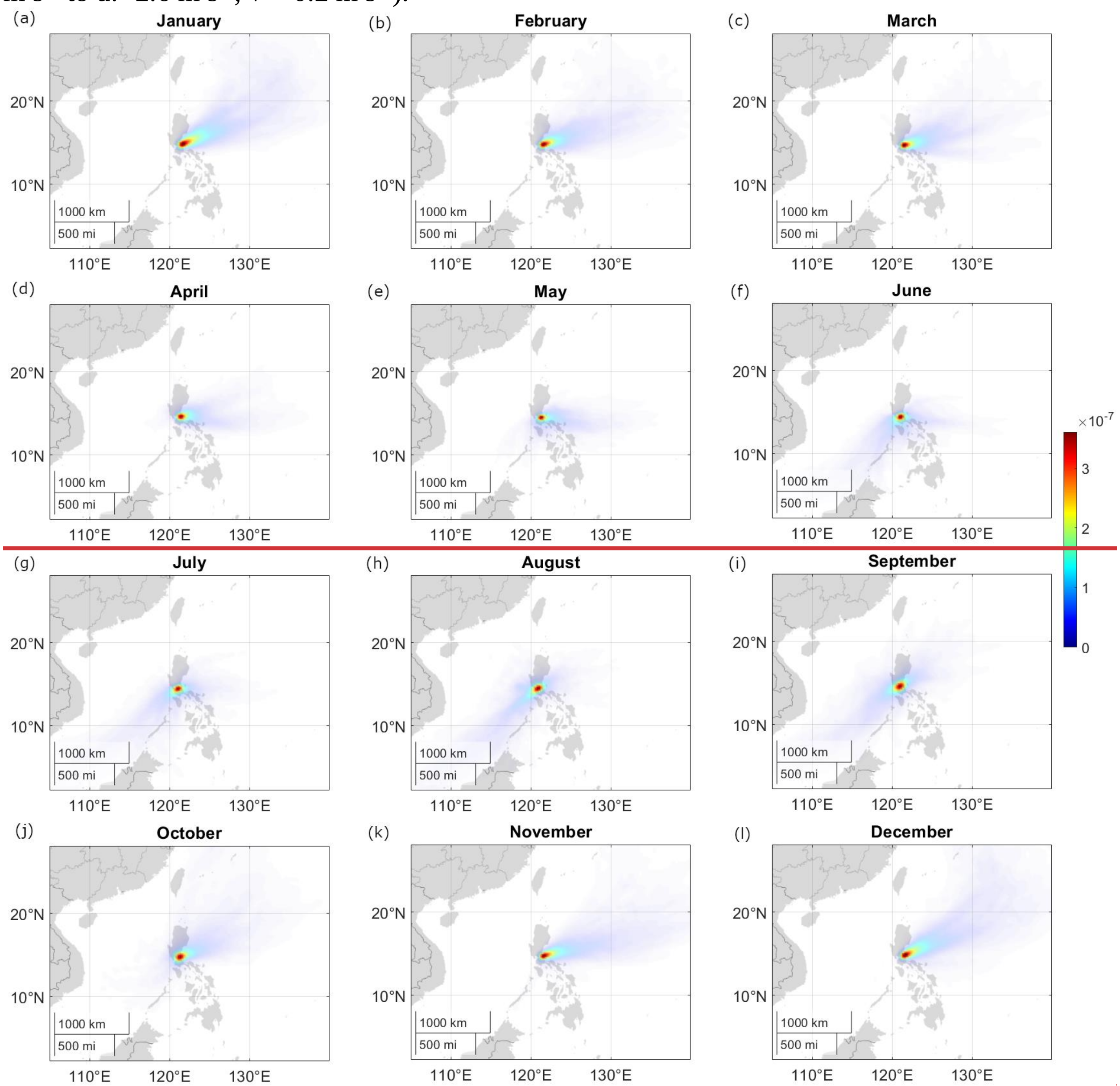

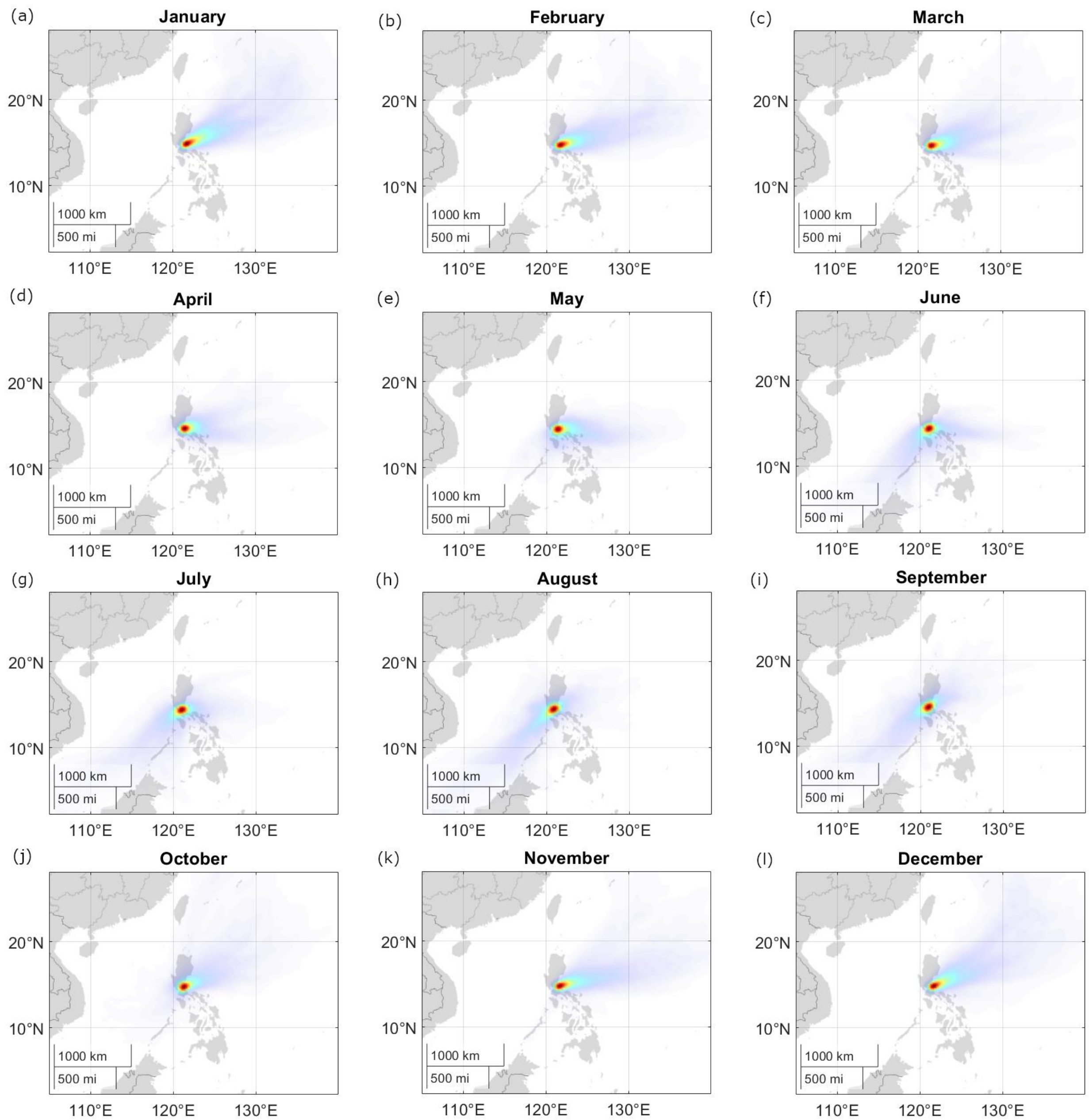

Figure 2: Density plots of HYSPLIT trajectories reaching Manila Observatory per month from 2009 to 2018. Red denotes areas with the greatest number of back trajectories within a 100 km radius. The colors represent density value contributions to Matlab-calculated cumulative probability distribution surfaces (100 km radius) from coordinates of three-day back trajectories of the specific months.

The transition times between the monsoons (when the wind directions shift and wind speeds change) are also the times of the highest (May, Fig. 1g, 621.2 m) and lowest (November, Fig. 1g, 279.6 m) median planetary boundary layer heights (MERRA-2). The median planetary boundary layer height was highest during the period (May) of highest temperatures, lowest relative humidity, reduced air pressure, and lowest monthly median low cloud fraction (MERRA-2) (Fig. 1e) (1.4 %). The lowest monthly median planetary boundary layer height was observed during the period (November) when temperatures were beginning to cool and air pressure was rising. The monthly maximum low cloud fraction was lowest in July (18.5 %) during the summer southwest monsoon while the monthly median and monthly maximum low cloud fractions (MERRA-2) (Fig. 1e) were highest (38.3 % max, 4.9 % median) in January during the winter northeast monsoon.

3.2 Aerosol Particle Characteristics

3.2.1 Aerosol Optical Depth

Monthly median AOD (AERONET, 500 nm) (Fig. 3a) over the Manila Observatory was highest from August (0.21) to October (0.23) around the time of the summer monsoon when winds were coming from the southwest (Figs. 2h to 2i) (Holben et al., 2001). This is the same time of year when biomass burning activities occur in the Indonesian region southwest of Metro Manila~~.~~ (Glover and Jessup, 1998; Kiely et al., 2019; Cahyono et al., 2022). Studies have shown that AOD in the Philippines increases during the biomass burning season in Indonesia (Nguyen et al., 2019b; Caido et al., 2022). Regional AOD (550 nm) over the larger Southeast Asia ~~region~~domain from MISR and MERRA-2 (Fig. 4) had a similarly large peak ~~from~~around the same time beginning in September ~~to~~until October which, however, was second only in magnitude to a March peak, which is influenced by biomass burning in Peninsular Southeast Asia (PSEA) (Gautam et al., 2013; Hyer et al., 2013; Dong and Fu, 2015; Wang et al., 2015; Yang et al., 2022)~~.~~. This is consistent with the peak in speciated AOD due to fine (radii <0.7 μm), spherical, and absorbing aerosols that were observed by MISR from March to April (Fig. S1). This larger peak in March, attributed to PSEA (which is ~2000 km west of the Philippines~~,~~), was not as prevalent in the AERONET AOD data over Manila Observatory in Metro Manila due to the dominant easterly winds in the Philippines in March (Fig. 2c) and more localized sources.

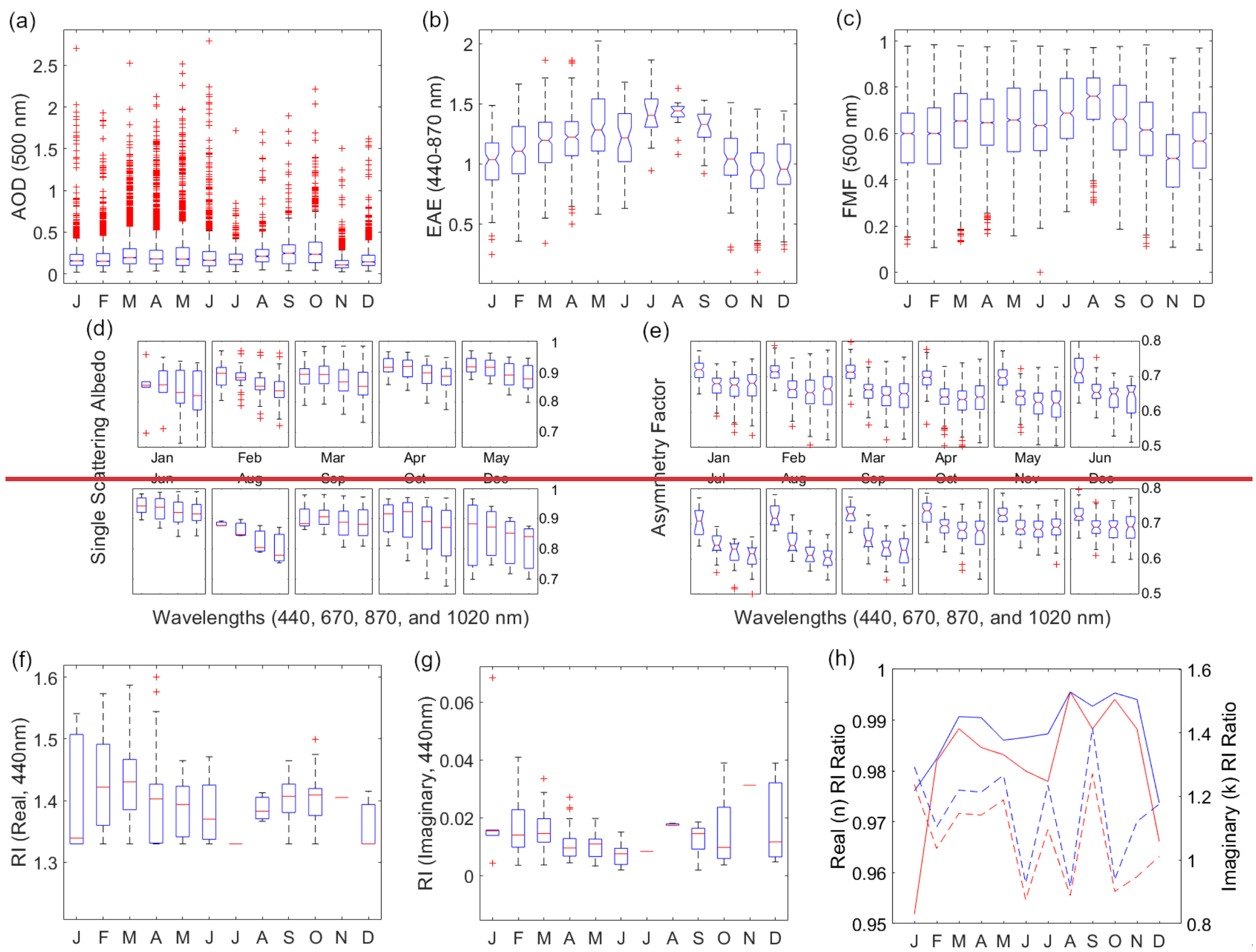
(a)
AOD (500 nm)
J F M A M J J A S O N D
(b)
EAE (440-870 nm)
J F M A M J J A S O N D
(c)
FMF (500 nm)
J F M A M J J A S O N D
(d)
Single Scattering Albedo
Jan Feb Mar Apr May
Jun Aug Sep Oct Dec
Wavelengths (440, 670, 870, and 1020 nm)
(e)
Asymmetry Factor
Jan Feb Mar Apr May Jun
Jul Aug Sep Oct Nov Dec
Wavelengths (440, 670, 870, and 1020 nm)
(f)
RI (Real, 440nm)
J F M A M J J A S O N D
(g)
RI (Imaginary, 440nm)
J F M A M J J A S O N D
(h)
Real (n) RI Ratio
Imaginary (k) RI Ratio
J F M A M J J A S O N D

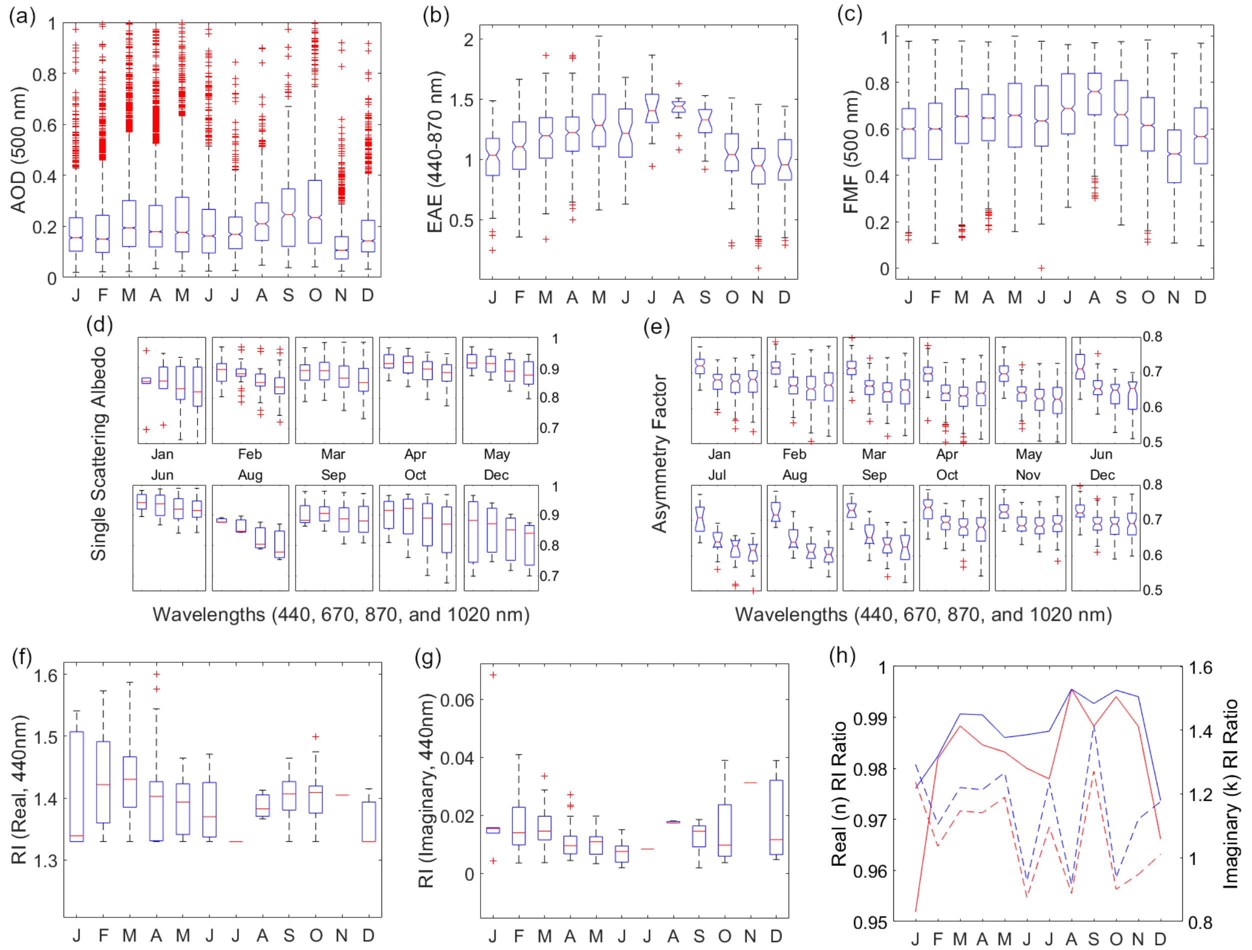

Figure 3: Monthly characteristics of AERONET aerosol particle parameters: (a) aerosol optical depth (AOD at 500 nm with y-axis until 1.0 only for larger boxplot resolution) with counts (Jan: 2107, Feb: 3931, Mar: 4923, Apr: 5755, May: 3389, Jun: 1653, Jul: 637, Aug: 483, Sep: 718, Oct: 1555, Nov: 2001, Dec: 1386), (b) extinction angstrom exponent (EAE at 440-870 nm) with counts (Jan: 102, Feb: 248, Mar: 312, Apr: 309, May: 137, Jun: 53, Jul: 14, Aug: 18, Sep: 18, Oct: 79, Nov: 77, Dec: 52), (c) spectral de-convolution algorithm (SDA) retrievals of fine mode fraction (FMF~~),~~ at 500 nm) with the same counts as AOD, (d) single scattering albedo (SSA) from 440 nm (leftmost boxplot) to 1020 nm (rightmost boxplot) with counts (Jan: 6, Feb: 31, Mar: 62, Apr: 50, May: 29, Jun: 8, Aug: 3, Sep: 5, Oct: 17, Dec: 3), (e) asymmetry factor (AF~~),~~) from 440 nm (leftmost boxplot) to 1020 nm (rightmost boxplot) with the same counts as EAE, (f) real and (g) imaginary refractive index (RI) values (440 nm~~),~~) with the same counts as SSA, and (h) refractive index ratios (where the blue line is the ratio of RI at 440 nm and ~~675~~670 nm, the red line is the ratio of RI at 440 nm and the average RI for the ~~670~~675–1020 nm wavelengths, and the broken lines are the imaginary refractive index ratios) for Metro Manila, Philippines based on data between January 2009 and October 2018.

There is a notable dip in the monthly median AERONET AOD over Manila Observatory from the peak in October to the lowest monthly median AOD (0.11) in November~~,~~ (Fig. 3a), just slightly above defined background levels (<0.1) (Holben et al., 2001), when the windspeeds were picking up and were coming from the east to northeast directions (Fig. 2k) in the direction of the Philippine Sea and the West Pacific Ocean. ~~This dip was also observed in the regional~~

~~AOD data (MISR and MERRA-2, Fig. 4).~~ This dip was also observed in the regional (30° × 30°) AOD data (MISR and MERRA-2, Fig. 4). This is most probably due to the decrease in the AOD contribution from fine (radii <0.7 μm) and spherical particles based on size speciated MISR AOD (Fig. S1). Larger and non-spherical particle contributions to AOD increase in November in the Southeast Asia region. The MERRA-2 AOD is relatively higher than the MISR AOD probably due to assimilation of MODIS data into MERRA-2. Studies in Asia (Xiao et al., 2009; Qi et al., 2013; Choi et al., 2019) have observed relatively higher MODIS AOD compared to MISR AOD.

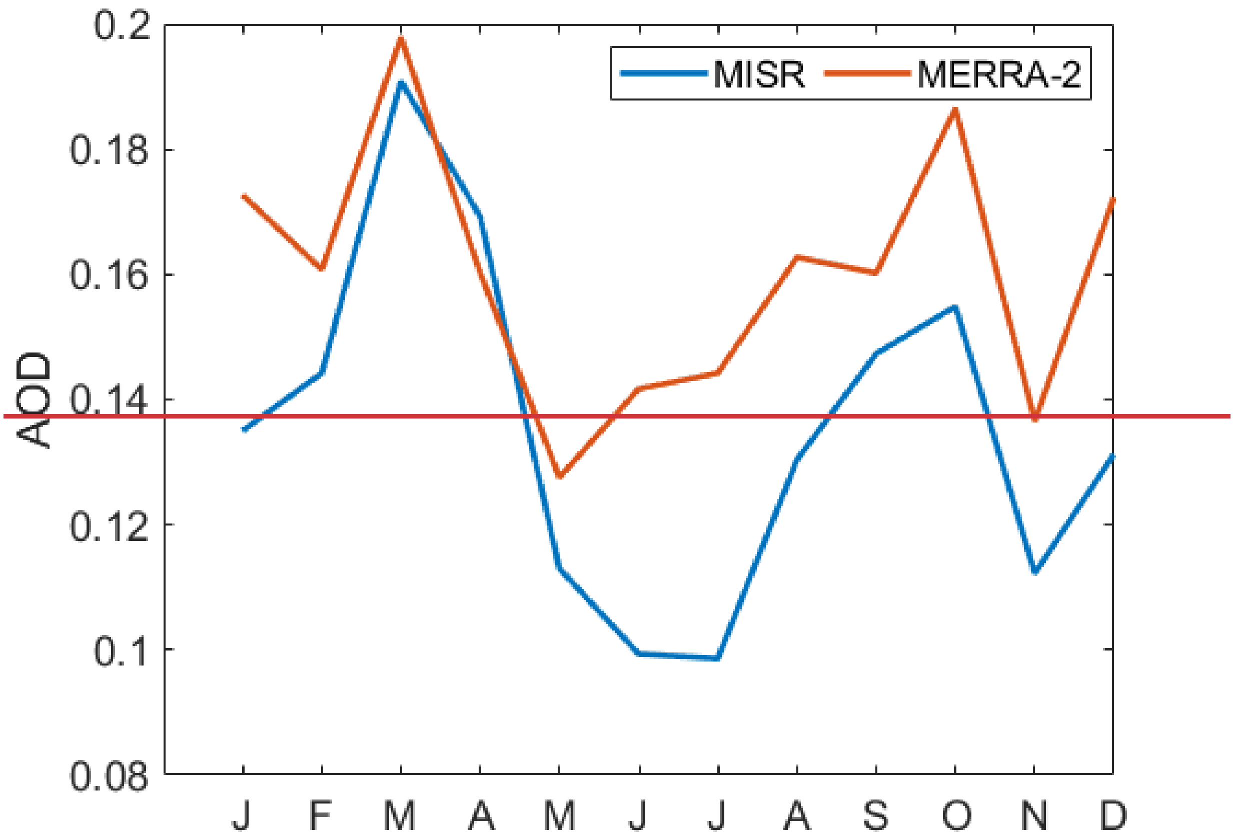

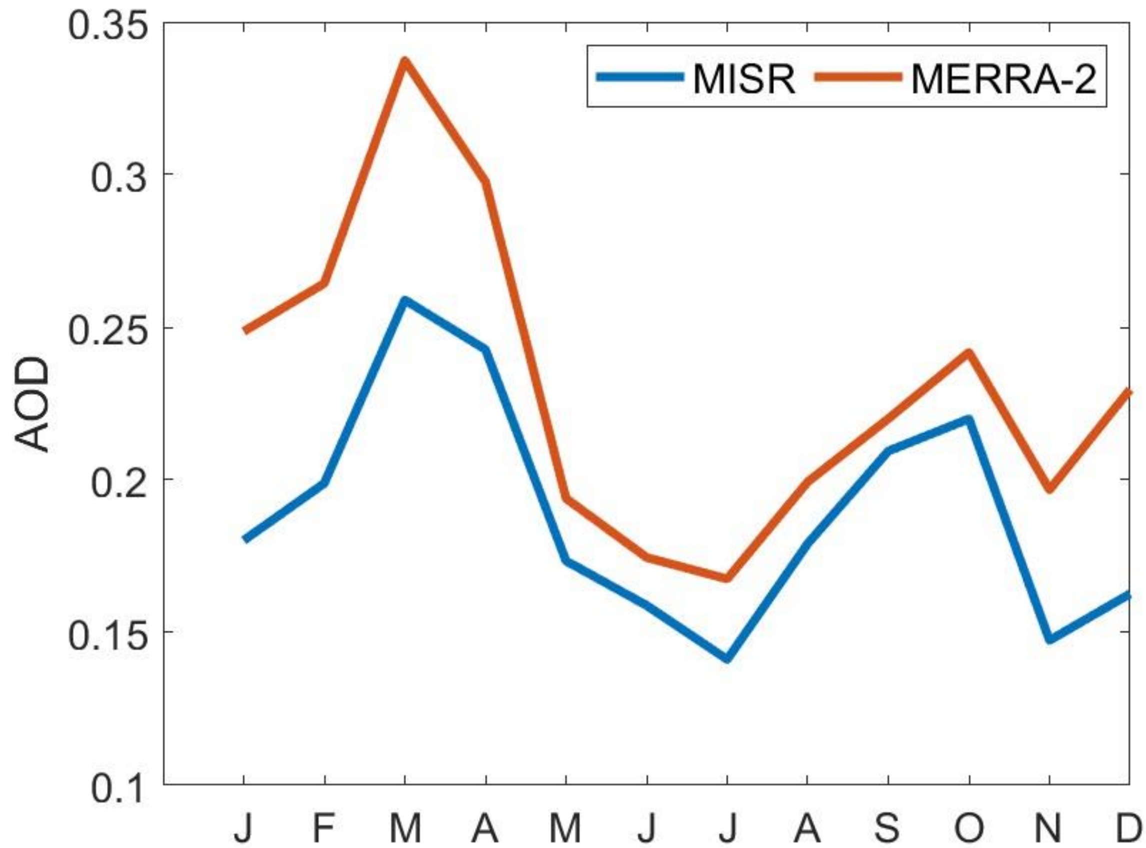

Figure 4: Monthly ~~median~~mean AOD (550 nm) in Southeast Asia (30° × 30°) from 2009 to 2018 from MISR (blue line) and MERRA-2 (red line).

There were 338 instances (~1.2 % of the time based on the total number of 28,538 valid AERONET AOD data points) of AOD values exceeding 1, indicative of heavy aerosol particle loading (Huang et al., 2021). Because AOD is extrinsic (it depends on mass), AOD describes total aerosol particle loading and we examine other aerosol particle parameters from AERONET to make more informed inferences about size and composition.

3.2.2 Extinction Angstrom Exponent and Fine Mode Fraction

The extinction angstrom exponent (EAE) relates the extinction of light at specific wavelengths and is indicative of aerosol particle size (Ångström, 1929). ~~The EAE is usually greater for smaller particles (~4 for very small particles that undergo Rayleigh scattering and 0 for particles as large as cloud drops) (Bergstrom et al., 2007), except for when the coarse mode has a large impact on the angstrom exponent (Schuster et al., 2006).~~The EAE is usually greater for smaller particles (~4 for very small particles that undergo Rayleigh scattering, > 2 for small particles, < 1 for large particles like sea salt and dust, and 0 for particles as large as cloud drops) (Schuster et al., 2006; Bergstrom et al., 2007). The highest monthly median EAE (Fig. 3b) from 2009 to 2018 over the Manila Observatory was observed from July (~1.4) to September (~1.3), during the southwest monsoon. This period is associated with the biomass burning southwest of the

Philippines (Oanh et al., 2018; Stahl et al., 2021; Crosbie et al., 2022). The median (per month) EAE ranged from ~0.9 in November to ~1.4 in August, a range which is within the values from previous studies collected from mixed sites and urban/industrial areas with both fine and coarse particles (Eck et al., 2005; Giles et al., 2012). The high EAE over Manila Observatory from July to September is probably regional in nature based on the MISR data showing increased EAE with increased AOD from fine, spherical, and absorptive particles (Fig. S1) in Southeast Asia during the same months.

EAE increases with AOD (Fig. ~~S1~~S2), which means that the greater particle loading is contributed by smaller particles (Smirnov et al., 2002). Of the high loading cases (AOD >1~~),~~) over Manila Observatory, the EAE values ~~ranged from~~were mostly greater than 0.~~6 to 1.6,~~8 indicating fine mode particles (Che et al., 2015). The EAE values in August were the highest compared to other months including having the highest minimum value of any month (0.71) (Fig. ~~S1~~S2), due to smaller particles (~EAE >1 for fine particles, Table 2). The lowest EAE values (0.08) and thus the largest particles were observed in December~~.~~, which again may be regional in nature with MISR EAE also lowest during this time with increased AOD from larger and non-spherical particles (Fig. S1).

The fine mode fraction (FMF) describes the prevalence of fine mode particles in the column of air above the surface. The fine mode fraction (Fig. 3c) from 2009 to 2018 was highest in August (monthly median of 0.75) and lowest in November (monthly median of 0.45). This is consistent with the EAE values discussed earlier with the prevalence of smaller particles in August and larger particles in November. In August (Fig. 2h) the southwest monsoon is known to coincide with ~~transported~~the transporting of fine smoke particles to Luzon. In November (Fig. 2k), the prevalent winds may have already shifted to easterly (Matsumoto et al., 2020) implying more marine-related sources associated with coarser particles.

3.2.3 Single Scattering Albedo

The single scattering albedo (SSA) is the most important aerosol particle parameter determining whether aerosol particles will have a warming or cooling effect (Reid et al., 1998). SSA is the ratio of the scattering coefficient to the total extinction (scattering and absorption) coefficient (Bohren and Clothiaux, 2006) of aerosol particles. Higher SSAs are related to more reflective aerosol particles while more absorbing aerosol particles will have lower SSA values; values range from 1 (reflective) to 0 (absorbing). Monthly median SSA values were largest in June (0.94~~,~~ at 440 nm), suggesting the presence of more reflective aerosol particles, and smallest in August (0.~~78,~~88 at 440 nm and 0.78 at 1020 nm) suggesting more absorptive particles that are similar in range to the SSA of biomass burning particles (Table 2). August is when biomass burning is prevalent to the southwest of the Philippines and associated with soot particles that are absorptive.

The sensitivity of SSA to different wavelengths depends on the type of aerosol particles present. More specifically, aerosol particle size and refractive index (which is related to aerosol particle composition) both affect the SSA (Dubovik and King, 2000; Bergstrom et al., 2007; Moosmüller and Sorensen, 2018). For dust-type particles, SSA increases with wavelength because of lower dust absorption in the higher visible to infrared wavelengths (Dubovik et al., 2002), while for urban particles (including black carbon), which absorb light at longer wavelengths, SSA decreases with wavelength (Reid et al., 1998; Bergstrom et al., 2002). The presence of organic carbon may affect this spectral dependence; however, because organic particles absorb in the UV, this lowers SSA at wavelengths shorter than 440 nm (Kirchstetter et al., 2004). Monthly median SSA generally decreased with increasing wavelength for all months with available data (Fig. 3d) presumably due to the influence of more urban particles in contrast to dust. Noteworthy though are the monsoon transition months of April, September, and October (Fig. 3d), which had increased SSA from 440 nm to 670 nm, possibly from organics along with black carbon due to transported smoke. The back-trajectories for these months (Figs. 2d, 2i, and 2j) suggest sources from the northeast that are closer to Luzon during these months compared to other months. This indicates the possibility of more local sources. Increasing the certainty of sources associated with aerosol particles necessitates looking at other available aerosol particle parameters, discussed subsequently.

3.2.4 Asymmetry Factor

The asymmetry factor quantifies the direction of scattering of light due to aerosol particles, with values ranging from -1 (back scatter) to 0 (uniform scattering) to 1 (forward scatter). It is important in modeling climate forcing because it affects the vertical distribution of the radiation in the atmosphere (Kudo et al., 2016; Zhao et al., 2018). The asymmetry factor is dependent on particle size, shape, and composition and the value of 0.7 is used in radiative models (Pandolfi et al., 2018).

Lower asymmetry factors are related to smaller particles (at constant AOD) (Bi et al., 2014). Measured values due to biomass burning, for example, are 0.54 (550 nm) in Brazil (Ross et al., 1998) and 0.45 – 0.53 (550 nm and including dust) over central India (Jose et al., 2016). There have been relatively higher values observed in western, central, and eastern Europe (0.57 – 0.61 at 520 – 550 nm) (Pandolfi et al., 2018) and the U.S. East Coast (0.7 at 550 nm) (Hartley and Hobbs, 2001). In Norway, the asymmetry factor for background summer conditions was 0.62 and was higher in the springtime at 0.81 (862 nm) during Arctic haze events (Herber et al., 2002). Highest values are associated with dust such as those measured in the Sahara being 0.72 – 0.73 (500 nm) (Formenti et al., 2000). Over Metro Manila, the asymmetry factors from the AERONET data at the 675, 870, and 1020 nm were similar across months (Fig. 3e). The monthly median asymmetry factors at 440 nm ranged from 0.70 (April and May) to 0.74 (October), while for 670, 870, and 1020 nm the monthly median asymmetry factors were smaller and ranged from 0.62 – 0.69. These values were closely related to those observed over the U.S. East Coast as mentioned earlier, perhaps due to the proximity of the location to the coast (10 km east of Manila Bay and 100 km west of the Philippine Sea) as well as its location in Manila, which is a large local source due mostly to vehicles (Cruz et al., 2019).

The monthly median asymmetry factor in Metro Manila was greatest towards the end of the year (October to December) for all the wavelengths, suggesting larger particles when winds (Figs. 2j to 2l) come from the Philippine Sea in the northeast. It was in March and April that the monthly median asymmetry factor was minimal for 440 nm and in August for 670, 870, and 1020 nm. These were the times when ~~the~~ aerosol particles were smallest. March to April represents the driest time of the year in Manila (Fig. 1b and 1h) perhaps preventing particle growth and where the local sources may be dominating, even as back-trajectories (Fig. 2c and 2d) extend all the way from the Philippine Sea to the east. This is corroborated by results from other studies showing that the asymmetry factor seems to be enhanced by relative humidity (Zhao et al., 2018). The unexpected low asymmetry factor values in August, however, are probably because of the source of the particles. August had the highest relative humidity and precipitable water (Fig. 1b and 1h) but is also when the back-trajectories (Fig. 2h) were from the southwest, possibly affected by the Indonesia fires, which could have transported more non-hygroscopic fine particles.

Fine particles have been observed to exhibit decreasing asymmetry factors with increasing wavelength (Bergstrom et al., 2003). This trend is observed in all the months for the monthly median asymmetry factors (Fig. 3e) suggesting the predominance of smaller aerosol particles. The greatest decrease in the asymmetry factor (all wavelengths) was in August, consistent with the lowest observed values of the year (670, 870, and 1020 nm). Transported biomass burning particles are the probable dominant particles during this time. They are usually composed of hygroscopic inorganics, non-hygroscopic soot, and relative non-hygroscopic organic fractions (Petters et al., 2009). Knowing the composition of biomass burning particles over the study region will help in the understanding of hygroscopicity and its impacts on radiation.

3.2.5 Refractive Index

Refractive index is an intrinsic parameter as it does not depend on the mass or the size of particles, and thus can be used to infer aerosol particle composition (Schuster et al., 2016). For the case of the AERONET data, which include refractive index values that are insensitive to coarse particles (Sinyuk et al., 2020), the focus of the discussion will be for fine mode particles and may be limited when coarse particles are involved. Refractive index measurements are complex since they include real and imaginary parts related to light scattering and absorption, respectively. All aerosol particles scatter light but only certain types absorb light significantly. The most prominent particle absorbers in the atmosphere are soot carbon, brown carbon (organic carbon that absorbs light), and free iron from dust (hematite and goethite in the ultraviolet to mid-visible) (Schuster et al., 2016). ~~For this study, we examine refractive index values at 440 nm wavelength because this is the wavelength used to calculate SSA (Andrews et al., 2017).~~For this study, we examine refractive index values at 440 nm wavelength. Pure sources of soot carbon have the highest real refractive index values (~1.85) as well as the highest imaginary refractive index (~0.71), both independent of wavelength (Koven and Fung, 2006; Van Beelen et al., 2014). Brown carbon and dust have relatively lower real refractive index values at 440 nm (~1.57 and ~1.54) and imaginary refractive index values (~0.063 and ~0.008) that decrease with increasing wavelength (Xie et al., 2017).

In this study the range of the monthly median real refractive index values (440 nm) was from 1.33 (December and January) to 1.43 (March) (Fig. 3f). Water uptake by aerosol particles decreases the real refractive index values (Xie et al., 2017) and thus the lowered real refractive indices over the Manila Observatory can be due to the presence of more water in the atmosphere in general and/or the increased presence of more hygroscopic particles. December and January are not necessarily the months that have the highest moisture content, but they are months when back-trajectories reaching the column over the Manila Observatory are from the Philippine Sea to the northeast presumably transporting hygroscopic particles. As reported in previous sections, relatively larger particles are observed around this time of the year and thus sea salt can be an important contributor. The greatest change in the monthly median real refractive index with increasing wavelength also was observed in December (Fig. 3h), possibly due the increased fractional contribution of constituents other than soot carbon (because the real refractive index of soot carbon is invariant with wavelength). Noteworthy as well is the month of August (Fig. 3f), which has the smallest range of real refractive index values, possibly indicating a more homogenous aerosol particle source compared to other months. August is the month with the highest relative humidity (Fig. 1b) as well as highest precipitable water (Fig. 1h), while this is also the month when long-range biomass burning emissions are observed to be highest, and when the real refractive index values would otherwise be expected to be highest.

Water content seems to play a significant role in the real refractive index values in Manila. March, when the monthly median real refractive index values are highest (Fig. 3f), is when precipitable water vapor (Fig. 1h) is among the lowest in the year. The months around March are also when maximum real refractive indices (1.57 in February, 1.59 in March, and 1.60 in April) were observed (Fig. 3f). March was when there was a relatively small change in real refractive index value with wavelength perhaps related to greater soot carbon fractions during this time, due possibly to the contribution of biomass burning from Peninsular Southeast Asia (Shen et al., 2014). Looking more closely at the imaginary refractive index values will help elucidate this issue.

Monthly median imaginary refractive index values (440 nm) ranged from 0.007 in June to 0.015 in September and December (Fig. 3g). These are low compared to those of the pure soot carbon mentioned earlier because of the mixed nature of the sampling site with contributions from brown carbon and dust. The highest imaginary refractive index values in September and December suggest the greatest fractional contribution of soot because the highest imaginary refractive index values are associated with soot. These are also similar in magnitude to biomass burning particles in the Amazon (0.013) (Guyon et al., 2003). The key distinction between soot carbon and other major absorbers (brown carbon and dust) is that its imaginary refractive index is invariant with wavelength. Both brown carbon and dust exhibit a decrease in the imaginary refractive index with increasing wavelength (Xie et al., 2017). The ratios of imaginary refractive index values (440 nm to average of 670–1020 nm) (Fig. 3h) show a relative invariance with wavelength (ranging from 0.88 to 1.4), which indicates the dominance of soot as the major absorber in the region (Eck et al., 2003). While observed wavelength invariance points to high soot contributions, the size of the particles can help distinguish between brown carbon, which reside mainly in the fine mode, and dust sources, which yield more coarse particles (Schuster et al., 2016). September is during the southwest monsoon, which is when, as noted in the earlier sections, fine particles were most prevalent. This is also the time when the imaginary refractive index varied most with wavelength (1.4 ratio of the imaginary refractive index at 440 nm and the imaginary refractive index average for 670 nm to 1020 nm in Fig. 3h) possibly with greater absolute contributions from brown carbon, even with the highest soot carbon fractional contributions. Brown carbon has been observed both from primary and aged aerosol particle emissions from biomass burning (Saleh et al., 2013). As noted earlier, December also had the highest imaginary refractive index values as well as relatively coarser particles, possibly due to larger dust absolute contributions even with the highest soot carbon fraction contributions. The lowest monthly median imaginary refractive index values in June, on the other hand, when fine mode particles prevail suggest highest fractional contributions of brown carbon relative to other months (Fig. 3h).

3.2.6 Volume Size Distributions

The volume size distribution (VSD) is another way to be able to more deeply characterize aerosol particles, specifically related to their effect on climate, weather, and clouds (Haywood and Boucher, 2000; Feingold, 2003). In the Manila Observatory dataset, there was a bi-modal VSD for the entire dataset (Fig. 5a). The fine mode median values peaked in the accumulation mode at 0.148 μm particle radius while the coarse mode median values peaked at 3.857 μm. (Fig. 5a and Table S1). The median coarse mode amplitudes and volume concentrations were higher than the fine mode amplitudes and volume concentrations for most of the year (DJF, MAM, and SON, Fig. 5b and Table S1), except during the southwest monsoon (JJA) when the fine mode amplitude and volume concentration was higher. This is consistent with observations earlier of fine mode prevalence during the southwest monsoon. Median VSD amplitudes (Fig. 5c) were greater in the afternoon, with higher peaks and volume concentrations for both the fine and coarse modes, compared to the morning. There was a slightly larger coarse median amplitude and volume concentration, compared to the accumulation mode median amplitude and volume concentration, for both the morning and afternoon size distributions. While the VSDs confirm several observations based on the analysis of the aerosol particle parameters presented earlier, not much further information is gained especially regarding chemical composition. Size distributions are a result of contributions from multiple sources, and thus being able to discriminate the sources based on their characteristic size distributions will help identify relevant sources.

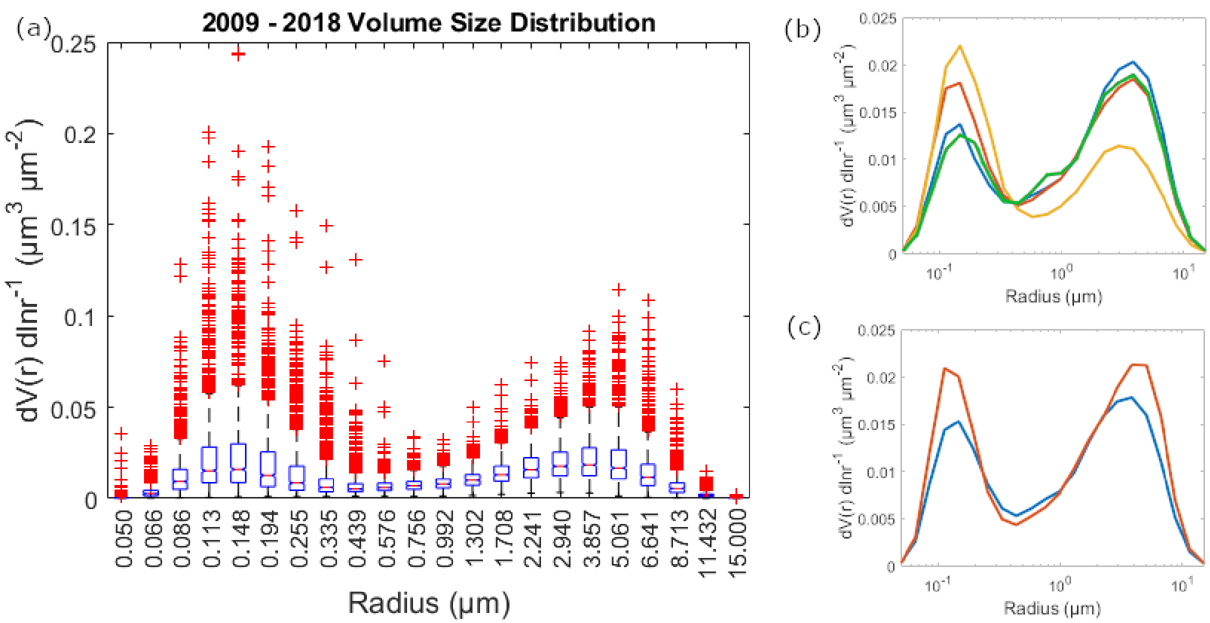

Figure 5: (a) VSD results derived from AERONET measurements at Metro Manila between January 2009 and October 2018. Median VSDs over the study period based on (b) season (blue: DJF, red: MAM, orange: JJA, green: SON) and (c) time of day (blue: AM, red: PM).

3.3 Clusters

3.3.1 VSD Cluster Profiles

Five clusters were identified to best represent the VSD (Fig. 6a). The average of the VSDs in each cluster varied depending on the height of the peaks in the accumulation mode and the coarse mode. In Metro Manila, the accumulation mode is associated with aged aerosol particles and combustion (Cruz et al., 2019). The majority of the data (830 count out of 1419 total VSD profiles) were clustered together in a profile (cluster 1) that had relatively low average magnitudes of volume concentration for both the accumulation (0.01 $\mu m^3\ \mu m^{-2}$) and coarse (0.02 $\mu m^3\ \mu m^{-2}$) modes, with the volume concentration magnitude of the coarse mode peak slightly higher than the volume concentration magnitude of the accumulation mode peak. The next prevalent cluster profile (284 counts, cluster 2) had an average fine mode peak for the volume concentration (0.04 $\mu m^3\ \mu m^{-2}$) which was more than twice as much than the previous profile but with a similar coarse mode peak for the volume concentration (0.02 $\mu m^3\ \mu m^{-2}$). The average coarse mode peak for the volume concentration (0.04 $\mu m^3\ \mu m^{-2}$) was the highest (compared to the four other cluster profiles) for the third prevalent cluster profile (166 counts, cluster 3); cluster 3 ~~was~~ also had a slightly shifted volume concentration peak in the coarse mode to a higher radius (5.06 µm) compared to other clusters. The coarse mode dominated this VSD compared to other profiles (lower magnitude for the accumulation mode peak for the volume concentration, 0.02 $\mu m^3\ \mu m^{-2}$). The two remaining cluster profiles exhibited high average magnitudes of volume concentration in both the accumulation and coarse modes. The fourth prevalent cluster profile (74 counts, cluster 4) had the highest average absolute magnitude for the volume concentration in the accumulation mode (0.11 $\mu m^3\ \mu m^{-2}$), while the fifth prevalent cluster profile (65 counts, cluster 5) had a slightly smaller accumulation mode peak for the volume concentration (0.07 $\mu m^3\ \mu m^{-2}$) that was shifted to a slightly higher radius (0.19 µm compared to 0.15 µm). Both clusters 4 and 5 had similar average coarse mode peak volume concentration magnitudes (0.04 $\mu m^3\ \mu m^{-2}$).

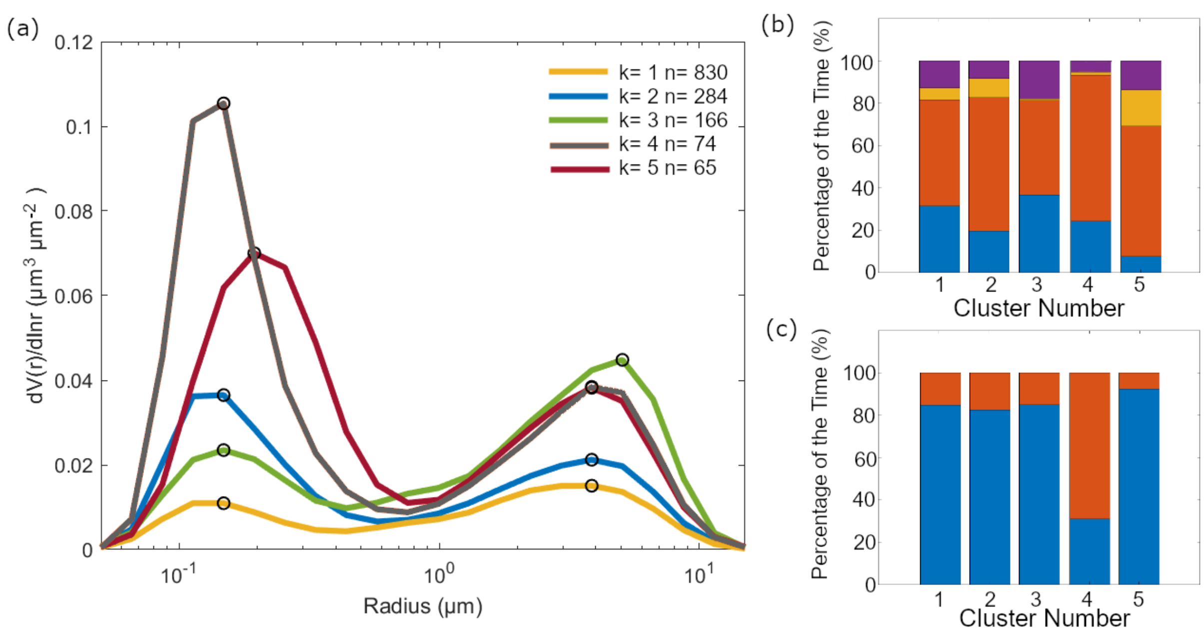

Figure 6: (a) Cluster analysis of VSD data yielding five characteristic and averaged VSDs with the number of points per cluster shown in the legend. The black circles on the curves show the peak locations in the submicrometer (<1 µm) and coarse (≥1 µm) modes. The relative abundance of each cluster is shown for different (b) seasons (blue: DJF, red: MAM, orange: JJA, violet: SON) and (c) times of day (blue: AM, red: PM).

The clusters were distributed across seasons (Fig. 6b), with clusters 1 and 2 being the most evenly distributed among the clusters. Cluster 3, which had the highest coarse mode peak, had the greatest contribution from September to November compared to other clusters. Cluster 4, which had the highest accumulated mode peak compared to other clusters, had the greatest contribution from March to May as well as to afternoon VSDs compared to other clusters (Fig. 6b and 6c). Relative contributions of VSDs from June to August were highest for cluster 5, which had the shifted accumulated mode peak.

Median total (AERONET) AOD values (Fig. 7b) were lowest (0.12) for cluster 1, though it had the second highest sea salt fractional contributions (31%) (Fig. 7a) to total AOD (MERRA-2) ~~(31%)~~ among all the clusters. Cluster 2 had relatively mid-range median total AOD values (0.27) that, along with clusters 4 and 5, were dominated by sulfate and organic carbon (46% and 20%). Cluster 3 had similar, but slightly lower median total AOD (0.25) compared to cluster 2. Cluster 3 was distinct because it had the largest total (0.04) and fractional contribution (37%) from sea salt among all clusters. Clusters 4 and 5 had the highest median total AOD values (0.47 and 0.56), with cluster 5 having the highest absolute and fractional sulfate contributions (0.14 and 64%) among the clusters. Integrating the above results with their corresponding aerosol particle properties can help associate the clusters to air masses.

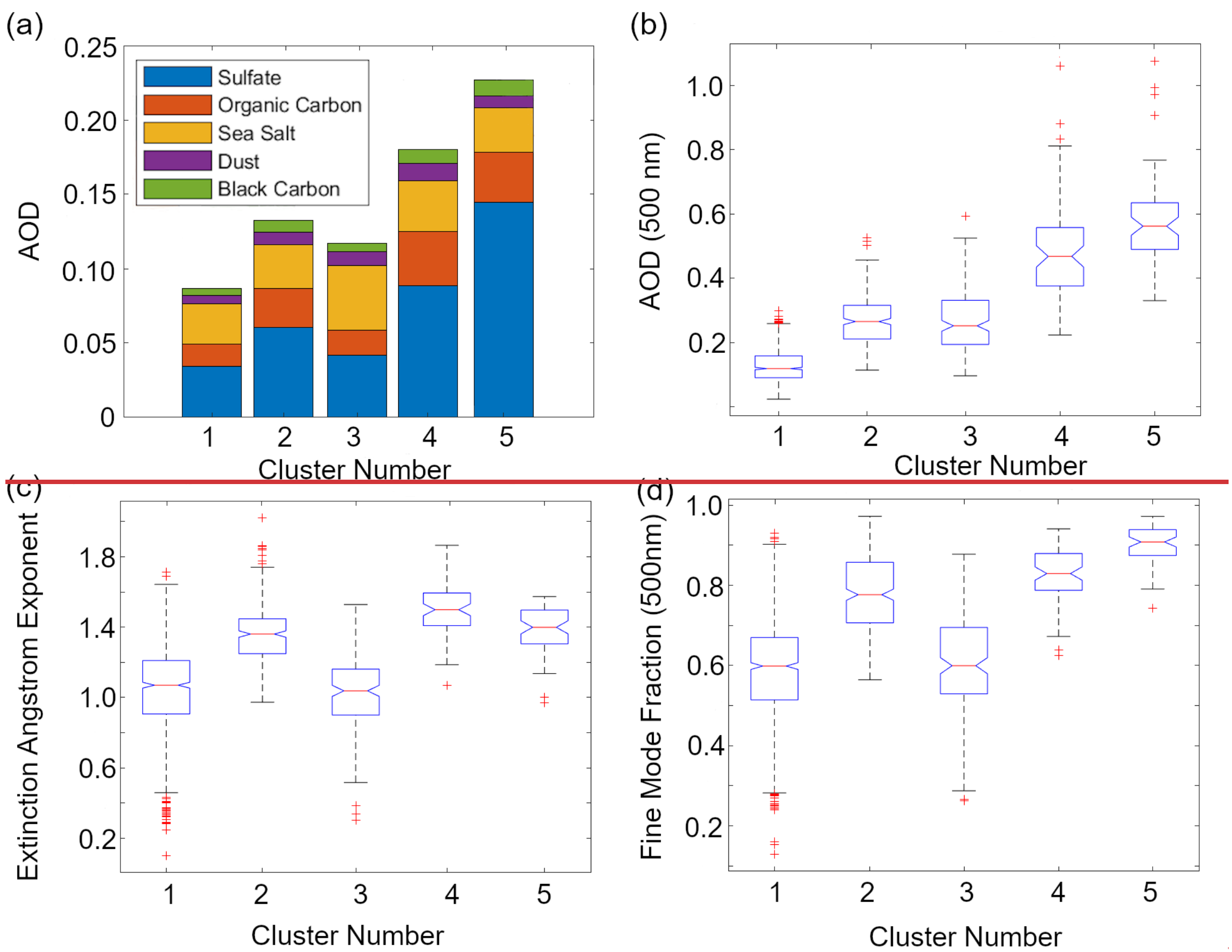

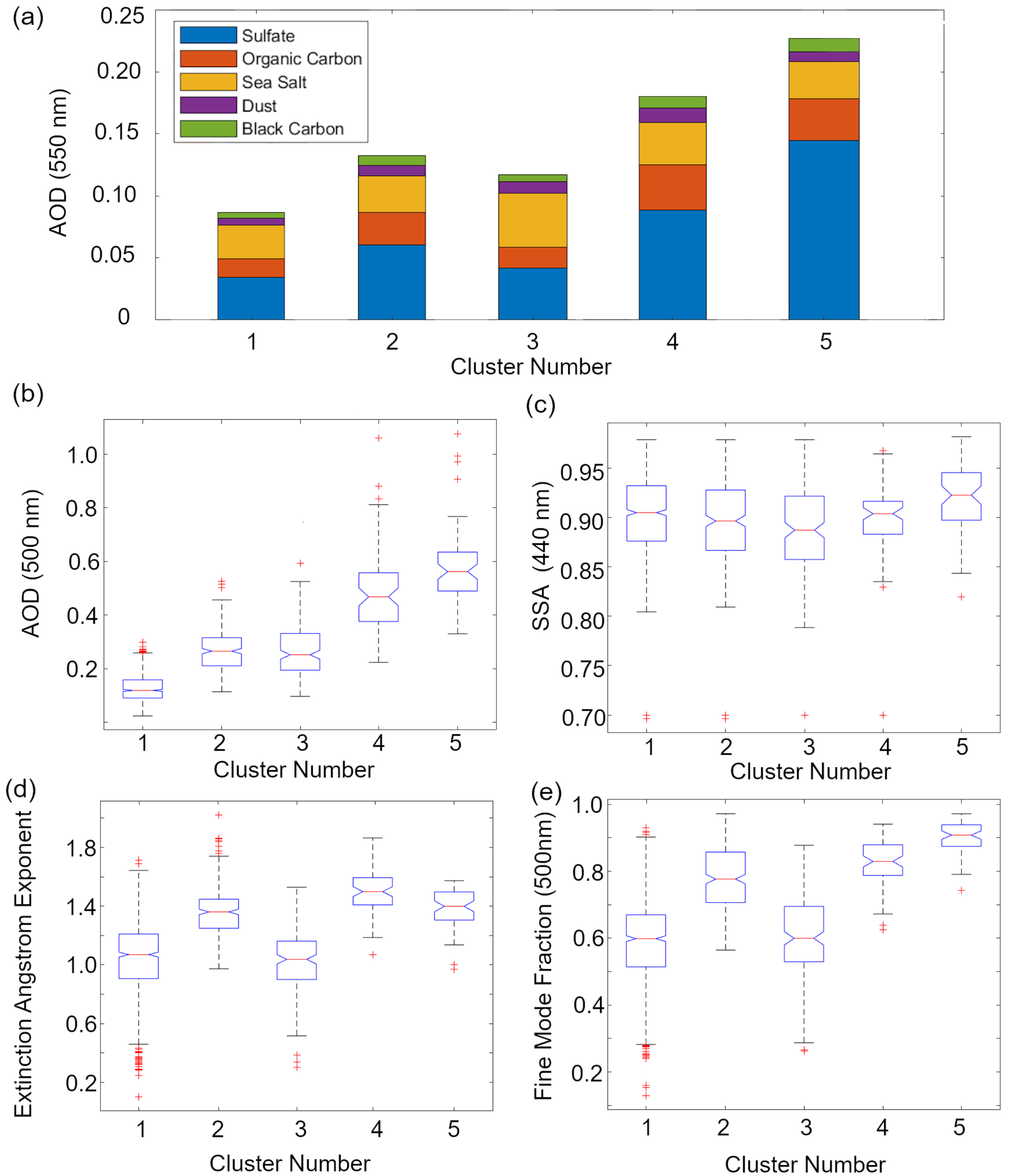

Figure 7: (a) Average compositional contributions to aerosol optical depth (AOD at 550 nm) from MERRA-2 per identified cluster~~.~~ (counts per cluster from 1 to 5: 830, 284, 166, 74, 65). Boxplots of AERONET (b) total AOD (500 nm), (c) single scattering albedo (SSA at 440 nm), (d) extinction angstrom exponent (EAE~~,~~ at 440 nm – 870 nm total), and (~~d~~e) fine mode fraction (FMF~~,~~ at 500 nm) per cluster.

3.3.2 Air Mass Types

Air masses have been classified in previous studies based on their AOD, EAE, FMF, and ~~FMF~~SSA values (e.g., Lee et al., 2010 and Aldhaif et al~~,~~., 2021). The criteria from different studies (Table 2) were applied per cluster. Median total AOD of cluster 1 (0.12) was less than 0.2 (Fig. 7b), which is the threshold for sea salt sources ~~(Kaskaoutis et al., 2007)~~(Kaskaoutis et al., 2009; Kaskaoutis et al., 2007). Half of the data points in cluster 1 also fall below the threshold for clean environments (AOD < 0.1) (Sorooshian et al., 2013). Based on its median ~~FMF (0.60) and~~ EAE (1.07, where EAE < 1 is coarse and EAE >1 is fine) and FMF (0.60) values (Fig. ~~7c~~7d and ~~7d~~7e), cluster 1 is a mixture of fine and coarse particles. The fine Cluster 1 is the only cluster with a median that meets that threshold value for clean marine sources (AOD < 0.2), and we know from Sect. 3.3.1 that its average VSD magnitude was greater for the coarse fraction and that its sea salt contribution to total AOD was second greatest among the clusters. Thus, ~~we can say that~~ most probably, cluster 1 is a background clean marine source, since it also is predominant throughout the seasons (Fig. 6b). This makes sense given the proximity of the ocean to Metro Manila from both the east and the west. The median SSA (0.90 at 440 nm) for cluster 1 (Fig. 7c), however, suggests the presence of absorbing particles most probably due to high black carbon in the local source (Cruz et al., 2019) that is mixed in with this generally clean marine source.

Most of the data from the other clusters all fall in the polluted category (Table 2), based on their median total AODs (>0.1) (Fig. 7b). Cluster 2 has a median FMF value of 0.78 (Fig. ~~7c~~7e), which suggests that most of the particles in this air mass are in the fine fraction. They are, however, not sufficiently dominant in the aerosol for them to be typical of urban/industrial sources. The average VSDs (Fig. 6a) of cluster 2 similarly suggest that their relative accumulation mode magnitude is higher than the coarse magnitude, but not much higher. Like cluster 1, cluster 2 is also more evenly distributed across the seasons (Fig. 6b~~)~~). The median SSA for cluster 2 (0.90 at 440 nm) is also similar to the SSA of cluster 1 (Fig. 7c) where the local and background particles are mixed. Cluster 2 could be a fine polluted background source superimposed on the dominant marine source. Metro Manila is a megacity with continuous and large amounts of sources that could be, due to its proximity to the ocean, interacting with the background.

Based on its median EAE value (1.04) (Fig. 7d), cluster 3 is mixed but mostly in the coarse fraction, consistent with its VSD profile (Fig. 6a) which has the highest coarse magnitude (FMF = 0.60) compared to the other clusters. The contribution of data from September to February is greatest in cluster 3, consistent with expected coarser particles during this period when the winds are initially shifting from the southwest before becoming more northeasterly, as previously noted. ~~This air mass can be a mixed polluted air mass, which is possibly transported due to the large sea salt contribution to total AOD (Sect. 3.3.1).~~Median SSA (0.89 at 440 nm) was lowest for cluster 3 (Fig. 7c), this and the relatively high coarse particle contribution suggests cluster 3 as a possible dust source based on past studies (Lee et al., 2010). This air mass can be a mixture of local sources and transported dust air masses, the large sea salt contribution (~37%) to total AOD (Sect. 3.3.1) can be related to long-range transport.

Both clusters 4 and 5 have median total FMF (0.83 and 0.91) (Fig. ~~7c~~7e) values exceeding the mark (> 0.8, Table 2) for urban/industrial air masses. Combining this and results from the previous sections confirms that cluster 4 can be an urban/industrial source given that it had the highest median accumulated mode peak and organic carbon contribution (~20%) to total AOD among the clusters. The median SSA for cluster 4 (0.90 at 440 nm) was similar to the median SSA of clusters 1 and 2 (Fig. 7c), but the maximum SSA value for this cluster was lowest in general among all the clusters suggesting cluster 4 has the net most absorptive effect. The cluster 4 air mass is probably from local sources and transported biomass burning emissions. The high median EAE (1.40, Fig. 7d) may be associated with aerosol particles due to biomass burning (Deep et al., 2021).

Cluster 5 had the highest median total AOD (0.56) and FMF (0.91) values (Fig. ~~7e~~7b and 7e). It also had the highest ~~(Fig. 7a)~~ sulfate contribution (~64%) to total AOD ~~as well as~~(Fig. 7a), the highest median SSA (0.92 at 440 nm, thus most reflective particles among the clusters) (Fig. 7c), and a shifted accumulation mode peak (Fig. 6a). These characteristics suggest that cluster 5 is a possible cloud processing air mass (Eck et al., 2012). The larger peak in the accumulation mode is possibly the cloud signature. Previous studies have attributed this larger mode to cloud processing due to the conversion of SO_2 to sulfate (Hoppel et al., 1994). Cloud processing is a major source of sulfate (Barth et al., 2000).

The distribution of the air masses based on the abundance of the VSD profiles per cluster suggest prevalent clean marine (58% of the total VSD counts) and background fine polluted (20%) air masses over Metro Manila. The mixed ~~polluted~~dust (12%), urban/industrial (5%), and cloud processing (5%) air masses contribute 22% ~~all together~~altogether. We can investigate more deeply and look at specific case studies that can better describe the air masses identified here.

3.4 Case Studies

Selected case studies are used to highlight periods with the highest AOD values and strongest clear sky (no rain and heavy clouds) daytime aerosol particle sources within the sampling period. As such, the clusters that are associated with the selected case studies are the clusters (3-5) with higher VSD concentration magnitudes.

3.4.1 Long Range Transport of Smoke

Both cases of long-range transport of smoke discussed below have similar VSDs (Fig. 8a and 9a) to the urban/industrial cluster VSD (cluster 4, Fig. 6a). Organic carbon was the dominant contributor to AOD (Fig. 8b and 9b) for both long-range transport cases. The first of two events occurred around 1 April 2020 with smoke presumed to come from East Asia. The VSD of this specific case (Fig. 8a) is most like the urban/industrial cluster (cluster 4 in 3.3.2, Fig. 6a) because of the high magnitude of its accumulated mode peak, its timing (April), and the enhanced organic carbon contribution to AOD in the area (Fig. 8b). Though the absolute black carbon contribution to AOD was highest here compared to the other case studies, and in general for the AERONET data, it was organic carbon that was more prevalent in terms of contribution to total AOD. Smoke is comprised of both soot carbon and organic carbon, amongst other constituents (Reid et al., 2005).

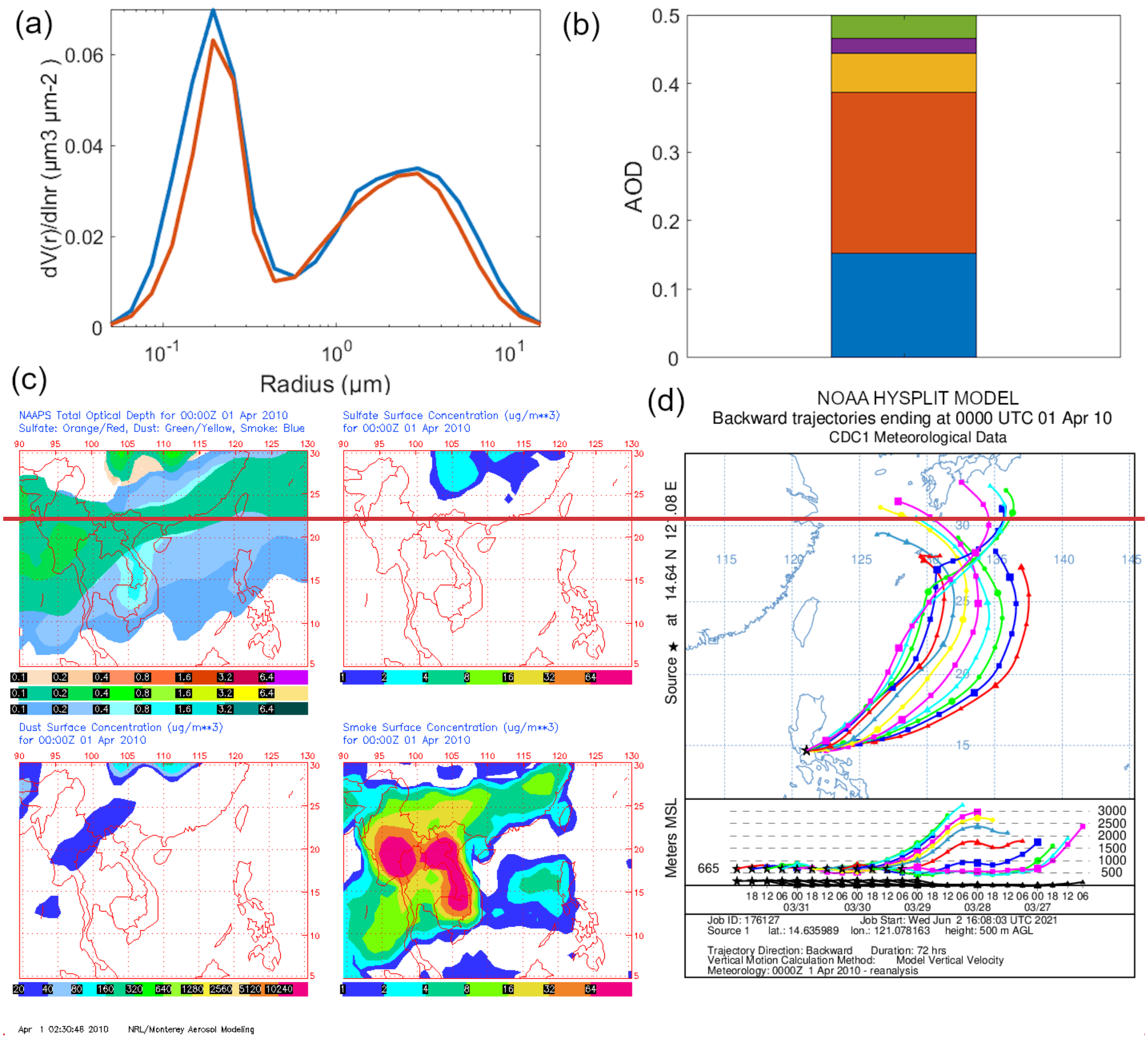

(a)
dV(r)/dlnr (μm3 μm-2)
Radius (μm)
(b)
AOD
(c)
NAAPS Total Optical Depth for 00:00Z 01 Apr 2010
Sulfate: Orange/Red, Dust: Green/Yellow, Smoke: Blue
Sulfate Surface Concentration (ug/m**3)
for 00:00Z 01 Apr 2010
Dust Surface Concentration (ug/m**3)
for 00:00Z 01 Apr 2010
Smoke Surface Concentration (ug/m**3)
for 00:00Z 01 Apr 2010
Apr 1 02:30:45 2010 NRL/Monterey Aerosol Modeling
(d)
NOAA HYSPLIT MODEL
Backward trajectories ending at 0000 UTC 01 Apr 10
CDC1 Meteorological Data
Source ★ at 14.64 N 121.08 E
Meters MSL
Job ID: 176127 Job Start: Wed Jun 2 16:08:03 UTC 2021
Source 1 lat.: 14.635989 lon.: 121.078163 height: 500 m AGL
Trajectory Direction: Backward Duration: 72 hrs
Vertical Motion Calculation Method: Model Vertical Velocity
Meteorology: 0000Z 1 Apr 2010 - reanalysis

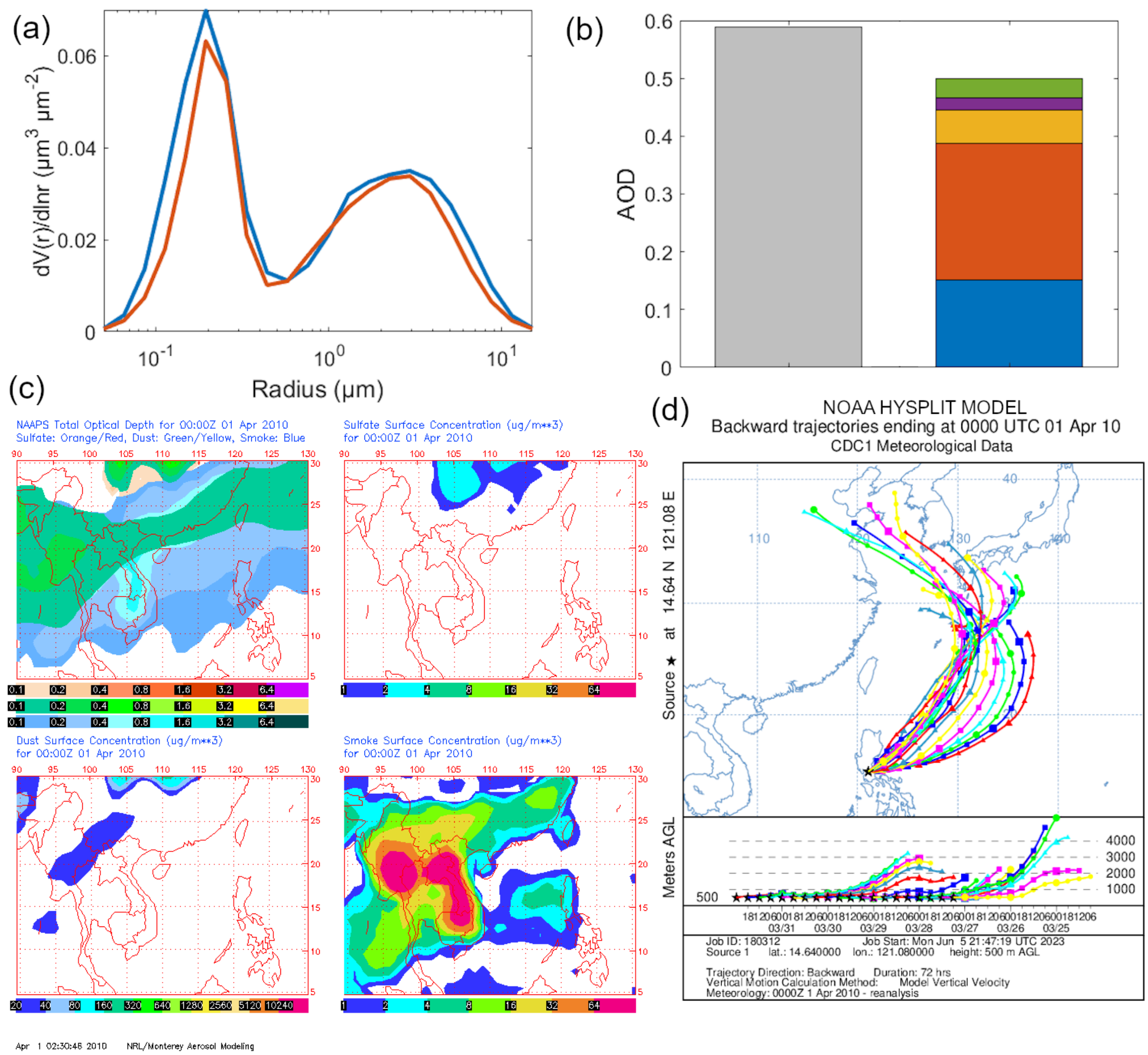

Figure 8: Case study of long-range transport (smoke – East Asia) around 1 April 2010. (a) AERONET VSDs at (blue) 00:01 and (red) 00:26 UTC, (b) AOD from AERONET (gray: median AOD at 500 nm) and MERRA-2 hourly (green: black carbon, violet: dust, yellow: sea salt, orange: organic carbon, blue: sulfate) compositional contributions to AOD (550 nm) closest in time to 00:01 UTC, (c) NAAPS maps of total and compositional hourly AOD (orange/red: sulfate, green/yellow: dust, blue: smoke) and sulfate, dust, and smoke surface concentrations at 00:00 UTC, and (d) HYSPLIT ~~three~~seven-day back-trajectories arriving at Manila Observatory at 00:00 UTC.

The smoke contribution to AOD from NAAPS (Fig. 8c) for the first smoke case was visible in the Philippines (0.2) and seemed to come from East Asia were the smoke contribution to AOD was greater (reaching 0.8) especially in Peninsular Southeast Asia. Smoke surface concentrations were also widespread (Fig. 8c) with greatest concentrations in East Asia that reached the Western Philippines, though seemingly disconnected over the sea. There were observed biomass burning emissions in the Peninsular Southeast Asia (southern China, Burma, and Thailand) at this time (Shen et al., 2014). The direction of the air mass coming into Metro Manila was from the northeast, which curved from the west in the direction of East Asia based on HYSPLIT back-trajectories (Fig. 8d).

The second smoke case was on 15 September 2009 with the source being Southeast Asia. The back-trajectories of this case study (Fig. 9d) are from the southwest of the Philippines, and in the direction of the Malaysia and Indonesia. NAAPS maps likewise show elevated AOD, specifically smoke contribution to AOD (Fig. 9c), as well as enhanced smoke surface contributions in the area around Metro Manila for this second smoke case study. The observed AOD and smoke surface concentration increased specifically from the southwest of the Philippines in the same direction of the back-trajectories. There were fires in the lowland (peat) forests of Borneo around this time (NASA, 2009). MERRA-2 AOD contributions for this case were greatest due to organic carbon as well as sulfate (Fig. 9b), and the absolute black carbon contributions were greatest compared to other cases. The VSD of this smoke case from Southeast Asia (Fig. 9a) resembled that from long-range transported smoke from East Asia (Fig. 8a) and the urban/industrial air mass (cluster 4, Fig. 6a). This case occurred in the afternoon, which was the prevalent time that the urban/industrial air mass was observed (Fig. 6c).

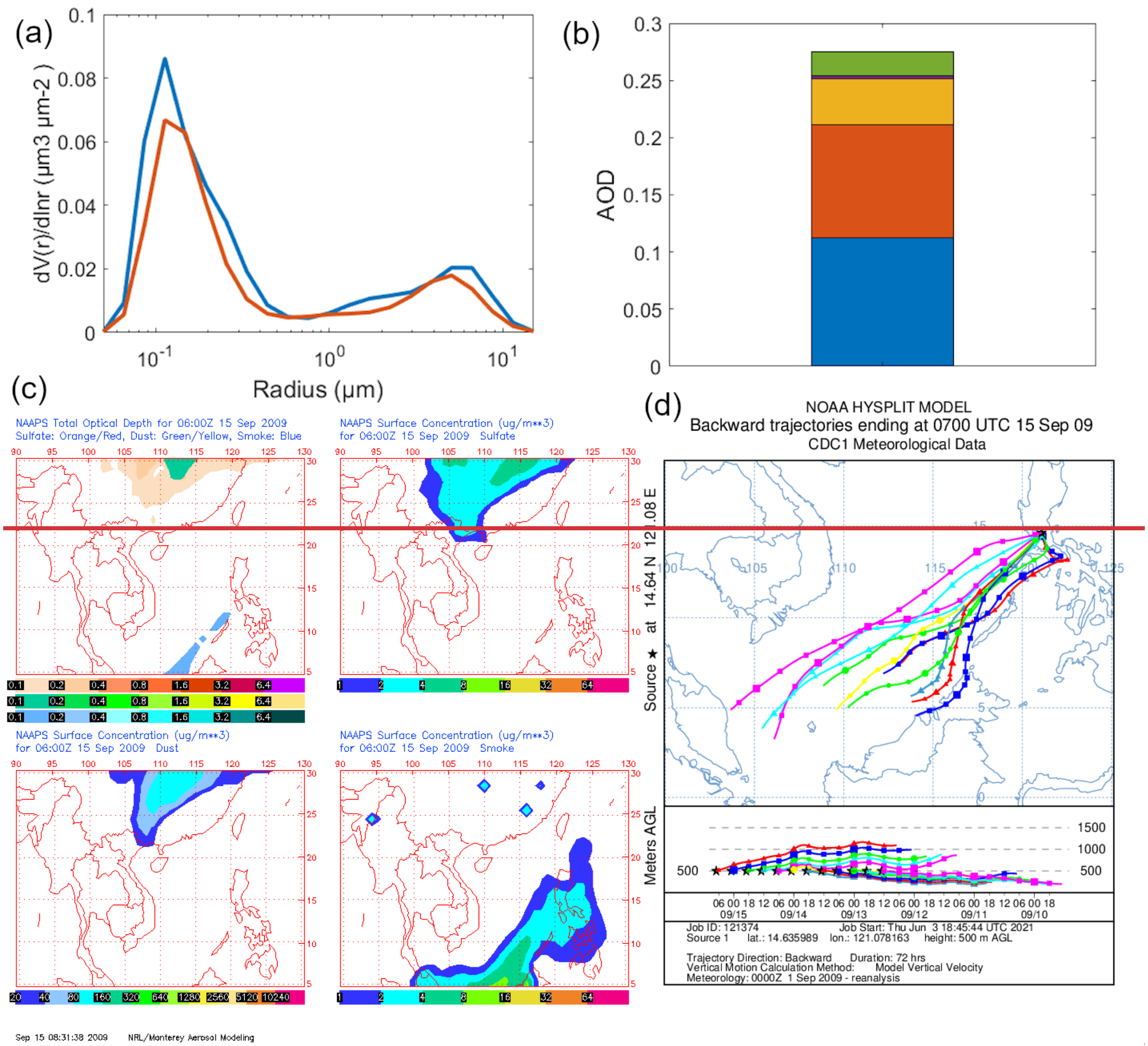
(a)
dV(r)/dlnr (μm3 μm-2)
Radius (μm)
(b)
AOD
(c)
NAAPS Total Optical Depth for 06:00Z 15 Sep 2009
Sulfate: Orange/Red, Dust: Green/Yellow, Smoke: Blue
NAAPS Surface Concentration (ug/m**3)
for 06:00Z 15 Sep 2009 Sulfate
NAAPS Surface Concentration (ug/m**3)
for 06:00Z 15 Sep 2009 Dust
NAAPS Surface Concentration (ug/m**3)
for 06:00Z 15 Sep 2009 Smoke
Sep 15 08:31:38 2009 NRL/Monterey Aerosol Modeling
(d)
NOAA HYSPLIT MODEL
Backward trajectories ending at 0700 UTC 15 Sep 09
CDC1 Meteorological Data
Source ★ at 14.64 N 121.08 E
Meters AGL
Job ID: 121374 Job Start: Thu Jun 3 18:45:44 UTC 2021
Source 1 lat.: 14.635989 lon.: 121.078163 height: 500 m AGL
Trajectory Direction: Backward Duration: 72 hrs
Vertical Motion Calculation Method: Model Vertical Velocity
Meteorology: 0000Z 1 Sep 2009 - reanalysis

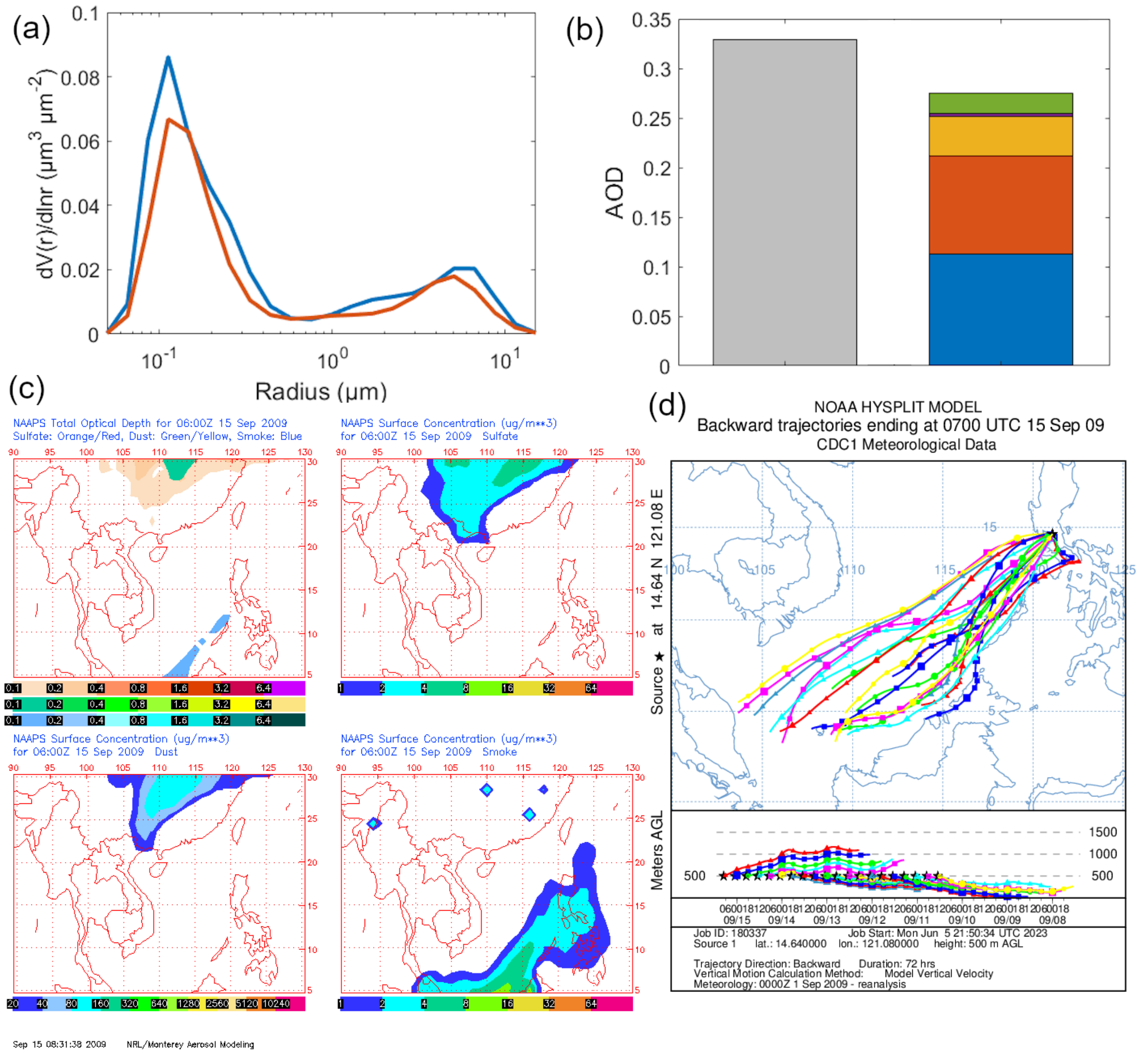

Figure 9: Case study of long-range transport (smoke – Southeast Asia) around 15 September 2009. (a) AERONET VSDs at (blue) 07:27 and (red) 07:52 UTC, (b) AOD from AERONET (gray: median AOD at 500 nm) and MERRA-2 hourly (green: black carbon, violet: dust, yellow: sea salt, orange: organic carbon, blue: sulfate) compositional contributions to AOD (550 nm) closest in time to 07:27 UTC, (c) NAAPS maps of total and compositional hourly AOD (orange/red: sulfate, green/yellow: dust, blue: smoke) and sulfate, dust, and smoke surface concentrations at 06:00 UTC, and (d) HYSPLIT ~~three~~seven-day back-trajectories arriving at Manila Observatory at 07:00 UTC.

3.4.2 Long Range Transport of Dust

The VSD of this specific case on 24 March 2018 (Fig. 10a) was most similar to the mixed ~~polluted~~dust cluster (cluster 3), which had a mixed size distribution but a more dominant coarse contribution. This is consistent with the most dominant contribution to AOD in the area, which was sea salt and dust (Fig. 10b). The back-trajectories were from East Asia around the same latitude as Taiwan (Fig. 10d). That area, at that time, had increased AOD in general from sulfate and dust (Fig. 10c). The AOD from both AERONET and MERRA-2 (Fig. 10b) are lower than 0.3 (the AOD threshold for dust in other studies, Table 2) because of the long distance from the source (thousands of kilometers). The dust and sulfate seemed to have been transported to Metro Manila from East Asia based on the NAAPS sulfate and dust surface concentrations (Fig. 10c).

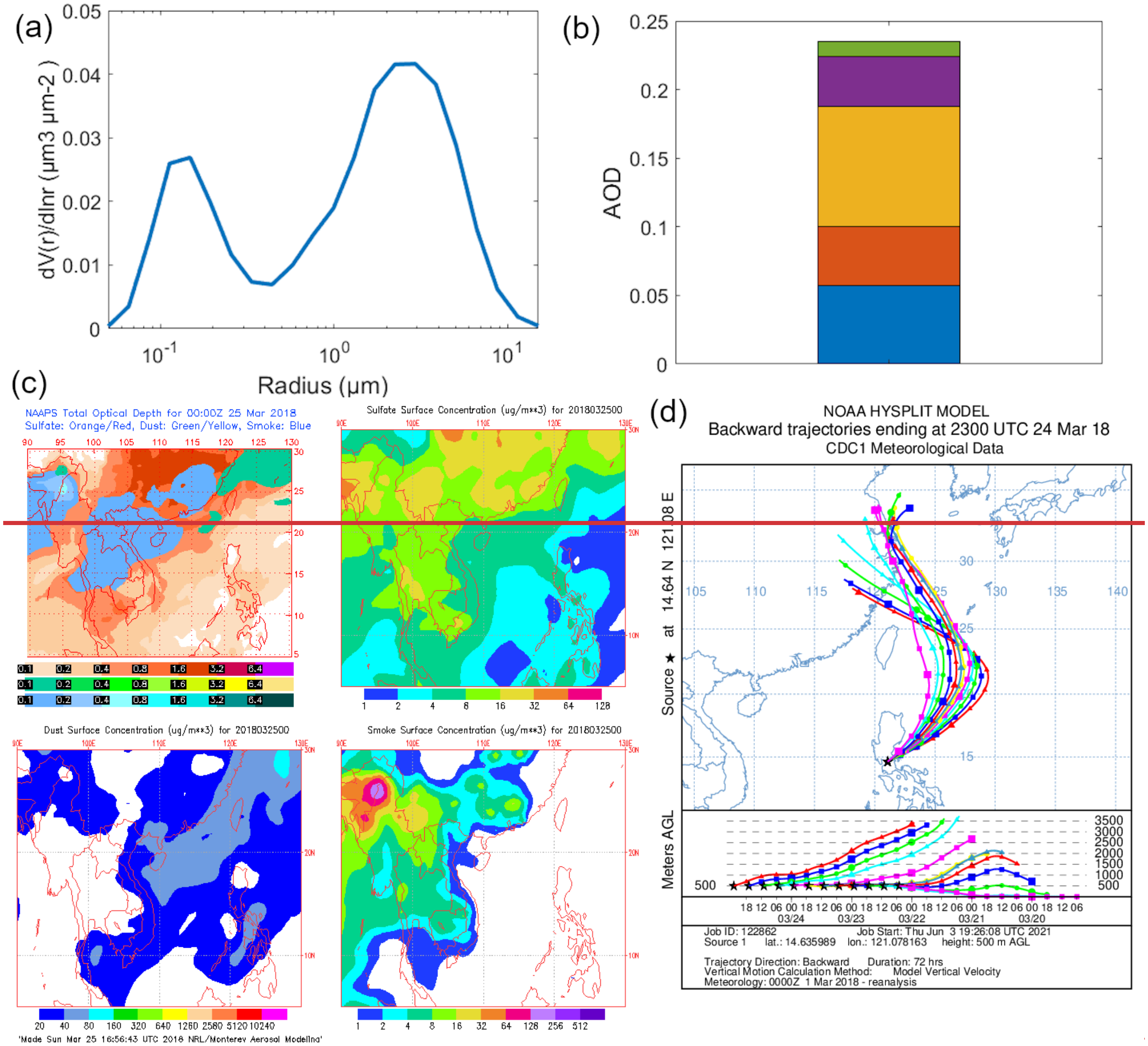

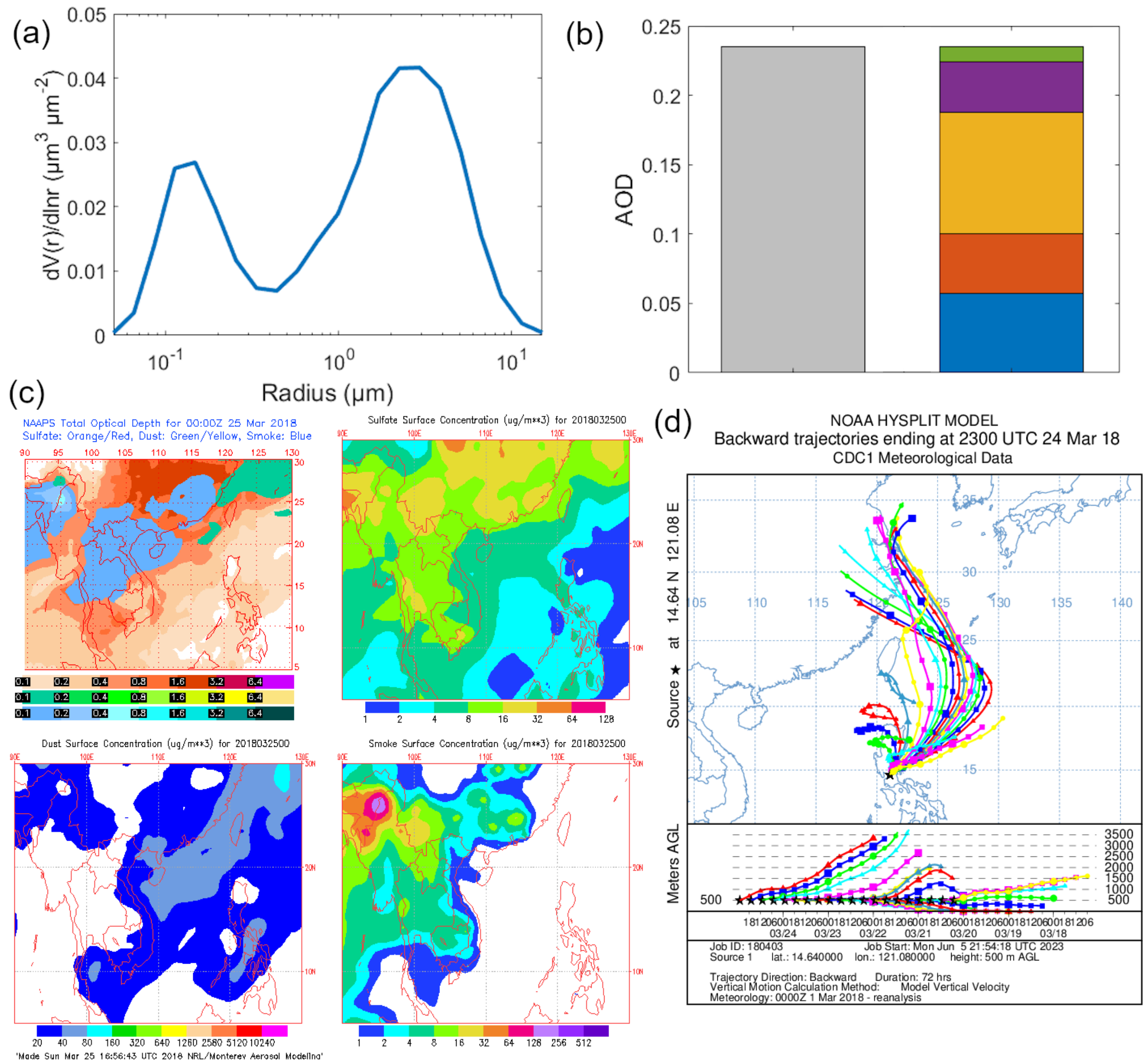

Figure 10: Case study of long-range transport (dust) around 24-25 March ~~2009~~2018. (a) AERONET VSD at (blue) 23:23 UTC, (b) AOD from AERONET (gray: AOD at 500 nm) and MERRA-2 hourly (green: black carbon, violet: dust, yellow: sea salt, orange: organic carbon, blue: sulfate) compositional contributions to AOD (550 nm) closest in time to 23:23 UTC, (c) NAAPS maps of total and compositional hourly AOD (orange/red: sulfate, green/yellow: dust, blue: smoke) and sulfate, dust, and smoke surface concentrations at 00:00 UTC on March 25, and (d) HYSPLIT ~~three~~seven-day back-trajectories arriving at Manila Observatory at 23:00 UTC.

~~3.5~~3.4.3 Cloud Processing

Sulfate dominated the AOD (Fig. 11b) for this case on 26 August 2009 in the area around Metro Manila. This along with its VSD exhibiting a second peak (Fig. 11a) in the accumulation mode make it very similar to the cloud processing cluster (cluster 5). Sulfate has been known to be enhanced through chemical productions in clouds and is used as a signature for cloud processing (Barth et al., 2000; Ervens et al., 2018). Aqueous production of sulfate is significant in areas with sources and clouds (Barth et al., 2000), and this case study has both. Aside from the high sulfate contribution to AOD, the cloud fraction (Aqua/MODIS, Terra/MODIS, Fig. S3) is very high (~100%) in the area of the back-trajectories (~~Aqua/MODIS, Terra/MODIS,~~ Fig. ~~S2~~11d). Interestingly, there is no regional AOD elevation observed in the NAAPS maps (Fig. 11c) for this time. There are increased surface smoke and sulfate levels in East Asia as well as southwest of the Philippines, and though the back-trajectories ~~(Fig. 11d)~~ do show a northeastward direction, they do not reach far enough into mainland East Asia. It is possible that even while there are known regional sources of sulfate in Southeast Asia (Smith et al., 2011; Li et al., 2017), this case could be local to the Philippines. There is in fact a large power plant northwest of Metro Manila (Jamora et al., 2020).

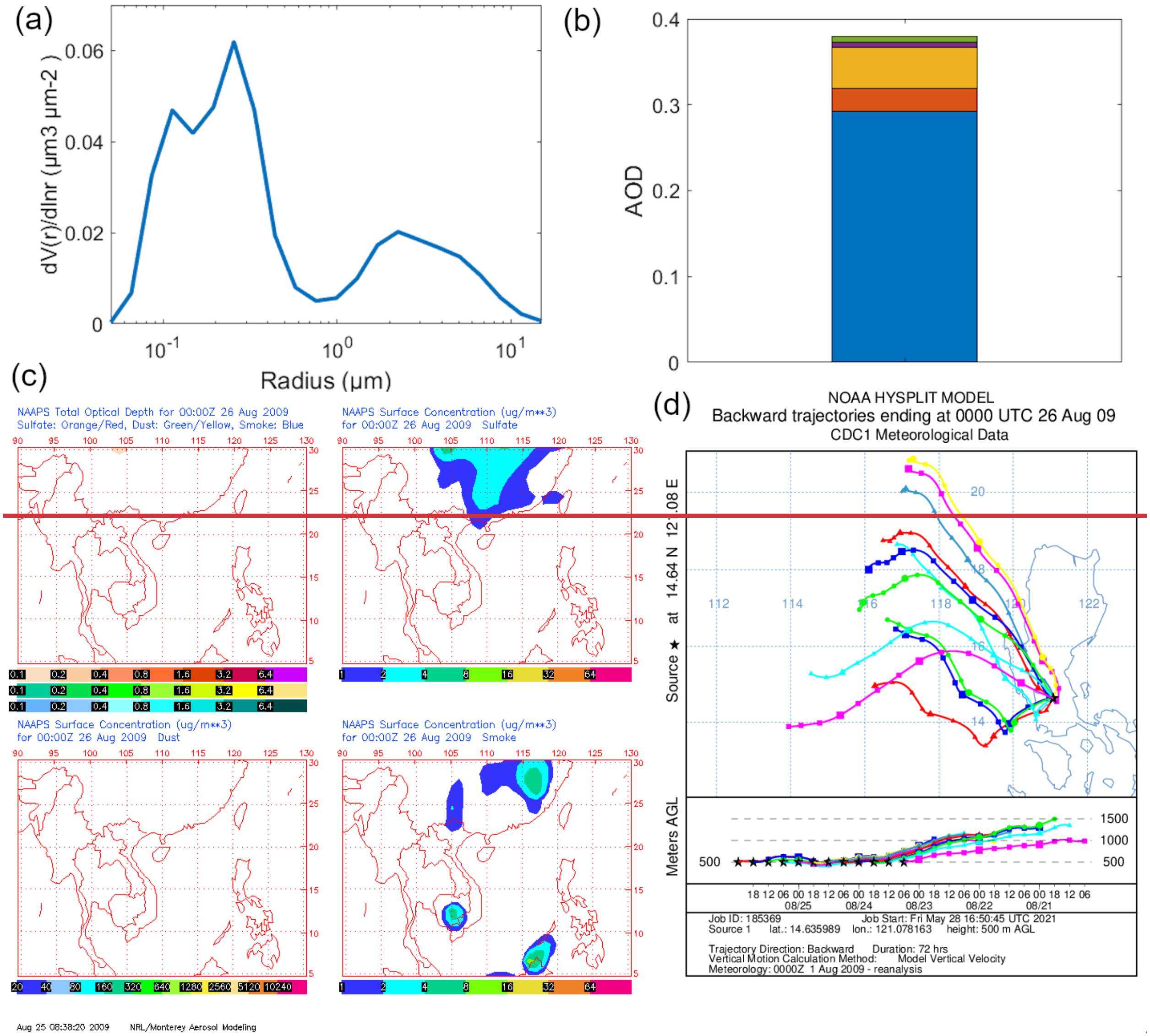
(a)
dV(r)/dlnr (μm3 μm-2)
Radius (μm)
(b)
AOD
(c)
NAAPS Total Optical Depth for 00:00Z 26 Aug 2009
Sulfate: Orange/Red, Dust: Green/Yellow, Smoke: Blue
NAAPS Surface Concentration (ug/m**3)
for 00:00Z 26 Aug 2009 Sulfate
NAAPS Surface Concentration (ug/m**3)
for 00:00Z 26 Aug 2009 Dust
NAAPS Surface Concentration (ug/m**3)
for 00:00Z 26 Aug 2009 Smoke
Aug 25 08:38:20 2009 NRL/Monterey Aerosol Modeling
(d)
NOAA HYSPLIT MODEL
Backward trajectories ending at 0000 UTC 26 Aug 09
CDC1 Meteorological Data
Source ★ at 14.64 N 121.08 E
Meters AGL
Job ID: 185369 Job Start: Fri May 28 16:50:45 UTC 2021
Source 1 lat.: 14.635989 lon.: 121.078163 height: 500 m AGL
Trajectory Direction: Backward Duration: 72 hrs
Vertical Motion Calculation Method: Model Vertical Velocity
Meteorology: 0000Z 1 Aug 2009 - reanalysis

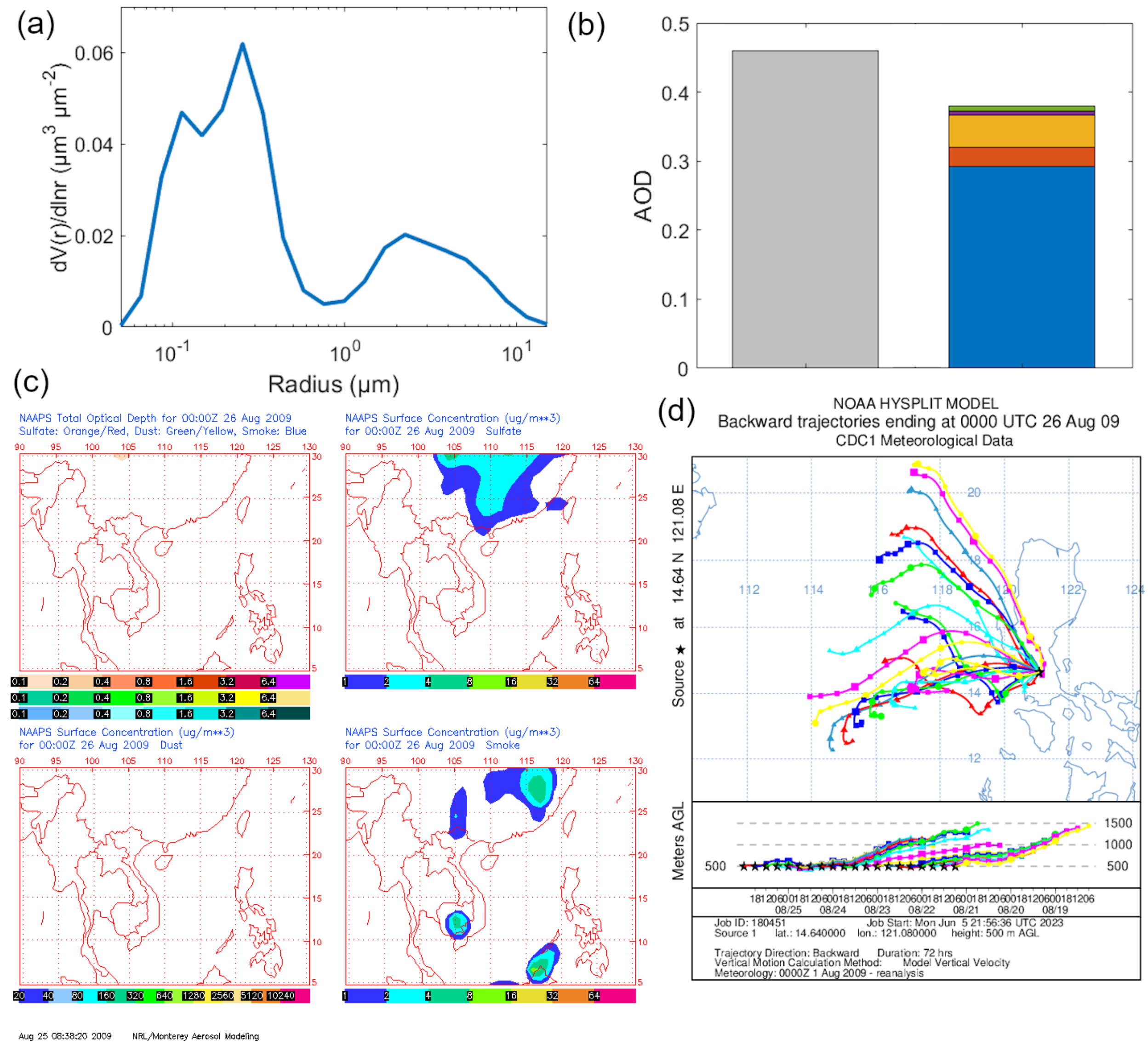

Figure 11: Case study of cloud processing on 26 August 2009. (a) AERONET VSDs at 00:18 UTC, (b) AOD from AERONET (gray: median AOD at 500 nm) and MERRA-2 hourly (green: black carbon, violet: dust, yellow: sea salt, orange: organic carbon, blue: sulfate) compositional contributions to AOD (550 nm) closest in time to 00:18 UTC, (c) NAAPS maps of total and compositional hourly AOD and contributions and smoke surface concentrations at 00:00 UTC, and (d) HYSPLIT ~~three~~seven-day back-trajectories arriving at Manila Observatory at 00:00 UTC.

~~3.6~~3.5 EOF Analysis of AOD in Southeast Asia

~~To contextualize the analysis of aerosol particle~~

The air masses in Metro Manila~~, major~~ are influenced by regional sources ~~of aerosol particles in Southeast Asia~~which were identified ~~based on the dominant principal components from~~through EOF analysis of AOD. Three principal components (PC, Fig. 12) explained most of the data variance (73.77%) (Fig. 12a) and were all well-separated from each other and are therefore most probably the major distinct aerosol particle sources in the region. They will be the focus of the subsequent discussion.

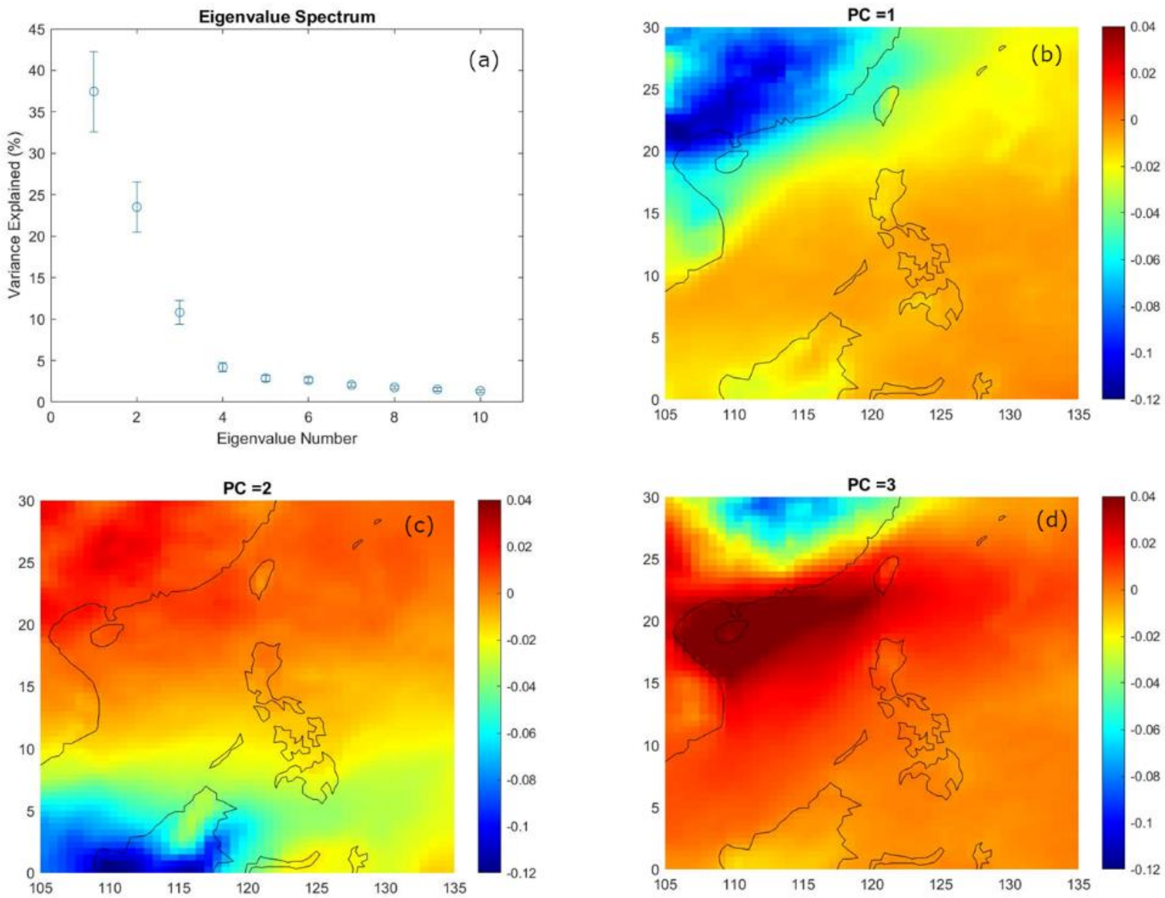

Figure 12: Results of the singular value decomposition. (a) Eigenvalue spectrum of the first ten eigenvalues, (b-d) maps of the coefficients of regression AOD anomalies onto the first three principal components.

The first PC explains 37.46% of the data variance (Fig. 12a) and, based on the map of the regression coefficients (Fig. 12b), separates mainland East Asia from the Philippines and Indonesia. East Asia is a globally recognized source for high AOD (Li et al., 2013), and its contribution to particles in Southeast Asia possibly corresponds to the first PC. The second PC explains 25.51% of the data variance (Fig. 12a) and separates ~~the~~ southern Southeast Asia from northern Southeast Asia at around 15°N (Fig. 12c). Southern Southeast Asia is a known regional source of aerosol particles due to biomass burning (Cohen et al., 2017) and could be associated with the second PC. The third PC explains 10.80% of the data variance (Fig. 12a) and separates northern East Asia from southern East Asia mainland and the rest of Southeast Asia (Fig. 12d).

To gain confidence in the association of the PCs with their sources, we present correlation maps between the first three PCs to the fractional contributions of sulfate and organic carbon to AOD for the entire dataset.

The correlation maps of the first PC and the sulfate contribution to AOD (Fig. 13a and 13d) show high and statistically significant correlations (gray areas) in mainland East Asia and Taiwan, parts of western Philippines and Borneo, which are the probable sulfate sources. Clues from the mean monthly wind vector maps in April (Fig. 14a and 14d) and mean monthly AOD in either March or April (Fig. S3c or S3e) most resembling the features of regression map of the first PC (Fig. 12b) and the PC time series peaking in March (Fig. S4) together suggest that the first PC may be associated with air masses that are present around March or April. Emissions sources and meteorology that are dominant during the peak dates in the PC time series offer clues to the attribution of each PC. The Southeast Asia region and the Philippines is influenced by the monsoon systems (Coronas, 1920; Matsumoto et al., 2020) and February to March is the time when the winds are transitioning from the northeasterly to easterly. The first PC could be affected by the easterly winds, which are dominant around March when its PC values peaked. The higher-level winds (free troposphere) (Fig. 14a) in April are from the west in mainland East Asia and are from the east in the Philippines and it is possible that the different wind regimes are distinguishing the sulfate sources in East Asia and the Philippines and beyond. Sulfate is a known product of industry in East Asia (Smith et al., 2011; Li et al., 2017) while the West Luzon and West Visayas islands have large power plants (Jamora et al., 2020).

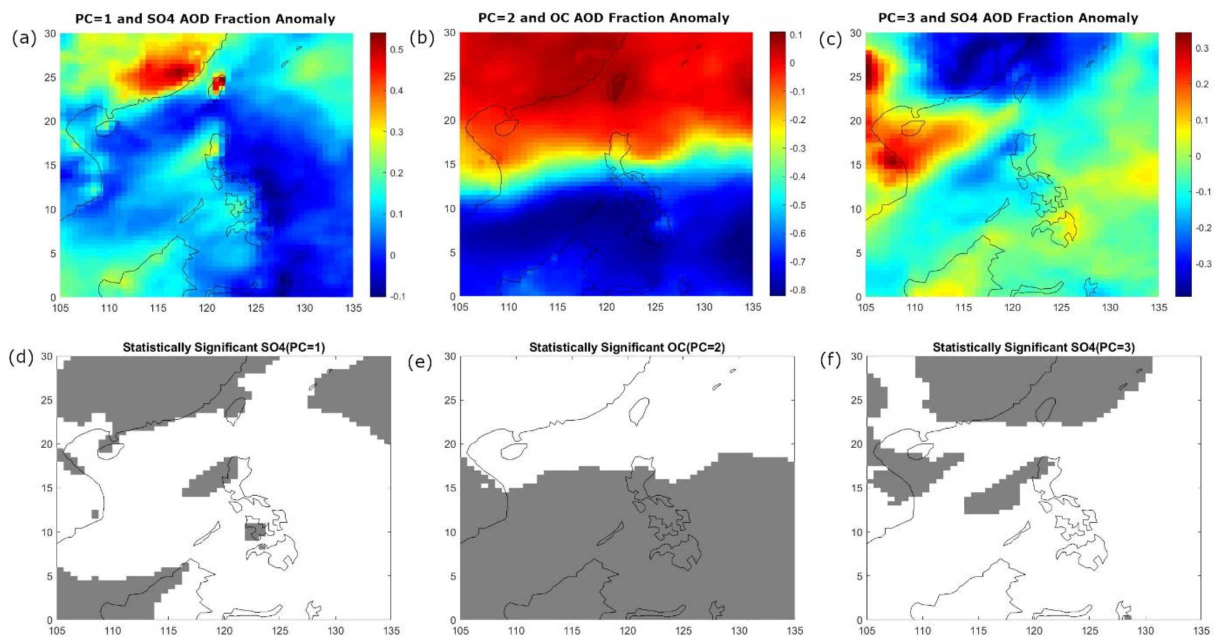

Figure 13: Correlation coefficients of principal components with (a/c) sulfate AOD fraction and (b) organic carbon AOD fraction. Statistically significant (90%, d-f) areas are shaded gray.

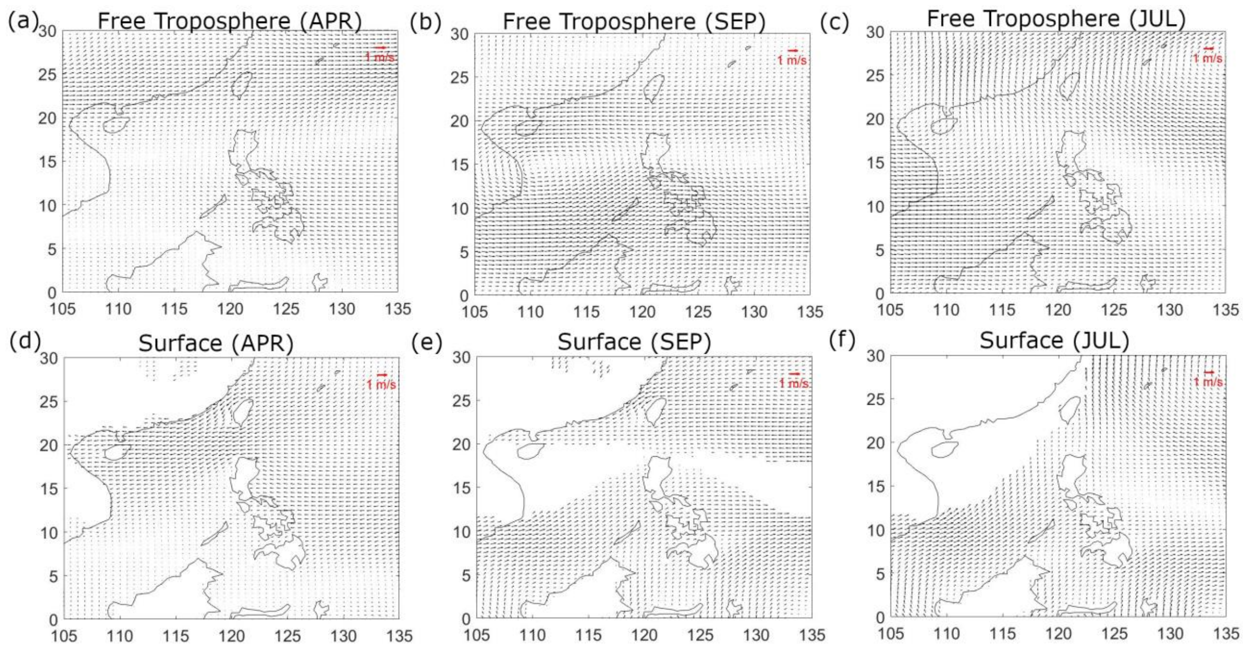

Figure 14: Monthly averaged winds for (a & d) April, (b & e) September, and (c & f) July from MERRA-2 at (725 hPa, a-c) the free troposphere approximate and at (1000 hPa, d-f) the surface.

The correlation maps of the second PC and the OC contribution to AOD (Fig. 13b and 13e) show high and statistically significant correlations from 0°N to 15°N. The large magnitude of the correlation coefficient (gray areas in Fig. 13b) stands out in ~~the~~ southern Southeast Asia and is the potential OC source. In this case, it is known that Indonesia is a major source of biomass burning during its fire season (Glover and Jessup, 1998), and thus the local significance established in the southern Southeast Asia is most likely due to the Indonesia biomass burning source. The burning season in Indonesia is from August to October, and that is the same time when the AOD values peak in the area (Fig. S3h, S3i, and S3j), as well as the peak of the second PC in the time series (Fig. S4). Winds are usually from the southwest and west due to the southwest monsoon from September to October, when the second PC peaked, and thus the second PC may be related to the southwest monsoon. During the same time the surface and free troposphere mean monthly winds (Fig. 14b and 14e) are from the southwest (in the general direction of Indonesia) towards the south portion of Southeast Asia and thus corroborate the observation that the second PC may be highlighting the regional effect of the Indonesia forest fires. Of interest is the line of separation of the northern and southern Southeast Asia in the principal component that is within the area of the monsoon trough (Wang et al., 2007). This line is also evident in the surface and the free troposphere maps where the southwest winds from the area of Indonesia meet the easterlies in north Southeast Asia (Fig. 14b and 14e) and which thus appears to be limiting the dispersion of the biomass burning emissions to southern Southeast Asia.

The third PC was also well correlated to the sulfate AOD fraction though, compared to the first PC correlation maps, there were distinctions between the northern and southern East Asia regions (Fig. 13c and 13f). The local Philippine source still came out in the correlation maps as a significant source. It was not clear from the PC time series (Fig. S4), which showed peaks in the third PC in February, how the dates were related to the PC profile. The free troposphere winds in

July (Fig. 14c), as well as the AOD monthly mean map in July (Fig. 14c), however, showed more similarities to the third PC regression map. Both showed a delineation between the northern East Asia and southern East Asia (including Hong Kong) features. Mean winds (Fig. 14c) in the free troposphere are from the west, due to the southwest monsoon, in the area around the Philippines, and they were from the northeast in north Southeast Asia. The interface of the winds is within the approximate location of the monsoon trough in July (Wang et al., 2007), and it is thus possible that the monsoon trough is causing the separation of the sulfate sources. This could be investigated further. The monsoon trough has been noted to scavenge aerosol particles from southern Southeast Asia (Reid et al., 2013). It is evident from the analysis that meteorology affects the transport and processing of aerosol particles in region which along with local sources contribute to the aerosol composition in Southeast Asia (Cruz et al., 2019; AzadiAghdam et al., 2019; Braun et al., 2020; Hilario et al., 2020b; Hilario et al., 2022).

4. Conclusion

Metro Manila has both urban and industrial local sources known to contribute to the dominance of fine mode particles in its air (Cruz et al., 2019). Ten years of AERONET data in Manila Observatory suggest that aerosol particles in Metro Manila were mixed in size but with a prevalent fine mode fraction (>50% FMF) throughout the year. Background clean marine aerosol particles (58% of the time) and fine polluted aerosol particles (20% of the time) were the most dominant clear sky day sources impacting the atmospheric column over Metro Manila based on cluster analysis of volume size distributions. The proximity of Metro Manila to the sea, both in the east and west~~,~~ along with local sources, transportation being the most prominent, together contribute to the prevalence of the marine and fine particles. The prevalence of marine particles could explain the relatively small AOD values in Metro Manila compared to other Southeast Asian megacities (Reid et al., 2013).

Regional sources and meteorology also impact monthly aerosol optical depth trends in Metro Manila from EOF analysis. Biomass burning from Borneo and Sumatra emerged in the study as the second most prevalent regional anthropogenic aerosol particle source in Southeast Asia. Though the monsoon trough limits the dispersion of aerosol particles throughout the entire Southeast Asia, biomass burning emissions impact southern Southeast Asia including Metro Manila during the southwest monsoon (July to September). The monsoon winds facilitate the transport of fine particles during the peak burning season in Borneo and Sumatra (August-September). This is experienced in Metro Manila as higher than usual aerosol particle loadings ~~during~~around the same period~~.~~ (August to October). Climatologically, August ~~is~~was also when ~~aerosol optical depth peaked over Metro Manila, concurrent~~there were particles with the greatest fine mode fractions that were relatively absorbing and non-hygroscopic possibly due to increased organic and elemental carbon fractional contributions. Though not as strong a source as the Borneo and Sumatra case, the peninsular Southeast Asia burning season (March-April) also contributed to extreme aerosol particle concentrations over Metro Manila.

High aerosol particle loadings due to transported dust, probably from East Asia, were observed in Metro Manila during the transition period between the southwest and northeast monsoons and during the northeast monsoon (December to February). These extreme events are transient because the lowest median aerosol particle loadings of the year were observed during the northeast monsoon when annual wind speeds were highest. Particles then were observed to be largest in diameter, with the greatest coarse fraction contribution, relatively high absorptivity, and most hygrosocopicity, compared to other months of the year. This is probably due to constituents other than soot, especially aged dust (Kim and Park, 2012; Geng et al., 2014) and sea salt which the northeast winds appear to be bringing in from the general direction of the Luzon Island and the Philippine Sea (West Pacific Ocean).

Cloud processing is one of the cases that were linked to very high aerosol particle loading in Metro Manila. This is associated with sulfate sources, which appear more localized in nature because of a power plant nearby. This sulfate source seems to be distinct from the industrial sulfate air mass from East Asia, which is the most dominant regional aerosol particle source in Southeast Asia (Li et al., 2013). Winds appear to limit the mixing of this notable East Asia air mass with local industrial sources in the region including the Philippines and Indonesia.

The formation of cloud systems in Southeast Asia is complex due to intersecting large- and small-scale mechanisms. Additionally, the interaction of particles and clouds in Southeast Asia is not yet well understood. In Metro Manila, both topography and meteorology affect aerosol particle distribution (Cruz et al., 2023). This baseline study on the aerosol particle characteristics in Metro Manila and in regional Southeast Asia shows how meteorology impacts varied aerosol particle sources (e.g., sulfate, elemental carbon, and organic carbon) and their distribution in the region. This can help in mitigating aerosol particle sources in the region and in the deepening of the understanding of the relationship of aerosol particles, meteorology, and clouds.

Data availability

Aerosol Robotic Network (AERONET) (2020), Version 3 Direct Sun Algorithm, Site: Manila Observatory, Philippines, Accessed: **[*28 September 2020*]**, https://aeronet.gsfc.nasa.gov/cgi-bin/webtool_aod_v3?stage=3&region=Asia&state=Philippines&site=Manila_Observatory&place_code=10&if_polarized=0

Aerosol Robotic Network (AERONET) (2020), Version 3 Direct Sun and Inversion Algorithm, Site: Manila Observatory, Philippines, Accessed: **[*28 September 2020*]**, https://aeronet.gsfc.nasa.gov/cgi-bin/webtool_inv_v3?stage=3&region=Asia&state=Philippines&site=Manila_Observatory&place_code=10&if_polarized=0

Multi-angle Imaging SpectroRadiometer (MISR) Jet Propulsion Laboratory (2018), Level 3 Component Global Aerosol product in netCDF format covering a month V004, Accessed: ***[22 November 2021],*** https://search.earthdata.nasa.gov/

Global Modeling and Assimilation Office (GMAO) (2015), MERRA-2 inst3_3d_asm_Np: 3d,3-Hourly,Instantaneous,Pressure-Level,Assimilation,Assimilated Meteorological Fields V5.12.4, Greenbelt, MD, USA, Goddard Earth Sciences Data and Information Services Center (GES DISC), Accessed: **[*10 March 2021*]**, https://doi.org/10.5067/QBZ6MG944HW0

Global Modeling and Assimilation Office (GMAO) (2015), MERRA-2 tavg1_2d_flx_Nx: 2d,1-Hourly,Time-Averaged,Single-Level,Assimilation,Surface Flux Diagnostics V5.12.4, Greenbelt,

MD, USA, Goddard Earth Sciences Data and Information Services Center (GES DISC), Accessed: **[*10 March 2021*]**, https://doi.org/10.5067/7MCPBJ41Y0K6

Global Modeling and Assimilation Office (GMAO) (2015), MERRA-2 tavg1_2d_csp_Nx: 2d,1-Hourly,Time-averaged,Single-Level,Assimilation,COSP Satellite Simulator V5.12.4, Greenbelt, MD, USA, Goddard Earth Sciences Data and Information Services Center (GES DISC), Accessed: **[*13 July 2021*]**, https://doi.org/10.5067/H0VVAD8F6MX5

Nguyen, P., E.J. Shearer, H. Tran, M. Ombadi, N. Hayatbini, T. Palacios, P. Huynh, G. Updegraff, K. Hsu, B. Kuligowski, W.S. Logan, and S. Sorooshian, The CHRS Data Portal, an easily accessible public repository for PERSIANN global satellite precipitation data, Nature Scientific Data, Vol. 6, Article 180296, 2019, Accessed: **[*11 March 2021*],** https://doi.org/10.1038/sdata.2018.296

Author contributions

GRL and AS designed the experiment. NL, SNU, GRL, GFG, HJO, JBS, and MTC, carried out various aspects of the data collection. GRL, AS, JBS, MOC, MRH, CC, and ~~CC~~LDG conducted analysis and interpretation of the data. GRL prepared the manuscript draft with contributions from the coauthors. AFA, LDG, MRH, GRL, and AS reviewed and edited the manuscript. AS led the management and funding acquisition. All authors approved the final version of the manuscript.

Competing interests

We declare that Armin Sorooshian is a member of the editorial board of Atmospheric Chemistry and Physics. The peer-review process was guided by an independent editor, and the authors have also no other competing interests to declare.

Acknowledgements

The authors acknowledge support from NASA grant 80NSSC18K0148 in support of the NASA CAMP^{2}Ex project, in addition to ONR grant N00014-21-1-2115. We acknowledge the US Naval Research Laboratory for providing the AERONET instrument. We acknowledge the use of imagery from the NASA Worldview application (https://worldview.earthdata.nasa.gov), part of the NASA Earth Observing System Data and Information System (EOSDIS).

References:

AERONET Inversion Products (Version 3): https://aeronet.gsfc.nasa.gov/new_web/Documents/Inversion_products_for_V3.pdf, access: June 25, 2021, 2019.

Alas, H. D., Müller, T., Birmili, W., Kecorius, S., Cambaliza, M. O., Simpas, J. B. B., Cayetano, M., Weinhold, K., Vallar, E., and Galvez, M. C.: Spatial characterization of black carbon mass concentration in the atmosphere of a southeast asian megacity: an air quality case study for Metro Manila, Philippines, Aerosol Air Qual. Res., 18, 2301-2317, https://doi.org/10.4209/aaqr.2017.08.0281, 2018.

Aldhaif, A. M., Lopez, D. H., Dadashazar, H., and Sorooshian, A.: Sources, frequency, and chemical nature of dust events impacting the United States East Coast, Atmos. Environ., 231, 117456, https://doi.org/10.1016/j.atmosenv.2020.117456, 2020.

Aldhaif, A. M., Lopez, D. H., Dadashazar, H., Painemal, D., Peters, A. J., and Sorooshian, A.: An Aerosol Climatology and Implications for Clouds at a Remote Marine Site: Case Study Over Bermuda, J. Geophys. Res.- Atmos., 126, e2020JD034038, https://doi.org/10.1029/2020JD034038, 2021.

Alizadeh-Choobari, O., and Gharaylou, M.: Aerosol impacts on radiative and microphysical properties of clouds and precipitation formation, Atmos. Res., 185, 53-64, https://doi.org/10.1016/j.atmosres.2016.10.021, 2017.

~~Andrews, E., Ogren, J. A., Kinne, S., and Samset, B.: Comparison of AOD, AAOD and column single scattering albedo from AERONET retrievals and in situ profiling measurements, Atmos. Chem. Phys., 17, 6041-6072, https://doi.org/10.5194/acp-17-6041-2017, 2017.~~
Amnuaylojaroen, T.: Air Pollution Modeling in Southeast Asia—An Overview, Vegetation Fires and Pollution in Asia, 531-544, https://doi.org/10.1007/978-3-031-29916-2_31, 2023.

Ångström, A.: On the atmospheric transmission of sun radiation and on dust in the air, Geografiska Annaler, 11, 156-166, 1929.

Arthur, D., and Vassilvitskii, S.: k-means++: The advantages of careful seeding, Stanford, 2006.

AzadiAghdam, M., Braun, R. A., Edwards, E.-L., Bañaga, P. A., Cruz, M. T., Betito, G., Cambaliza, M. O., Dadashazar, H., Lorenzo, G. R., and Ma, L.: On the nature of sea salt aerosol at a coastal megacity: Insights from Manila, Philippines in Southeast Asia, Atmos. Environ., 216, 116922, https://doi.org/10.1016/j.atmosenv.2019.116922, 2019.

Bagtasa, G.: Contribution of tropical cyclones to rainfall in the Philippines, Journal of Climate, 30, 3621-3633, 2017.

Bañares, E. N., Narisma, G. T. T., Simpas, J. B. B., Cruz, F. A. T., Lorenzo, G. R. H., Cambaliza, M. O. L., and Coronel, R. C.: Seasonal and diurnal variations of observed convective rain events in metro Manila, Philippines, Atmos. Res., 105646, https://doi.org/10.1016/j.atmosres.2021.105646, 2021.

Barth, M., Rasch, P., Kiehl, J., Benkovitz, C., and Schwartz, S.: Sulfur chemistry in the National Center for Atmospheric Research Community Climate Model: Description, evaluation, features, and sensitivity to aqueous chemistry, J. Geophys. Res.- Atmos., 105, 1387-1415, https://doi.org/10.1029/1999JD900773, 2000.

Bautista VII, A. T., Pabroa, P. C. B., Santos, F. L., Racho, J. M. D., and Quirit, L. L.: Carbonaceous particulate matter characterization in an urban and a rural site in the Philippines, Atmospheric Pollution Research, 5, 245-252, https://doi.org/10.5094/APR.2014.030, 2014.

Bergstrom, R. W., Russell, P. B., and Hignett, P.: Wavelength dependence of the absorption of black carbon particles: Predictions and results from the TARFOX experiment and implications for the aerosol single scattering albedo, J. Atmos. Sci., 59, 567-577, https://doi.org/10.1175/1520-0469(2002)059<0567:WDOTAO>2.0.CO;2, 2002.

Bergstrom, R. W., Pilewskie, P., Schmid, B., and Russell, P. B.: Estimates of the spectral aerosol single scattering albedo and aerosol radiative effects during SAFARI 2000, J. Geophys. Res.-Atmos., 108, https://doi.org/10.1029/2002JD002435, 2003.

Bergstrom, R. W., Pilewskie, P., Russell, P. B., Redemann, J., Bond, T. C., Quinn, P. K., and Sierau, B.: Spectral absorption properties of atmospheric aerosols, Atmos. Chem. Phys., 7, 5937-5943, https://doi.org/10.5194/acp-7-5937-2007, 2007.

Bi, J., Huang, J., Hu, Z., Holben, B., and Guo, Z.: Investigating the aerosol optical and radiative characteristics of heavy haze episodes in Beijing during January of 2013, J. Geophys. Res.-Atmos., 119, 9884-9900, https://doi.org/10.1002/2014JD021757, 2014.

Björnsson, H., and Venegas, S.: A manual for EOF and SVD analyses of climatic data, CCGCR Report, 97, 112-134, 1997.

Bohren, C. F., and Clothiaux, E. E.: Fundamentals of atmospheric radiation: an introduction with 400 problems, John Wiley & Sons, 2006.

Braun, R. A., Aghdam, M. A., Bañaga, P. A., Betito, G., Cambaliza, M. O., Cruz, M. T., Lorenzo, G. R., MacDonald, A. B., Simpas, J. B., and Stahl, C.: Long-range aerosol transport and impacts on size-resolved aerosol composition in Metro Manila, Philippines, Atmos. Chem. Phys., 20, 2387-2405, https://doi.org/10.5194/acp-20-2387-2020, 2020.

Buchard, V., Randles, C., Da Silva, A., Darmenov, A., Colarco, P., Govindaraju, R., Ferrare, R., Hair, J., Beyersdorf, A., and Ziemba, L.: The MERRA-2 aerosol reanalysis, 1980 onward. Part II: Evaluation and case studies, Journal of Climate, 30, 6851-6872, https://doi.org/10.1175/JCLI-D-16-0613.1, 2017.

Cahyono, W. E., Setyawati, W., Hamdi, S., Cholianawati, N., Kombara, P. Y., and Sari, W. J.: Observations of aerosol optical properties during tropical forest fires in Indonesia, Materials Today: Proceedings, 63, S445-S450, https://doi.org/10.1016/j.matpr.2022.04.113, 2022.

Caido, N. G., Ong, P. M., Rempillo, O., Galvez, M. C., and Vallar, E.: Spatiotemporal analysis of MODIS aerosol optical depth data in the Philippines from 2010 to 2020, Atmosphere, 13, 939, https://doi.org/10.3390/atmos13060939, 2022.

Chang, C.-P., Wang, Z., McBride, J., and Liu, C.-H.: Annual cycle of Southeast Asia—Maritime Continent rainfall and the asymmetric monsoon transition, Journal of climate, 18, 287-301, https://doi.org/10.1175/JCLI-3257.1, 2005.

Che, H., Xia, X., Zhu, J., Wang, H., Wang, Y., Sun, J., Zhang, X., and Shi, G.: Aerosol optical properties under the condition of heavy haze over an urban site of Beijing, China, Environ. Sci. Pollut. R., 22, 1043-1053, https://doi.org/10.1007/s11356-014-3415-5, 2015.

Chen, Q., McGowan, S., Gouramanis, C., Fong, L., Balasubramanian, R., and Taylor, D.: Rapidly rising transboundary atmospheric pollution from industrial and urban sources in

Southeast Asia and its implications for regional sustainable development, Environ. Res. Lett., 15, 1040a1045, https://doi.org/10.1088/1748-9326/abb5ce, 2020.

Choi, M., Lim, H., Kim, J., Lee, S., Eck, T. F., Holben, B. N., Garay, M. J., Hyer, E. J., Saide, P. E., and Liu, H.: Validation, comparison, and integration of GOCI, AHI, MODIS, MISR, and VIIRS aerosol optical depth over East Asia during the 2016 KORUS-AQ campaign, Atmos. Meas. Tech., 12, 4619-4641, https://doi.org/10.5194/amt-12-4619-2019, 2019.

Cohen, J. B.: Quantifying the occurrence and magnitude of the Southeast Asian fire climatology, Environmental Research Letters, 9, 114018, https://dx.doi.org/10.1088/1748-9326/9/11/114018, 2014.

Cohen, J. B., Lecoeur, E., and Hui Loong Ng, D.: Decadal-scale relationship between measurements of aerosols, land-use change, and fire over Southeast Asia, Atmos. Chem. Phys., 17, 721-743, https://doi.org/10.5194/acp-17-721-2017, 2017.

Coronas, J.: The Climate and Weather of the Philippines, 1903-1918, by Rev. José Coronas. SJ, Chief, Meteorological Division, Weather Bureau, Manila Observatory, Manila,: Bureau of Printing, 1920.

Crosbie, E., Sorooshian, A., Monfared, N. A., Shingler, T., and Esmaili, O.: A multi-year aerosol characterization for the greater Tehran area using satellite, surface, and modeling data, Atmosphere, 5, 178-197, https://doi.org/10.3390/atmos5020178, 2014.

Crosbie, E., Ziemba, L. D., Shook, M. A., Robinson, C. E., Winstead, E. L., Thornhill, K. L., Braun, R. A., MacDonald, A. B., Stahl, C., and Sorooshian, A.: Measurement report: Closure analysis of aerosol–cloud composition in tropical maritime warm convection, Atmos. Chem. Phys., 22, 13269-13302, https://doi.org/10.5194/acp-22-13269-2022, 2022.

Cruz, F., Narisma, G. T., Villafuerte II, M. Q., Chua, K. C., and Olaguera, L. M.: A climatological analysis of the southwest monsoon rainfall in the Philippines, Atmos. Res., 122, 609-616, https://doi.org/10.1016/j.atmosres.2012.06.010, 2013.

Cruz, M. T., Bañaga, P. A., Betito, G., Braun, R. A., Stahl, C., Aghdam, M. A., Cambaliza, M. O., Dadashazar, H., Hilario, M. R., Lorenzo, G. R., Ma, L., MacDonald, A. B., Pabroa, C., Yee, J. R., Simpas, J. B., and Sorooshian, A.: Size-resolved composition and morphology of particulate matter during the southwest monsoon in Metro Manila, Philippines, Atmos. Chem. Phys., 19, 10675–10696, https://doi.org/10.5194/acp-19-10675-2019, 2019.

Cruz, M. T., Simpas, J. B., Sorooshian, A., Betito, G., Cambaliza, M. O. L., Collado, J. T., Eloranta, E. W., Holz, R., Topacio, X. G. V., and Del Socorro, J.: Impacts of regional wind circulations on aerosol pollution and planetary boundary layer structure in Metro Manila, Philippines, Atmos. Environ., 293, 119455, https://doi.org/10.1016/j.atmosenv.2022.119455, 2023.

Deep, A., Pandey, C. P., Nandan, H., Singh, N., Yadav, G., Joshi, P., Purohit, K., and Bhatt, S.: Aerosols optical depth and Ångström exponent over different regions in Garhwal Himalaya, India, Environmental Monitoring and Assessment, 193, 324, https://doi.org/10.1007/s10661-021-09048-4, 2021.

Di Girolamo, L., Holz, R., Reid, J., Tanelli, S., van den Heever, S., Narsma, G., and Simpas, J.: Cloud and aerosol monsoonal processes-Philippines experiment (CAMP2Ex), NASA White Paper, 2015.

Diner, D. J., Di Girolamo, L., and Nolin, A.: Preface to the MISR special issue, Remote Sens. Environ., 107, 1, https://doi.org/10.1016/j.rse.2006.11.001, 2007.

Dong, X., and Fu, J. S.: Understanding interannual variations of biomass burning from Peninsular Southeast Asia, part II: Variability and different influences in lower and higher atmosphere levels, Atmospheric Environment, 115, 9-18, https://doi.org/10.1016/j.atmosenv.2015.05.052, 2015.

Dorado, S. V., Holdsworth, J. L., Lagrosas, N. C., Villarin, J. R., Narisma, G., Ellis, J., and Perez, R.: Characterization of urban atmosphere of Manila with lidar, filter sampling, and radiosonde, Lidar Remote Sensing for Industry and Environment Monitoring, 2001, 591-598,

Dubovik, O., Holben, B., Kaufman, Y., Yamasoe, M., Smirnov, A., Tanré, D., and Slutsker, I.: Single-scattering albedo of smoke retrieved from the sky radiance and solar transmittance measured from ground, J. Geophys. Res.- Atmos., 103, 31903-31923, https://doi.org/10.1029/98JD02276, 1998.

Dubovik, O., and King, M. D.: A flexible inversion algorithm for retrieval of aerosol optical properties from Sun and sky radiance measurements, J. Geophys. Res.- Atmos., 105, 20673-20696, https://doi.org/10.1029/2000JD900282, 2000.

Dubovik, O., Holben, B., Eck, T. F., Smirnov, A., Kaufman, Y. J., King, M. D., Tanré, D., and Slutsker, I.: Variability of absorption and optical properties of key aerosol types observed in worldwide locations, J. Atmos. Sci., 59, 590-608, https://doi.org/10.1175/1520-0469(2002)059<0590:VOAAOP>2.0.CO;2, 2002.

Eck, T., Holben, B., Reid, J., O'neill, N., Schafer, J., Dubovik, O., Smirnov, A., Yamasoe, M., and Artaxo, P.: High aerosol optical depth biomass burning events: A comparison of optical properties for different source regions, Geophys. Res. Lett., 30, https://doi.org/10.1029/2003GL017861, 2003.

Eck, T., Holben, B., Dubovik, O., Smirnov, A., Goloub, P., Chen, H., Chatenet, B., Gomes, L., Zhang, X. Y., and Tsay, S. C.: Columnar aerosol optical properties at AERONET sites in central eastern Asia and aerosol transport to the tropical mid-Pacific, J. Geophys. Res.- Atmos., 110, https://doi.org/10.1029/2004JD005274, 2005.

Eck, T., Holben, B., Reid, J., Mukelabai, M., Piketh, S., Torres, O., Jethva, H., Hyer, E., Ward, D., and Dubovik, O.: A seasonal trend of single scattering albedo in southern African biomass-burning particles: Implications for satellite products and estimates of emissions for the world's largest biomass-burning source, J. Geophys. Res.- Atmos., 118, 6414-6432, https://doi.org/10.1002/jgrd.50500, 2013.

Eck, T. F., Holben, B., Reid, J., Dubovik, O., Smirnov, A., O'neill, N., Slutsker, I., and Kinne, S.: Wavelength dependence of the optical depth of biomass burning, urban, and desert dust aerosols, J. Geophys. Res.- Atmos., 104, 31333-31349, https://doi.org/10.1029/1999JD900923, 1999.

Eck, T. F., Holben, B. N., Reid, J., Giles, D., Rivas, M., Singh, R. P., Tripathi, S., Bruegge, C., Platnick, S., and Arnold, G.: Fog-and cloud-induced aerosol modification observed by the Aerosol Robotic Network (AERONET), J. Geophys. Res.- Atmos., 117, https://doi.org/10.1029/2011JD016839, 2012.

Ervens, B., Sorooshian, A., Aldhaif, A. M., Shingler, T., Crosbie, E., Ziemba, L., Campuzano-Jost, P., Jimenez, J. L., and Wisthaler, A.: Is there an aerosol signature of chemical cloud processing?, Atmos. Chem. Phys., 18, 16099-16119, https://doi.org/10.5194/acp-18-16099-2018, 2018.

Faloona, I.: Sulfur processing in the marine atmospheric boundary layer: A review and critical assessment of modeling uncertainties, Atmos. Environ., 43, 2841-2854, https://doi.org/10.1016/j.atmosenv.2009.02.043, 2009.

Feingold, G.: Modeling of the first indirect effect: Analysis of measurement requirements, Geophys. Res. Lett., 30, https://doi.org/10.1029/2003GL017967, 2003.

Flores, J.: Climate of the Philippines, Climates of the Northern and Eastern Asia, 159-213, 1969.

Formenti, P., Andreae, M. O., and Lelieveld, J.: Measurements of aerosol optical depth above 3570 m asl in the North Atlantic free troposphere: results from ACE-2, Tellus B, 52, 678-693, https://doi.org/10.1034/j.1600-0889.2000.00006.x, 2000.

Garay, M. J., Bull, M. A., Nastan, A. M., Witek, M. L., Seidel, F. C., Diner, D. J., Kahn, R. A., Limbacher, J. A., and Kalashnikova, O. V.: Data Product Specification for the MISR Level 2 Aerosol Product, Jet Propulsion Laboratory, California Institute of Technology. JPL D-100649. https://asdc.larc.nasa.gov/documents/misr/DPS_AEROSOL_V023.20180125.pdf, 2018.

Gautam, R., Hsu, N. C., Eck, T. F., Holben, B. N., Janjai, S., Jantarach, T., Tsay, S.-C., and Lau, W. K.: Characterization of aerosols over the Indochina peninsula from satellite-surface observations during biomass burning pre-monsoon season, Atmos. Environ., 78, 51-59, https://doi.org/10.1016/j.atmosenv.2012.05.038, 2013.

Gelaro, R., McCarty, W., Suárez, M. J., Todling, R., Molod, A., Takacs, L., Randles, C. A., Darmenov, A., Bosilovich, M. G., and Reichle, R.: The modern-era retrospective analysis for research and applications, version 2 (MERRA-2), J. Climate, 30, 5419-5454, https://doi.org/10.1175/JCLI-D-16-0758.1, 2017.

Geng, H., Hwang, H., Liu, X., Dong, S., and Ro, C.-U.: Investigation of aged aerosols in size-resolved Asian dust storm particles transported from Beijing, China, to Incheon, Korea, using low-Z particle EPMA, Atmos. Chem. Phys., 14, 3307-3323, https://doi.org/10.5194/acp-14-3307-2014, 2014.

Giles, D. M., Holben, B. N., Eck, T. F., Sinyuk, A., Smirnov, A., Slutsker, I., Dickerson, R., Thompson, A., and Schafer, J.: An analysis of AERONET aerosol absorption properties and classifications representative of aerosol source regions, J. Geophys. Res.- Atmos., 117, https://doi.org/10.1029/2012JD018127, 2012.

Giles, D. M., Sinyuk, A., Sorokin, M. G., Schafer, J. S., Smirnov, A., Slutsker, I., Eck, T. F., Holben, B. N., Lewis, J. R., and Campbell, J. R.: Advancements in the Aerosol Robotic Network (AERONET) Version 3 database–automated near-real-time quality control algorithm with improved cloud screening for Sun photometer aerosol optical depth (AOD) measurements, Atmos. Meas. Tech., 12, 169-209, https://doi.org/10.5194/amt-12-169-2019, 2019.

Glover, D., and Jessup, T.: The Indonesian fires and haze of 1997: the economic toll, Economy and Environment Program for SE Asia (EEPSEA) Singapore and the World Wildlife Fund (WWF) Indonesia, Jakarta, 1998.

Guyon, P., Boucher, O., Graham, B., Beck, J., Mayol-Bracero, O. L., Roberts, G. C., Maenhaut, W., Artaxo, P., and Andreae, M. O.: Refractive index of aerosol particles over the Amazon tropical forest during LBA-EUSTACH 1999, J. Aerosol Sci., 34, 883-907, https://doi.org/10.1016/S0021-8502(03)00052-1, 2003.

Hartley, W. S., and Hobbs, P. V.: An aerosol model and aerosol-induced changes in the clear-sky albedo off the east coast of the United States, J. Geophys. Res.- Atmos., 106, 9733-9748, https://doi.org/10.1029/2001JD900025, 2001.

Haywood, J., and Boucher, O.: Estimates of the direct and indirect radiative forcing due to tropospheric aerosols: A review, Rev. Geophys., 38, 513-543, https://doi.org/10.1029/1999RG000078, 2000.

Hendrickson, B. N., Brooks, S. D., Thornton, D. C., Moore, R. H., Crosbie, E., Ziemba, L. D., Carlson, C. A., Baetge, N., Mirrielees, J. A., and Alsante, A. N.: Role of sea surface microlayer properties in cloud formation, Frontiers in Marine Science, 7, 596225, https://doi.org/10.3389/fmars.2020.596225, 2021.

Herber, A., Thomason, L. W., Gernandt, H., Leiterer, U., Nagel, D., Schulz, K. H., Kaptur, J., Albrecht, T., and Notholt, J.: Continuous day and night aerosol optical depth observations in the Arctic between 1991 and 1999, J. Geophys. Res.- Atmos., 107, AAC 6-1-AAC 6-13, https://doi.org/10.1029/2001JD000536, 2002.

Hilario, M. R. A., Cruz, M. T., Bañaga, P. A., Betito, G., Braun, R. A., Stahl, C., Cambaliza, M. O., Lorenzo, G. R., MacDonald, A. B., AzadiAghdam, M., Pabroa, P. C., Yee, J. R., Simpas, J. B., and Sorooshian, A.: Characterizing weekly cycles of particulate matter in a coastal megacity: The importance of a seasonal, size-resolved, and chemically-speciated analysis, J. Geophys. Res.- Atmos., 125, e2020JD032614, https://doi.org/10.1029/2020JD032614, 2020a.

Hilario, M. R. A., Cruz, M. T., Cambaliza, M. O. L., Reid, J. S., Xian, P., Simpas, J. B., Lagrosas, N. D., Uy, S. N. Y., Cliff, S., and Zhao, Y.: Investigating size-segregated sources of elemental composition of particulate matter in the South China Sea during the 2011 Vasco cruise, Atmos. Chem. Phys., 20, 1255-1276, https://doi.org/10.5194/acp-20-1255-2020, 2020b.

Hilario, M. R. A., Crosbie, E., Shook, M., Reid, J. S., Cambaliza, M. O. L., Simpas, J. B. B., Ziemba, L., DiGangi, J. P., Diskin, G. S., and Nguyen, P.: Measurement report: Long-range transport patterns into the tropical northwest Pacific during the CAMP 2 Ex aircraft campaign: chemical composition, size distributions, and the impact of convection, Atmos. Chem. Phys., 21, 3777-3802, https://doi.org/10.5194/acp-21-3777-2021, 2021a.

Hilario, M. R. A., Olaguera, L. M., Narisma, G. T., and Matsumoto, J.: Diurnal characteristics of summer precipitation over Luzon Island, Philippines, Asia-Pacific Journal of Atmospheric Sciences, 57, 573-585, https://doi.org/10.1007/s13143-020-00214-1, 2021b.

Hilario, M. R. A., Bañaga, P. A., Betito, G., Braun, R. A., Cambaliza, M. O., Cruz, M. T., Lorenzo, G. R., MacDonald, A. B., Pabroa, P. C., and Simpas, J. B.: Stubborn aerosol: why particulate mass concentrations do not drop during the wet season in Metro Manila, Philippines, Environmental Science: Atmospheres, 2, 1428-1437, https://doi.org/10.1039/D2EA00073C, 2022.

Hogan, T. F., Liu, M., Ridout, J. A., Peng, M. S., Whitcomb, T. R., Ruston, B. C., Reynolds, C. A., Eckermann, S. D., Moskaitis, J. R., and Baker, N. L.: The navy global environmental model, Oceanography, 27, 116-125, https://doi.org/10.5670/oceanog.2014.73, 2014.

Holben, B. N., Eck, T. F., Slutsker, I. a., Tanre, D., Buis, J., Setzer, A., Vermote, E., Reagan, J. A., Kaufman, Y., and Nakajima, T.: AERONET—A federated instrument network and data archive for aerosol characterization, Remote Sens. Environ., 66, 1-16, https://doi.org/10.1016/S0034-4257(98)00031-5, 1998.

Holben, B. N., Tanre, D., Smirnov, A., Eck, T., Slutsker, I., Abuhassan, N., Newcomb, W., Schafer, J., Chatenet, B., and Lavenu, F.: An emerging ground-based aerosol climatology: Aerosol optical depth from AERONET, J. Geophys. Res.- Atmos., 106, 12067-12097, https://doi.org/10.1029/2001JD900014, 2001.

Hong, Y., and Di Girolamo, L.: Cloud phase characteristics over Southeast Asia from A-Train satellite observations, Atmos. Chem. Phys., 20, 8267-8291, https://doi.org/10.5194/acp-20-8267-2020, 2020.

Hong, Y., and Di Girolamo, L.: An overview of aerosol properties in clear and cloudy sky based on CALIPSO observations, Earth and Space Science, 9, e2022EA002287, https://doi.org/10.1029/2022EA002287, 2022.

Hoppel, W., Frick, G., Fitzgerald, J., and Larson, R.: Marine boundary layer measurements of new particle formation and the effects nonprecipitating clouds have on aerosol size distribution, J. Geophys. Res.- Atmos., 99, 14443-14459, https://doi.org/10.1029/94JD00797, 1994.

Huang, C., Li, J., Sun, W., Chen, Q., Mao, Q.-J., and Yuan, Y.: Long-Term Variation Assessment of Aerosol Load and Dominant Types over Asia for Air Quality Studies Using

Multi-Sources Aerosol Datasets, Remote Sensing, 13, 3116, https://doi.org/10.3390/rs13163116, 2021.

Hyer, E. J., Reid, J. S., Prins, E. M., Hoffman, J. P., Schmidt, C. C., Miettinen, J. I., and Giglio, L.: Patterns of fire activity over Indonesia and Malaysia from polar and geostationary satellite observations, Atmos. Res., 122, 504-519, https://doi.org/10.1016/j.atmosres.2012.06.011, 2013.

Jamora, J. B., Gudia, S. E. L., Go, A. W., Giduquio, M. B., and Loretero, M. E.: Potential CO2 reduction and cost evaluation in use and transport of coal ash as cement replacement: A case in the Philippines, Waste Manage., 103, 137-145, https://doi.org/10.1016/j.wasman.2019.12.026, 2020.

Jose, S., Gharai, B., Niranjan, K., and Rao, P.: Investigation on seasonal variations of aerosol properties and its influence on radiative effect over an urban location in central India, Atmos. Environ., 133, 41-48, https://doi.org/10.1016/j.atmosenv.2016.03.029, 2016.

Kaskaoutis, D., Kosmopoulos, P., Kambezidis, H., and Nastos, P.: Aerosol climatology and discrimination of different types over Athens, Greece, based on MODIS data, Atmos. Environ., 41, 7315-7329, https://doi.org/10.1016/j.atmosenv.2007.05.017, 2007.

Kaskaoutis, D., Badarinath, K., Kumar Kharol, S., Rani Sharma, A., and Kambezidis, H.: Variations in the aerosol optical properties and types over the tropical urban site of Hyderabad, India, Journal of Geophysical Research: Atmospheres, 114, https://doi.org/10.1029/2009JD012423, 2009.

Kiely, L., Spracklen, D. V., Wiedinmyer, C., Conibear, L., Reddington, C. L., Archer-Nicholls, S., Lowe, D., Arnold, S. R., Knote, C., and Khan, M. F.: New estimate of particulate emissions from Indonesian peat fires in 2015, Atmospheric Chemistry and Physics, 19, 11105-11121, https://doi.org/10.5194/acp-19-11105-2019, 2019.

Kim, J.-S., and Park, K.: Atmospheric aging of Asian dust particles during long range transport, Aerosol Sci. Tech., 46, 913-924, https://doi.org/10.1080/02786826.2012.680984, 2012.

Kirchstetter, T. W., Novakov, T., and Hobbs, P. V.: Evidence that the spectral dependence of light absorption by aerosols is affected by organic carbon, J. Geophys. Res.- Atmos., 109, https://doi.org/10.1029/2004JD004999, 2004.

Koven, C. D., and Fung, I.: Inferring dust composition from wavelength-dependent absorption in Aerosol Robotic Network (AERONET) data, J. Geophys. Res.- Atmos., 111, https://doi.org/10.1029/2005JD006678, 2006.

Kudo, R., Nishizawa, T., and Aoyagi, T.: Vertical profiles of aerosol optical properties and the solar heating rate estimated by combining sky radiometer and lidar measurements, Atmos. Meas. Tech., 9, 3223-3243, https://doi.org/10.5194/amt-9-3223-2016, 2016.

Kumar, K. R., Sivakumar, V., Reddy, R. R., Gopal, K. R., and Adesina, A. J.: Identification and classification of different aerosol types over a subtropical rural site in Mpumalanga, South

Africa: seasonal variations as retrieved from the AERONET Sunphotometer, Aerosol Air Qual. Res., 14, 108-123, https://doi.org/10.4209/aaqr.2013.03.0079, 2014.

Kumar, K. R., Yin, Y., Sivakumar, V., Kang, N., Yu, X., Diao, Y., Adesina, A. J., and Reddy, R.: Aerosol climatology and discrimination of aerosol types retrieved from MODIS, MISR and OMI over Durban (29.88 S, 31.02 E), South Africa, Atmos. Environ., 117, 9-18, https://doi.org/10.1016/j.atmosenv.2015.06.058, 2015.

Kuttippurath, J., and Raj, S.: Two decades of aerosol observations by AATSR, MISR, MODIS and MERRA-2 over India and Indian Ocean, Remote Sens. Environ., 257, 112363, https://doi.org/10.1016/j.rse.2021.112363, 2021.

Lee, H.-H., Iraqui, O., Gu, Y., Yim, S. H.-L., Chulakadabba, A., Tonks, A. Y.-M., Yang, Z., and Wang, C.: Impacts of air pollutants from fire and non-fire emissions on the regional air quality in Southeast Asia, Atmos. Chem. Phys., 18, 6141-6156, https://doi.org/10.5194/acp-18-6141-2018, 2018.

Lee, J., Kim, J., Song, C., Kim, S., Chun, Y., Sohn, B., and Holben, B.: Characteristics of aerosol types from AERONET sunphotometer measurements, Atmospheric Environment, 44, 3110-3117, https://doi.org/10.1016/j.atmosenv.2010.05.035, 2010.

Li, G., Bei, N., Cao, J., Huang, R., Wu, J., Feng, T., Wang, Y., Liu, S., Zhang, Q., and Tie, X.: A possible pathway for rapid growth of sulfate during haze days in China, Atmos. Chem. Phys., 17, 3301-3316, https://doi.org/10.5194/acp-17-3301-2017, 2017.

Li, J., Carlson, B. E., and Lacis, A. A.: Application of spectral analysis techniques in the intercomparison of aerosol data: 1. An EOF approach to analyze the spatial-temporal variability of aerosol optical depth using multiple remote sensing data sets, J. Geophys. Res.- Atmos., 118, 8640-8648, https://doi.org/10.1002/jgrd.50686, 2013.

Li, Z., Niu, F., Fan, J., Liu, Y., Rosenfeld, D., and Ding, Y.: Long-term impacts of aerosols on the vertical development of clouds and precipitation, Nat. Geosci., 4, 888-894, https://doi.org/10.1038/ngeo1313, 2011.

Lin, N.-H., Sayer, A. M., Wang, S.-H., Loftus, A. M., Hsiao, T.-C., Sheu, G.-R., Hsu, N. C., Tsay, S.-C., and Chantara, S.: Interactions between biomass-burning aerosols and clouds over Southeast Asia: Current status, challenges, and perspectives, Environ. Pollut., 195, 292-307, https://doi.org/10.1016/j.envpol.2014.06.036, 2014.

Lloyd, S.: Least squares quantization in PCM, IEEE T. Inform. Theory, 28, 129-137, https://doi.org/10.1109/TIT.1982.1056489, 1982.

Lynch, P., Reid, J. S., Westphal, D. L., Zhang, J., Hogan, T. F., Hyer, E. J., Curtis, C. A., Hegg, D. A., Shi, Y., and Campbell, J. R.: An 11-year global gridded aerosol optical thickness reanalysis (v1. 0) for atmospheric and climate sciences, Geosci. Model Dev., 9, https://doi.org/10.5194/gmd-9-1489-2016, 2016.

Matsumoto, J., Olaguera, L. M. P., Nguyen-Le, D., Kubota, H., and Villafuerte, M. Q.: Climatological seasonal changes of wind and rainfall in the Philippines, Int. J. Climatol., 40, 4843-4857, https://doi.org/10.1002/joc.6492, 2020.

Moosmüller, H., and Sorensen, C.: Small and large particle limits of single scattering albedo for homogeneous, spherical particles, J. Quant. Spectrosc. Ra., 204, 250-255, https://doi.org/10.1016/j.jqsrt.2017.09.029, 2018.

Mora, M., Braun, R. A., Shingler, T., and Sorooshian, A.: Analysis of remotely sensed and surface data of aerosols and meteorology for the Mexico Megalopolis Area between 2003 and 2015, J. Geophys. Res.- Atmos., 122, 8705-8723, https://doi.org/10.1002/2017JD026739, 2017.

Nakata, M., Mukai, S., and Yasumoto, M.: Seasonal and regional characteristics of aerosol pollution in east and southeast Asia, Frontiers in Environmental Science, 6, 29, ~~2018.~~https://doi.org/10.3389/fenvs.2018.00029, 2018.

Fires and Smoke in Borneo: https://earthobservatory.nasa.gov/images/40182/fires-and-smoke-in-borneo), 2009.

Nguyen, P., Shearer, E. J., Tran, H., Ombadi, M., Hayatbini, N., Palacios, T., Huynh, P., Braithwaite, D., Updegraff, G., and Hsu, K.: The CHRS Data Portal, an easily accessible public repository for PERSIANN global satellite precipitation data, Scientific Data, 6, 1-10, https://doi.org/10.1038/sdata.2018.296, ~~2019~~2019a.

Nguyen, T. T., Pham, H. V., Lasko, K., Bui, M. T., Laffly, D., Jourdan, A., and Bui, H. Q.: Spatiotemporal analysis of ground and satellite-based aerosol for air quality assessment in the Southeast Asia region, Environmental Pollution, 255, 113106, https://doi.org/10.1016/j.envpol.2019.113106, 2019b.

North, G. R., Bell, T. L., Cahalan, R. F., and Moeng, F. J.: Sampling errors in the estimation of empirical orthogonal functions, Mon. Weather Rev., 110, 699-706, https://doi.org/10.1175/1520-0493(1982)110<0699:SEITEO>2.0.CO;2, 1982.

O'Neill, N., Eck, T., Smirnov, A., Holben, B., and Thulasiraman, S.: Spectral discrimination of coarse and fine mode optical depth, J. Geophys. Res.- Atmos., 108, https://doi.org/10.1029/2002JD002975, 2003.

Oanh, N. K., Upadhyay, N., Zhuang, Y.-H., Hao, Z.-P., Murthy, D., Lestari, P., Villarin, J., Chengchua, K., Co, H., and Dung, N.: Particulate air pollution in six Asian cities: Spatial and temporal distributions, and associated sources, Atmospheric environment, 40, 3367-3380, https://doi.org/10.1016/j.atmosenv.2006.01.050, 2006.

Oanh, N. T. K., Permadi, D. A., Hopke, P. K., Smith, K. R., Dong, N. P., and Dang, A. N.: Annual emissions of air toxics emitted from crop residue open burning in Southeast Asia over the period of 2010–2015, Atmos. Environ., 187, 163-173, https://doi.org/10.1016/j.atmosenv.2018.05.061, 2018.

Ong, H. J. J., Lagrosas, N., Uy, S. N., Gacal, G. F. B., Dorado, S., Tobias Jr, V., and Holben, B.: Determination of Monthly Aerosol Types in Manila Observatory and Notre Dame of Marbel University from Aerosol Robotic Network (AERONET) measurements, AGU Fall Meeting Abstracts, 2016, A54E-03,

Pace, G., Sarra, A. d., Meloni, D., Piacentino, S., and Chamard, P.: Aerosol optical properties at Lampedusa (Central Mediterranean). 1. Influence of transport and identification of different aerosol types, Atmos. Chem. Phys., 6, 697-713, https://doi.org/10.5194/acp-6-697-2006, 2006.

Pandolfi, M., Alados-Arboledas, L., Alastuey, A., Andrade, M., Angelov, C., Artiñano, B., Backman, J., Baltensperger, U., Bonasoni, P., and Bukowiecki, N.: A European aerosol phenomenology–6: scattering properties of atmospheric aerosol particles from 28 ACTRIS sites, Atmos. Chem. Phys., 18, 7877-7911, https://doi.org/10.5194/acp-18-7877-2018, 2018.

Petters, M. D., Carrico, C. M., Kreidenweis, S. M., Prenni, A. J., DeMott, P. J., Collett Jr, J. L., and Moosmüller, H.: Cloud condensation nucleation activity of biomass burning aerosol, J. Geophys. Res.- Atmos., 114, https://doi.org/10.1029/2009JD012353, 2009.

Plymale, N. T., Szekely, J. E., and Rubinstein, A. H.: Statistical Cluster Analysis of Global Aerosol Optical Depth for Simplified Atmospheric Modeling, J. Appl. Meteorol. Clim., https://doi.org/10.1175/JAMC-D-21-0150.1, 2021.

PSA: Highlights of the Philippine population 2015 census of population, Philippine Statistics Authority, 2016.

Qi, Y., Ge, J., and Huang, J.: Spatial and temporal distribution of MODIS and MISR aerosol optical depth over northern China and comparison with AERONET, Chinese science bulletin, 58, 2497-2506, https://doi.org/10.1007/s11434-013-5678-5, 2013.

Ramage, C. S.: Monsoon meteorology, Academic Press, New York, 1971.

Randles, C., Da Silva, A., Buchard, V., Colarco, P., Darmenov, A., Govindaraju, R., Smirnov, A., Holben, B., Ferrare, R., and Hair, J.: The MERRA-2 aerosol reanalysis, 1980 onward. Part I: System description and data assimilation evaluation, J. Climate, 30, 6823-6850, https://doi.org/10.1175/JCLI-D-16-0609.1, 2017.

Reid, J., Koppmann, R., Eck, T., and Eleuterio, D.: A review of biomass burning emissions part II: intensive physical properties of biomass burning particles, Atmos. Chem. Phys., 5, 799-825, https://doi.org/10.5194/acp-5-799-2005, 2005.

Reid, J., Xian, P., Hyer, E., Flatau, M., Ramirez, E., Turk, F., Sampson, C., Zhang, C., Fukada, E., and Maloney, E.: Multi-scale meteorological conceptual analysis of observed active fire hotspot activity and smoke optical depth in the Maritime Continent, Atmos. Chem. Phys., 12, 2117, https://doi.org/10.5194/acp-12-2117-2012, 2012.

Reid, J., Maring, H., Narisma, G., van den Heever, S., Di Girolamo, L., Ferrare, R., Holz, R., Lawson, P., Mace, G., and Simpas, J.: The coupling between tropical meteorology, aerosol lifecycle, convection, and radiation, during the Cloud, Aerosol and Monsoon Processes

Philippines Experiment (CAMP 2 Ex), B. Am. Meteorol. Soc., https://doi.org/10.1175/BAMS-D-21-0285.1, 2023.

Reid, J. S., Hobbs, P. V., Liousse, C., Martins, J. V., Weiss, R. E., and Eck, T. F.: Comparisons of techniques for measuring shortwave absorption and black carbon content of aerosols from biomass burning in Brazil, J. Geophys. Res.- Atmos., 103, 32031-32040, https://doi.org/10.1029/98JD00773, 1998.

Reid, J. S., Hyer, E. J., Johnson, R. S., Holben, B. N., Yokelson, R. J., Zhang, J., Campbell, J. R., Christopher, S. A., Di Girolamo, L., and Giglio, L.: Observing and understanding the Southeast Asian aerosol system by remote sensing: An initial review and analysis for the Seven Southeast Asian Studies (7SEAS) program, Atmos. Res., 122, 403-468, https://doi.org/10.1016/j.atmosres.2012.06.005, 2013.

Reid, J. S., Lagrosas, N. D., Jonsson, H. H., Reid, E. A., Sessions, W. R., Simpas, J. B., Uy, S. N., Boyd, T., Atwood, S. A., and Blake, D. R.: Observations of the temporal variability in aerosol properties and their relationships to meteorology in the summer monsoonal South China Sea/East Sea: the scale-dependent role of monsoonal flows, the Madden–Julian Oscillation, tropical cyclones, squall lines and cold pools, Atmos. Chem. Phys., 15, 1745-1768, https://doi.org/10.5194/acp-15-1745-2015, 2015.

Rizza, U., Mancinelli, E., Morichetti, M., Passerini, G., and Virgili, S.: Aerosol optical depth of the main aerosol species over Italian cities based on the NASA/MERRA-2 model reanalysis, Atmosphere, 10, 709, https://doi.org/10.3390/atmos10110709, 2019.

Rolph, G., Stein, A., and Stunder, B.: Real-time environmental applications and display system: READY, Environ. Modell. Softw., 95, 210-228, https://doi.org/10.1016/j.envsoft.2017.06.025, 2017.

Ross, J. L., Hobbs, P. V., and Holben, B.: Radiative characteristics of regional hazes dominated by smoke from biomass burning in Brazil: Closure tests and direct radiative forcing, J. Geophys. Res.- Atmos., 103, 31925-31941, https://doi.org/10.1029/97JD03677, 1998.

Saleh, R., Hennigan, C., McMeeking, G., Chuang, W., Robinson, E., Coe, H., Donahue, N., and Robinson, A.: Absorptivity of brown carbon in fresh and photo-chemically aged biomass-burning emissions, Atmos. Chem. Phys., 13, 7683-7693, https://doi.org/10.5194/acp-13-7683-2013, 2013.

Schlosser, J. S., Braun, R. A., Bradley, T., Dadashazar, H., MacDonald, A. B., Aldhaif, A. A., Aghdam, M. A., Mardi, A. H., Xian, P., and Sorooshian, A.: Analysis of aerosol composition data for western United States wildfires between 2005 and 2015: Dust emissions, chloride depletion, and most enhanced aerosol constituents, J. Geophys. Res.- Atmos., 122, 8951-8966, https://doi.org/10.1002/2017JD026547, 2017.

Schuster, G., Dubovik, O., and Arola, A.: Remote sensing of soot carbon–Part 1: Distinguishing different absorbing aerosol species, Atmos. Chem. Phys., 16, 1565-1585, https://doi.org/10.5194/acp-16-1565-2016, 2016.

Schuster, G. L., Dubovik, O., Holben, B. N., and Clothiaux, E. E.: Inferring black carbon content and specific absorption from Aerosol Robotic Network (AERONET) aerosol retrievals, J. Geophys. Res.- Atmos., 110, https://doi.org/10.1029/2004JD004548, 2005.
Schuster, G. L., Dubovik, O., and Holben, B. N.: Angstrom exponent and bimodal aerosol size distributions, J. Geophys. Res.- Atmos., 111, https://doi.org/10.1029/2005JD006328, 2006.

Sharma, M., Kaskaoutis, D. G., Singh, R. P., and Singh, S.: Seasonal variability of atmospheric aerosol parameters over Greater Noida using ground sunphotometer observations, Aerosol Air Qual. Res., 14, 608-622, https://doi.org/10.4209/aaqr.2013.06.0219, 2014.

Shen, Z., Liu, J., Horowitz, L., Henze, D., Fan, S., Mauzerall, D. L., Lin, J.-T., and Tao, S.: Analysis of transpacific transport of black carbon during HIPPO-3: implications for black carbon aging, Atmos. Chem. Phys., 14, 6315-6327, https://doi.org/10.5194/acp-14-6315-2014, 2014.

Sinyuk, A., Holben, B. N., Eck, T. F., Giles, D. M., Slutsker, I., Korkin, S., Schafer, J. S., Smirnov, A., Sorokin, M., and Lyapustin, A.: The AERONET Version 3 aerosol retrieval algorithm, associated uncertainties and comparisons to Version 2, Atmospheric Measurement Techniques, 13, 3375-3411, https://doi.org/10.5194/amt-13-3375-2020, 2020.

Smirnov, A., Holben, B. N., Dubovik, O., O'Neill, N. T., Eck, T. F., Westphal, D. L., Goroch, A. K., Pietras, C., and Slutsker, I.: Atmospheric aerosol optical properties in the Persian Gulf, J. Atmos. Sci., 59, 620-634, https://doi.org/10.1175/1520-0469(2002)059<0620:AAOPIT>2.0.CO;2, 2002.

Smith, S. J., Aardenne, J. v., Klimont, Z., Andres, R. J., Volke, A., and Delgado Arias, S.: Anthropogenic sulfur dioxide emissions: 1850–2005, Atmos. Chem. Phys., 11, 1101-1116, https://doi.org/10.5194/acp-11-1101-2011, 2011.

Sorooshian, A., Wang, Z., Feingold, G., and L'Ecuyer, T. S.: A satellite perspective on cloud water to rain water conversion rates and relationships with environmental conditions, J. Geophys. Res.- Atmos., 118, 6643-6650, https://doi.org/10.1002/jgrd.50523, 2013.

Stahl, C., Cruz, M. T., Bañaga, P. A., Betito, G., Braun, R. A., Aghdam, M. A., Cambaliza, M. O., Lorenzo, G. R., MacDonald, A. B., and Hilario, M. R. A.: Sources and characteristics of size-resolved particulate organic acids and methanesulfonate in a coastal megacity: Manila, Philippines, Atmos. Chem. Phys., 20, 15907-15935, https://doi.org/10.5194/acp-20-15907-2020, 2020.

Stahl, C., Crosbie, E., Bañaga, P. A., Betito, G., Braun, R. A., Cainglet, Z. M., Cambaliza, M. O., Cruz, M. T., Dado, J. M., and Hilario, M. R. A.: Total organic carbon and the contribution from speciated organics in cloud water: airborne data analysis from the CAMP 2 Ex field campaign, Atmos. Chem. Phys., 21, 14109-14129, https://doi.org/10.5194/acp-21-14109-2021, 2021.

Stein, A., Draxler, R. R., Rolph, G. D., Stunder, B. J., Cohen, M., and Ngan, F.: NOAA's HYSPLIT atmospheric transport and dispersion modeling system, B. Am. Meteorol. Soc., 96, 2059-2077, https://doi.org/10.1175/BAMS-D-14-00110.1, 2015.

Stevens, B., and Feingold, G.: Untangling aerosol effects on clouds and precipitation in a buffered system, Nature, 461, 607-613, https://doi.org/10.1038/nature08281, 2009.

Sullivan, R. C., Levy, R. C., da Silva, A. M., and Pryor, S. C.: Developing and diagnosing climate change indicators of regional aerosol optical properties, Scientific Reports, 7, 1-13, https://doi.org/10.1038/s41598-017-18402-x, 2017.

Tao, W. K., Chen, J. P., Li, Z., Wang, C., and Zhang, C.: Impact of aerosols on convective clouds and precipitation, Rev. Geophys., 50, https://doi.org/10.1029/2011RG000369, 2012.

Tsay, S.-C., Hsu, N. C., Lau, W. K.-M., Li, C., Gabriel, P. M., Ji, Q., Holben, B. N., Welton, E. J., Nguyen, A. X., and Janjai, S.: From BASE-ASIA toward 7-SEAS: A satellite-surface perspective of boreal spring biomass-burning aerosols and clouds in Southeast Asia, Atmospheric environment, 78, 20-34, ~~2013.~~https://doi.org/10.1016/j.atmosenv.2012.12.013, 2013.

Van Beelen, A., Roelofs, G., Hasekamp, O., Henzing, J., and Röckmann, T.: Estimation of aerosol water and chemical composition from AERONET Sun–sky radiometer measurements at Cabauw, the Netherlands, Atmos. Chem. Phys., 14, 5969-5987, https://doi.org/10.5194/acp-14-5969-2014, 2014.

Wall, C. J., Norris, J. R., Possner, A., McCoy, D. T., McCoy, I. L., and Lutsko, N. J.: Assessing effective radiative forcing from aerosol–cloud interactions over the global ocean, Proceedings of the National Academy of Sciences, 119, e2210481119, https://doi.org/10.1073/pnas.2210481119, 2022.

Wang, L., Lau, K.-H., Fung, C.-H., and Gan, J.-P.: The relative vorticity of ocean surface winds from the QuikSCAT satellite and its effects on the geneses of tropical cyclones in the South China Sea, Tellus A, 59, 562-569, https://doi.org/10.1111/j.1600-0870.2007.00249.x, 2007.

Wang, S.-H., Welton, E. J., Holben, B. N., Tsay, S.-C., Lin, N.-H., Giles, D., Stewart, S. A., Janjai, S., Nguyen, X. A., and Hsiao, T.-C.: Vertical distribution and columnar optical properties of springtime biomass-burning aerosols over Northern Indochina during 2014 7-SEAS campaign, Aerosol and Air Quality Research, 15, 2037-2050, https://doi.org/10.4209/aaqr.2015.05.0310, 2015.

Wu, M.-c., and Choy, C.-w.: An Observational Study of the Changes in the Intensity and Motion of Tropical Cyclones crossing Luzon, Tropical Cyclone Research and Review, 4, 95-109, https://doi.org/10.6057/2015TCRRh3.01, 2016.

Xian, P., Reid, J. S., Atwood, S. A., Johnson, R. S., Hyer, E. J., Westphal, D. L., and Sessions, W.: Smoke aerosol transport patterns over the Maritime Continent, Atmos. Res., 122, 469-485, https://doi.org/10.1016/j.atmosres.2012.05.006, 2013.

Xiao, N., Shi, T., Calder, C. A., Munroe, D. K., Berrett, C., Wolfinbarger, S., and Li, D.: Spatial characteristics of the difference between MISR and MODIS aerosol optical depth retrievals over mainland Southeast Asia, Remote Sensing of Environment, 113, 1-9, https://doi.org/10.1016/j.rse.2008.07.011, 2009.

Xie, Y., Li, Z., Zhang, Y., Zhang, Y., Li, D., Li, K., Xu, H., Zhang, Y., Wang, Y., and Chen, X.: Estimation of atmospheric aerosol composition from ground-based remote sensing measurements of Sun-sky radiometer, J. Geophys. Res.- Atmos., 122, 498-518, https://doi.org/10.1002/2016JD025839, 2017.

Yang, S., Lau, W. K., Ji, Z., Dong, W., and Yang, S.: Impacts of radiative effect of pre-monsoon biomass burning aerosols on atmospheric circulation and rainfall over Southeast Asia and southern China, Climate Dynamics, 59, 417-432, https://doi.org/10.1007/s00382-021-06135-7, 2022.

Yumul Jr, G. P., Cruz, N. A., Dimalanta, C. B., Servando, N. T., and Hilario, F. D.: The 2007 dry spell in Luzon (Philippines): its cause, impact and corresponding response measures, Climatic change, 100, 633-644, https://doi.org/10.1007/s10584-009-9677-0, 2010.

Zhao, G., Di Girolamo, L., Dey, S., Jones, A. L., and Bull, M.: Examination of direct cumulus contamination on MISR-retrieved aerosol optical depth and angstrom coefficient over ocean, Geophysical Research Letters, 36, https://doi.org/10.1029/2009GL038549, 2009.

Zhao, G., Zhao, C., Kuang, Y., Bian, Y., Tao, J., Shen, C., and Yu, Y.: Calculating the aerosol asymmetry factor based on measurements from the humidified nephelometer system, Atmos. Chem. Phys., 18, 9049-9060, https://doi.org/10.5194/acp-18-9049-2018, 2018.